UNIVERSIDADE DE LISBOA
FACULDADE DE FARMÁCIA

SMART HYBRID COMPOUNDS TO TARGET THE RESPIRATORY ELECTRON TRANSPORT CHAIN OF *MYCOBACTERIUM TUBERCULOSIS*

Diogo Miguel de Oliveira Nunes

Dissertação orientada pela Professora Francisca da Conceição Lopes e coorientada pela Professora Maria de Jesus de Almeida Rainha Perry da Câmara Saldanha Rocha.

MESTRADO EM QUÍMICA
MEDICINAL E BIOFARMACÊUTICA

2022

UNIVERSIDADE DE LISBOA
FACULDADE DE FARMÁCIA

SMART HYBRID COMPOUNDS TO TARGET THE RESPIRATORY ELECTRON TRANSPORT CHAIN OF *MYCOBACTERIUM TUBERCULOSIS*

Diogo Miguel de Oliveira Nunes

Dissertação orientada pela Professora Francisca da Conceição Lopes e coorientada pela Professora Maria de Jesus de Almeida Rainha Perry da Câmara Saldanha Rocha.

MESTRADO EM QUÍMICA
MEDICINAL E BIOFARMACÊUTICA

2022

Part of the work discussed in this dissertation was also presented in the following(s) scientific communication(s):

Clariano M, Nunes D, Canudo D, Perry MJ, Lopes F. Pyrroloquinolone-based hybrid compounds multitargeting the electron transport chain of *Mycobacterium tuberculosis* – Oral communication – XXVI Encontro Galego-Português de Química, Santiago de Compostela, November 16th – 18th, 2022.

Nunes D, Perry MJ, Lopes F. Smart hybrid pharmacological tools to target the mycobacterial respiration – Flash communication – iMed Conference 14.0 –AstraZeneca Foundation Innovate Competition, October 12th – 16th, 2022

Clariano M, Nunes D, Canudo D, Perry MJ, Lopes F. Exploiting the electron transport chain of *Mycobacterium tuberculosis* as a target in the development of new anti-tuberculosis drugs – Flash communication – 14th National Organic Chemistry Meeting & 7th National Medicinal Chemistry Meeting, April 20th - 22nd, 2022

Clariano M, Nunes D, Canudo D, Perry MJ, Lopes F. Pyrroloquinolone based hybrids for multitarget approach on tuberculosis – Poster – 5th Meeting of CQUL - "Forging bonds", July 12th to 14th, 2022

Clariano M, Nunes D, Canudo D, Perry MJ, Lopes F. Development of new drugs multitargeting the electron transport chain of *Mycobacterium tuberculosis* – Poster – 13th iMed.ULisboa meeting, July 5th – 6th, 2022

Clariano M, Nunes D, Canudo D, Perry MJ, Lopes F. Potential of the electron transport chain of *Mycobacterium tuberculosis* in the development of new anti-tuberculosis drugs – Poster – Ciência 2022 – Science and Technology in Portugal Summit, May 16th - 18th, 2022

This research was funded by projects UIDB/04138/2020 (FCT), UIDP/04138/2020 (FCT), and LISBOA-01-0145-FEDER-030266 | PTDC/MED-FAR/30266/2017 (FEDER and FCT), and by the Research Grant for students BII/5/FF/2022, within the project “Verão com Ciência – 2022” (FCT).

The NMR spectrometers are part of the National NMR Network, supported by Infrastructure Project Nº022161 (co-financed by FEDER through COMPETE2020, POCI and PORL and FCT through PIDDAC). The mass spectrometer is part of the Portuguese MS Network, LISBOA-01-0145-FEDER-022125, supported by Lisboa2020, under the Portugal2020 Partnership Agreement, through the European Regional Development Fund.

Acknowledgments

The work here presented was developed in the Research Institute for Medicines (iMed.ULisboa), Faculty of Pharmacy, Universidade de Lisboa, under the supervision of professors Francisca Lopes and Maria de Jesus Perry. I would like to express my gratitude to them for allowing me to work on this thesis project and for the continuous support, advice, and inspiration that made this project possible.

To my supervisors, professors Francisca Lopes and Maria de Jesus Perry, I also thank them for their constant availability, support, and motivation, even in the gloomiest times, and all the knowledge and advice they shared with me. Their contribution was essential, both for the planning and execution of this project, as well as for the interpretation of all of the results, and I have truly enjoyed the time I spent working with them.

To Marta Clariano, who mentored me and accompanied in the lab, I thank her for her support, companionship, and friendship. I thank her for all the advice, teachings, and knowledge she shared with me, and for her patience, dedication, motivation, and positivity that helped me to always keep going. I am very grateful to have shared a lab and a bench with her, and without her, this thesis project would have been much more difficult.

To my lab colleagues from the Medicinal Chemistry group, I thank them for their presence and sociality in the lab that contributed to a great lab environment. I also thank them for all the advice and exchange of scientific knowledge. To my master colleagues, Joana, Mariana, Salma, and Filipe, I thank them in particular for their companionship and friendship that made going to the lab much easier.

I would also like to thank Audrey Jordaan, from the University of Cape Town, for performing the antimycobacterial screenings presented in this thesis, Professor Ana Margarida Madureira, for performing the cytotoxicity assay presented in this thesis, and to Dr. Andreia Bento da Silva, for the mass spectrometry analysis.

Last, but certainly not least, I would like to express my gratitude to my family and friends. I am grateful for my family, in particular for my parents, for giving me a stable environment to grow, for supporting me in all of my decisions, and for all the opportunities they gave me throughout my life. I am very grateful for all the friends I made during my master's degree, Carolina, Bárbara, Keisly, Joana, Mariana, Raquel, Filipe, Salma, Rafaela, and Ginevra, as well as my older, lifelong friends, Carolina, Maria, Rita, Rita, and Mauro. I thank them for being my support system whenever I need it.

Abstract

While tuberculosis (TB) is curable and preventable, it continues to be a global epidemic, with a quarter of the world's population estimated to be infected with *Mycobacterium tuberculosis* (Mtb), its causative agent. Global TB control has been hampered by multiple factors, such as the emergence of drug-resistant tuberculosis and an inefficient targeting of latency.

The discovery of effective, safe, and compliance-friendly antitubercular (anti-TB) drugs remains a largely unmet medical need in the last 40 years. Although three drugs (bedaquiline, delamanid, and pretomanid) were recently approved, their displayed side-effects undermine widespread use. Therefore, new drugs active against drug-resistant and latent TB are urgently needed.

The mycobacterial electron transport chain (ETC) has emerged recently as an interesting target for novel anti-TB drugs. As both replicant and latent bacteria require a sustained supply of ATP, it is believed that the inhibition of the ETC is an effective strategy to eliminate latent populations and therefore improve TB control.

This project includes the synthesis and characterization of a small library of hybrid pharmacological tools that combine a structural feature designed to target cytochrome-bc1-aa3 with a nitric oxide releasing group, capable of inhibiting cytochrome bd. These tools thus offer the potential to block two key components of mycobacterial respiration.

In this thesis, the synthesis and structural characterization of a small library of hybrid compounds are presented. Compound aqueous solubility and stability was evaluated by HPLC, the antimycobacterial activity was tested against *Mtb* H37Rv and *Mtb* cydKO, and the toxicity was tested in HEK293 cell lines. The hybrid compounds' proposed mechanism of action was corroborated by the activity assays and compound **8c** presented itself as a promising anti-TB agent. Additionally, a nitrofuranylamide **(7c')** was isolated and presented itself has a very interesting lead molecule for anti-TB therapy, with sub-micromolar activity, no cytotoxicity, and a good pharmacokinetic and physicochemical profile.

Keywords: Tuberculosis, *Mycobacterium tuberculosis*, electron transport chain, hybrid pharmacological tools.

Resumo

A tuberculose, apesar de ser uma doença evitável e curável, mantém-se como uma epidemia global. Estima-se que em 2021, a tuberculose tenha sido a décima terceira maior causa de morte global e a segunda maior causa de morte induzida por um agente infecioso e que determinou, aproximadamente, 1,6 milhões de mortes. No mesmo ano, 10,6 milhões de pessoas terão contraído a doença e estimativas recentes indicam que um quarto da população mundial está infetado com o *Mycobacterium tuberculosis* (Mtb), o seu agente etiológico.

O Mtb é um agente patogénico humano obrigatório, com várias características distintivas que o tornam um agente infecioso de excelência. Esta bactéria aproveita a resposta imunitária do hospedeiro para aumentar o grau de transmissão. Para além disso, possuí um arsenal metabólico extenso capaz de metabolizar os xenobióticos e uma parede celular única, com um elevado número de bombas de efluxo, que lhe confere uma alta impermeabilidade, permitindo-lhe adaptar-se às múltiplas pressões ambientais criadas pelo hospedeiro, adquirindo assim uma elevada resistência natural a fármacos. Por fim, esta micobactéria possui uma capacidade única de permanecer no hospedeiro num estado latente, caracterizado por uma fisiologia e metabolismo distinto, crescimento reduzido, tolerância a fármacos aumentada, e uma capacidade de não se deixar detetar pelo sistema imunitário.

Um regime terapêutico anti-tubercular tem como objetivo diminuir a severidade da doença, evitar reincidências e o desenvolvimento de resistência, e para tal, necessita eliminar todas as populações de bacilos do hospedeiro. Devido às características próprias das bactérias latentes, os regimes terapêuticos anti-tuberculares têm durações bastante prolongadas e características de polimedicação, apresentando por isso efeitos adversos cumulativos. Consequentemente, os regimes terapêuticos anti-tuberculares têm baixa adesão e tolerância por parte dos doentes, podendo resultar na emergência de tuberculose resistente a fármacos, que está associada a uma maior letalidade, e a um sucesso terapêutico inferior.

Desta forma, o desenvolvimento de um regime terapêutico curto, potente, e eficiente em todas as formas de infeção é uma prioridade no controlo da tuberculose. Para tal, é essencial desenvolver novos fármacos que sejam eficientes, seguros, e bem-tolerados, e que preferencialmente atuem por novos mecanismos de ação, de forma a evitar a emergência de resistência. Esta premência não foi considerada nos últimos anos, sendo que apenas três fármacos anti-tuberculares (bedaquilina, delamanida e pretomanida) foram aprovados nos últimos quarenta anos, todos com efeitos secundários que comprometem a sua utilização prolongada. Assim, é crucial investir na descoberta e desenvolvimento de novos fármacos ativos contra a tuberculose latente e resistente, preferencialmente com novos mecanismos de ação e alvos diferentes.

A cadeia de transporte de eletrões do Mtb surgiu recentemente como um alvo promissor para novos fármacos anti-tuberculares. Atualmente, cerca de 30% dos novos fármacos em ensaios clínicos têm como alvo um elemento da cadeia de transporte de eletrões, e cerca de 65% dos regimes farmacológicos em ensaios clínicos de fase III incluem um fármaco que inibe a cadeia de transporte de eletrões. Como ambas as formas bacterianas, latentes e replicantes, requerem um fornecimento contínuo de ATP,

o metabolismo energético é um alvo apelativo, já que a sua inibição e consequente disrupção do fornecimento de ATP permite eliminar eficientemente as populações replicantes e latentes, e consequentemente, diminuir a duração dos regimes terapêuticos e a emergência de resistência.

Este projeto inclui a síntese e caracterização de uma pequena biblioteca de ferramentas farmacológicas híbridas, capazes de inibir o citocromo bc1-aa3, a oxidase principal do Mtb, e, em simultâneo, o citocromo bd, uma oxidase alternativa que o bacilo utiliza em situações de hipoxia. Deste modo, pretende-se que estes compostos consigam inibir eficientemente a produção de ATP, e eliminar ambas as populações bacterianas replicantes e latentes. Os compostos híbridos têm uma estrutura comum, com um esqueleto de pirroloquinolona, provavelmente capaz de inibir o citocromo bc1-aa3 uma vez que é inibidor do citocromo bc1 do *Plasmodium falciparum*, uma proteína com alta homologia com o citocromo bc1-aa3 do Mtb; e um esqueleto de nitrofurano, que podendo ser reduzido *in vivo* pelas nitroreductases do Mtb, liberta óxido nítrico capaz de inibir o citocromo bd. As duas estruturas serão ligadas por um braço de ligação, que será a porção variável da biblioteca de compostos.

Os compostos foram sintetizados por uma estratégia de síntese divergente, iniciada com a síntese do esqueleto da pirroloquinolona, com rendimentos elevados. De seguida, vários braços de ligação foram acoplados, com rendimentos moderados. Quando necessário, foi efetuada uma redução das funções químicas do braço de ligação (grupos nitro e nitrilo), por forma a garantir a presença de um grupo amina livre. Por fim, o esqueleto de nitrofurano foi acoplado, com rendimentos baixos, através de dois tipos de ligação: ligações amida **(7a – 7d)** e ligações imina **(8a – 8c)**. Todos os compostos foram obtidos puros, exceto o composto **7d**, cujas tentativas de purificação não foram bem sucedidas. Na síntese do composto **7c**, isolou-se um produto de degradação – uma nitrofuranilamida (composto **7c'**) – que foi caracterizado. Como o composto **7c** foi somente obtido puro posteriormente, por restrições temporais não foram efetuados os ensaios subsequentes para este composto.

A solubilidade aquosa dos compostos foi determinada por HPLC para os compostos **7c'** e **8c**. Este ensaio não foi efetuado com os restantes compostos (**(7a), (7b), (8a)** e **(8b)**) por se ter verificado que tinham sofrido degradação extensiva. Ambos os compostos **7c'** e **8c** demonstraram ter boa solubilidade aquosa, que juntamente com as propriedades físico-químicas previstas indicam que estes compostos, provavelmente, terão uma boa biodisponibilidade oral.

Também se avaliou a estabilidade química (em tampão PBS), em plasma, e metabólica (em microssomas de ratinho), por HPLC para os compostos **7c'** e **8c**. Ambos demonstraram ter um bom perfil farmacocinético, sendo que o composto **7c'** demonstrou ser mais estável que o composto **8c** nos três meios testados. Comparando a estabilidade do composto **7c'** com outros compostos híbridos, nenhuma correlação foi identificada entre a ausência do esqueleto da pirroloquinolona e uma melhoria no perfil farmacocinético.

A atividade anti-micobacteriana dos compostos **7c'**, **8c**, e de alguns intermediários foi testada contra duas estirpes de *M. tuberculosis* (uma estirpe nativa, H37Rv, e uma estirpe mutante, cydKO). Os resultados estão de acordo com o mecanismo de ação proposto em que os compostos híbridos têm como alvos ambos o

citocromos, bc1-aa3 e bd, e a necessidade do grupo nitro ser substituinte num ciclo heteroaromático. O composto **8c** apresentou atividade anti-micobacteriana com valores de MIC na gama micromolar, demonstrando que estes compostos híbridos são agentes anti-tuberculares promissores. O composto **7c'** foi o composto mais ativo, apresentando atividade anti-micobacteriana com valores de MIC na gama sub-micromolar, podendo indicar um mecanismo de ação distinto, uma vez que esta molécula não contém a subunidade pirroloquinolona.

A toxicidade dos compostos **7c'** e **8c**, tal como do percursor **6c**, foi testada contra a linha celular HEK293. Os compostos **7c'** e **6c** não apresentaram citotoxicidade, enquanto o composto **8c** apresentou citotoxicidade superior, apesar de demonstrar alguma seletividade para as células bacterianas.

Deste modo, os próximos passos deste projeto incluem a realização de ensaios de atividade dos compostos **7c'** e **8c** em outras bactérias, de forma a avaliar a seletividade destes compostos; a avaliação biológica e farmacocinética dos restantes compostos híbridos; e o aumento da biblioteca de compostos híbridos.

Palavras-chave: Tuberculose, *Mycobacterium tuberculosis*, cadeia de transporte de eletrões, ferramentas farmacológicas híbridas.

Table of Contents

List of Tables

List of Figures

List of Abbreviations

ADC – bovine albumin, dextrose, and catalase supplement.

Anti-TB – antitubercular

ATB – active tuberculosis

BDQ – bedaquiline

BMBN – bromomethylbenzonitrile

Boc – *tert*-butyloxycarbonyl

CAS – casitone

CFZ – clofazimine

CL_{int} –Intrinsic Clearence

DLM – delamanid

DR – drug resistant

DS – drug susceptible

ETC – electron transport chain

HBA – hydrogen bond acceptor

HBD – hydrogen bond donor

LTBI – latent tuberculosis infection

MDR – multidrug-resistant

MK – menaquinone

MKH_2 – menaquinol

Mtb – *Mycobacterium tuberculosis*

NBB – nitrobenzyl bromide

NDH – NADH dehydrogenases

NTZ – nitazoxanide

OxPhos – oxidative phosphorylation

PMF – proton motive force

PTM – pretomanid

PTSA – p-toluenesulfonic acid

PYQ – pyrroloquinolone

PZA – pyrazinamide

RNS – reactive nitrogen species

ROS – reactive oxygen species

SDH – succinate dehydrogenase

TB – tuberculosis

TCA – tricarboxylic acid cycle

TDR – total drug-resistant

TPSA – total polar surface area

Tw – Tween 80

Tx – tyloxapol

XDR – extensively drug-resistant

Chapter I

Introduction

Chapter I – Introduction

I. 1. Epidemiology

Currently, the World Health Organization (WHO) estimates that near 2 billion people are infected with *Mycobacterium tuberculosis* (Mtb), equivalent to a fourth of the world's population. Although only 5 to 10% of that population will develop tuberculosis (TB) in their lifetime; TB was the thirteenth leading cause of death worldwide and the top cause from a singular infectious agent in 2019, and is expected to be the second leading cause of death from a singular infectious agent in 2021, only after COVID-19. [1], [2]

TB can affect anyone, regardless of age and sex, but the highest burden is in adult males. In 2021, an estimated 10.6 million people contracted TB, a 4.5% increase compared with the previous year, reversing years of slow decline on new TB cases trend. In the same year, annual TB deaths increased for the second year in a row, reversing the decreasing trend observed since 2005, with 1.4 million deaths in HIV-negative people and an additional 187 thousand deaths in HIV-positive people. **Figure I.1** describes the global trend in the estimated number of incident TB cases and TB deaths between 2000 and 2021. [2], [3]

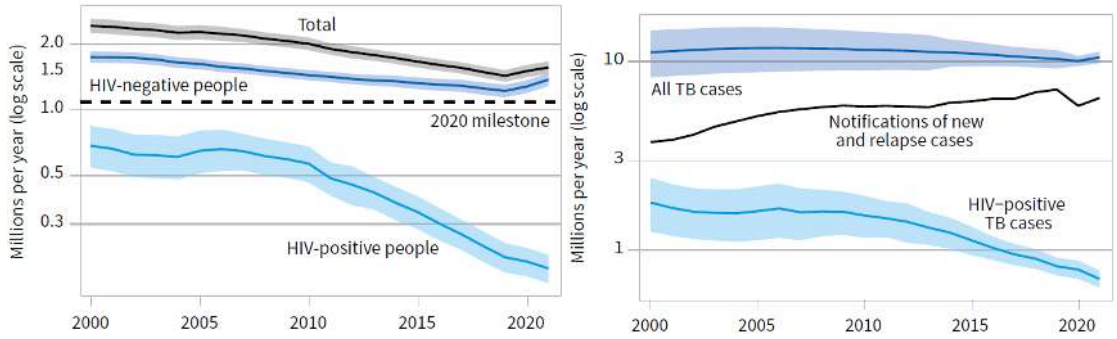

Figure I.1 | Global trends in estimated TB deaths (left) and incident TB cases (right), 2000-2021
The shaded areas represent uncertainty intervals. The horizontal dashed line shows the 2020 milestone defined in the 'End TB Strategy'. Reproduced from World Health Organization, 2022. [2]

The current TB endemic is fuelled by poverty, malnutrition, overcrowding, HIV, and deficient healthcare systems, but also by an insufficient comprehension of the spectrum of TB pathogenesis, which may be essential in the development of new diagnosis and treatment regimens. Furthermore, it is expected that the COVID-19 pandemic will result into a rise on TB incidence, with an observed maximum incidence in 2022. [4]–[6]

In 2014 and 2015, aiming to eradicate tuberculosis by 2035, all WHO members and the UN developed a concerted strategy in a global effort, the 'End TB strategy', with three main goals by 2035: a decrease of TB deaths by 95%, a decrease of TB incidence by 90%, and a decrease of the percentage of families facing "catastrophic total costs"[1] to 0%. Despite global efforts and global conferences on TB, 2020 results fall short compared to the defined milestones, with a decrease of TB deaths of 11% (2020 milestone: 20%), a decrease of TB incidence of 9.2% (2020 milestone: 35%), and 47% of people with TB still facing catastrophic costs. (2020 milestone: 0%). [6]

1 Defined as when TB related costs account for >20% of their household income.

I. 2. Mycobacterium tuberculosis

Mtb is an obligate human pathogen and the causative agent of TB. As humans are the only major natural reservoir of Mtb, this bacterium has to cause infection to transmit between individuals. Understanding the Mtb virulence is still a challenging task today, as no single genomic characteristic explains its obligate pathogen lifestyle, virulence, and transmission. Moreover, Mtb bacillary burden in TB patients is generally much lower than what would be expected considering its pathology, as the TB clinical spectrum is a consequence of interactions between host, environmental, and pathogen factors. [7]–[10]

One of Mtb virulence key mechanisms is its ability to subvert the host immune response. Contrary to many other pathogens who avoid the host immune system, the Mtb has a vast number of hyperconserved human T cell epitopes, suggesting an immune subversion strategy where the host immune response benefits the pathogen by enhancing its transmission. Moreover, Mtb is able to infect and multiply in human macrophages, and to effectively avoid complete elimination by the host immune system. [7]–[9]

Mtb is a slow-growing, acid-fast[2] mycobacteria with the genetic potential to synthetize every essential amino acid, vitamin, and co-factor, and a disproportional number of lipid metabolic pathways. Furthermore, despite being an obligate aerobe, Mtb has the ability to survive in anaerobic conditions. Mtb's expanded metabolic capacity is a distinctive characteristic comparing to most obliged pathogens which need the host to fulfil their metabolic needs and explains the Mtb formidable ability to metabolize xenobiotics, which halts drug development. [9], [10]

The Mtb cell wall is the primary host-pathogen interaction spot, a major determinant of the bacillus durability and robustness, the target of many current antimycobacterial drugs, and an impermeability barrier. The Mtb cell envelop includes a large number of efflux pumps, and is several times less permeable to chemotherapeutic agents compared with other bacterial cell walls, causing a natural high innate resistance and a major hindrance to antitubercular (anti-TB) drug development. [4], [9]

Additionally, Mtb has shown the ability to reside inside the host during long periods of time on a latent, non-replicative condition. In this condition, the host has a latent tuberculosis infection (LTBI), and although they remain asymptomatic, the infection has the potential to reactivate in a later stage, when the host is immunocompromised. Although it is still not fully understood how Mtb alternates between its latent and active state, latency is believed to be induced by multiple host tissue growth-limitation factors. This state is characterized by a distinctive metabolism, where ribosomal functions and aerobic respiration decrease, and lipid metabolism increases, with triacyclglycerols being the Mtb main energy reservoir. Furthermore, Mtb also uses mycolic glycolipids, the cell wall immunostimulatory components, as an energy source during latency, in a process that simultaneously decreases the host immune response, provides energy and accumulates intermediaries required when the bacterium re-enters the cell cycle. [9]–[12]

[2] Acid fastness is the physical property that gives a bacterium the ability to resist decolorization by acids during staining procedures. Acid-fast bacilli generally have thick cell walls, rich in lipids.

I. 3. Physiopathology

TB is spread through aerial transmission of droplet nuclei[3] containing viable Mtb bacteria produced by individuals with active tuberculosis (ATB), and expelled via coughing, talking, sneezing, or singing. Droplet nuclei can remain suspended in the air for several hours, and if an individual inhales air containing these small particles, infection may occur. [13]–[15]

In order to infect a new host, Mtb must surpass several physical and chemical barriers on the upper respiratory airways that effectively clear 99% of inhaled Mtb, such as the secretion of mucus, enzymes, and inflammatory mediators. Infection occurs most frequently when small droplets reach the pulmonary alveoli [**Figure I.2 – Panel (1)**], and accordingly, pulmonary TB is the most frequent type of TB. [9], [13]–[15]

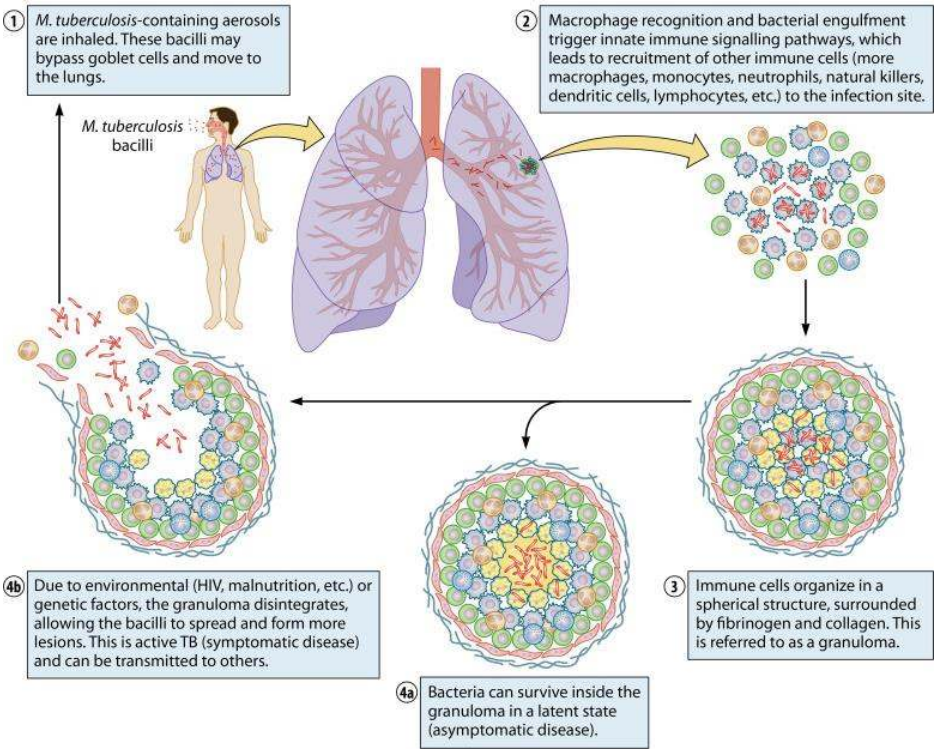

Figure I.2 | The pathophysiology of the *Mycobacterium tuberculosis* infection.
Reproduced from Luies, 2020. [15]

As Mtb bacilli reach the pulmonary alveoli, host innate immune cells, such as dendritic cells, macrophages, neutrophils, and monocytes, quickly phagocyte the bacilli in the host's first line of defense. Although the innate immune system can effectively control most bacterial infections, Mtb has the ability to subvert the host response and chronically infect immune cells, which frequently become Mtb bacilli replication niches. [**Figure I.2 – Panel (2)**] [15]–[19]

Macrophages are the first immune cells encountered by Mtb and are the primary replicative niche in human hosts. Mtb recognition by macrophages induce phagocytose and bacilli sequestrum in phagosomes, which typically eradicate pathogens through a tightly controlled process called phagosomal maturation, characterized by the

[3] Droplet nuclei are aerosols formed from the evaporation of respiratory droplets and are the vehicle for airborne respiratory disease transmission.

phagosomal fusion with lysosomes, and consequent phagolysosome formation. Nevertheless, some Mtb bacilli can inhibit this process, and avoid the hostile phagolysosome environment characterized by a very acidic pH and high concentrations of reactive oxygen species (ROS) and toxic peptides. By doing so, the bacilli have a chance to survive and replicate in the phagosome, by expressing stress adaptation genes who counter the nitrosative, oxidative phagosomal environment scarce in oxygen and nutrients, and consequently establish a chronic infection in the macrophages. [15]–[17], [19], [20]

Mtb bacteria have developed several mechanisms to avoid the host immune response to survive for long periods of time. The Mtb key pathogenic strategy is to inhibit macrophage apoptosis, as this process isolates Mtb bacilli in degradation vesicles and recruits the host adaptative immune response, and therefore is a key host strategy to limit the infection. Simultaneously, Mtb induces macrophages necrosis, as this type of cell death allows the viable Mtb bacilli to be released into the intracellular fluid and therefore disseminate the bacteria to nearby cells, creating secondary infection loci. The infected alveolar macrophages also have an important role in the mycobacterial dissemination by migrating within the lungs and recruiting additional phagocytic cells that exert immune pressure on the Mtb. This process, crucial to the adaptative immune response initiation, results on the formation of the granuloma, the histopathologic hallmark of TB infection. [15], [16], [19], [21]

The granuloma is a highly complex, dynamic, and heterogeneous structure who sequesters Mtb and limits its replication and dissemination, but also develops into the bacilli long-term survival niche. This structure is composed by a central core comprised of Mtb-infected and non-infected macrophages, in different maturation and differentiation states, accompanied by other phagocytic cells, surrounded by T-cells and B-cells. Granulomas can be derived from an individual Mtb bacillus and can vary immensely in the same or in between hosts on their cellular composition, oxygenation levels, inflammatory milieu, and bacterial burden. However, all granulomas have a highly drug selectivity that limit anti-TB drug efficacy, and an extremely hypoxic and nutrient-starved environment. [**Figure I.2 – Panel (3)**] [9], [13], [15], [19], [20]

In the granuloma's stressful environment, the bacilli enter a persistent, quiescent state that can be maintained for several decades, undetected by the immune system. This state is characterized by a remodelled physiology, a decreased metabolic rate, and a diminished growth rate, that create a higher drug tolerance to antibiotic treatment. Additionally, Mtb imprisonment in the granuloma and the non-vascularized location of granulomas further render Mtb bacilli inaccessible and recalcitrant to antibiotic treatment. [17], [18], [21], [22]

In immunocompetent individuals, the bacilli dissemination is contained in the granulomas in its quiescent state in a few weeks, and the patient is said to have latent tuberculosis. [**Figure I.2 – Panel (4a)**] An individual with LTBI has an infection with viable Mtb, but it has no symptoms, and cannot spread Mtb to other people. However, they might need preventive treatment to avoid TB development. LTBI is a highly heterogeneous condition, manifesting as a complex spectrum of different physiologic and metabolic Mtb subpopulations in each host. It is estimated that without preventive treatment, 5 to 10% of LTBI patients will develop ATB in their lifetime. [1], [5], [14], [15]

TB is a highly heterogeneous disease with a complex spectra of infection pathophysiology, ranging from a LTBI to an ATB, passing through incipient TB[4] and subclinical TB infection[5]. The progression of TB is not always linear, and it depends highly on genetic and phenotypic bacterial variation, the host immune system, as well as interactions between host and bacteria. [5], [19], [21]

ATB emerges when the host immune system can not contain the bacilli growth, normally 1 to 2 years after Mtb infection, on patients with a weak or supressed immune system, due to physiologic or pathologic factors. In an immunocompromised host, the granulomas liquify and expand, resulting in the release of viable bacilli from the degraded granuloma to re-infect pulmonary tissue. The granuloma loss of structural integrity and extensive inflammation results in cavity formation and substantial tissue damage, which enhance the release of Mtb bacilli to the respiratory airways, enabling Mtb-containing droplets release and consequent transmission. [**Figure I.2 – Panel (4b)**] [13]–[15], [17], [18], [20]–[22]

Individuals with ATB present symptoms that may include chest pains, chronic coughing, haemoptysis, fatigue, sustained weight loss, wasting, loss of appetite, chills, fever, and nocturnal sweats. ATB patients may spread Mtb to other people, and have abnormal chest radiograph, or a positive sputum smear or culture. Untreated ATB has a fatality rate over 70%, and therefore it is crucial for ATB patients to receive anti-TB therapy. [14], [23]–[25]

[4] An incipient TB infection is an infection by viable Mtb that will likely progress to ATB in absence of external therapeutical intervention, but that is yet to induce clinical TB symptoms, radiographic abnormalities, or microbiological evidence consistent with ATB.
[5] A subclinical TB infection is an infection by viable Mtb that is yet to cause clinical TB symptoms but has already induced other abnormalities detected in radiologic or microbiological assays.

I. 4. Current pharmacological TB control tools

I. 4. 1. Active Tuberculosis

Anti-TB therapeutic regimes date as early as the 1940s and have three main goals: decrease disease severity by reducing active Mtb bacilli in patients; eliminating all bacilli populations in the host to prevent relapses; and prevent drug resistance development. As anti-TB drugs work by decreasing drug-susceptible (DS) bacilli, long exposition to anti-TB drugs may lead to the enrichment of drug-resistant (DR) bacteria in the host, and therefore lead to the emergence of DR-Mtb strains, in a process of secondary resistance. Similarly to DS-Mtb strains, DR-Mtb strains can also be transmitted to new hosts, in a process of primary resistance. Thereby, patients can be infected by DR-Mtb strains (primary resistance) and accumulate resistance-inducing mutations (secondary resistance), leading ultimately to the development of strains resistant to all anti-TB drugs. [6], [12], [20], [26]–[28]

In order to achieve complete sterilization and avoid relapses, DS-TB therapeutic regimens must prevent the growth of dormant bacilli and are therefore very lengthy. Current therapeutic regimens for DS-TB include an initial intensive 2-month daily combination of four first-line drugs [rifampicin, isoniazid, ethambutol, and pyrazinamide (PZA)], and a following 4-month dual regime comprising rifampicin and isoniazid. The chemical structure, MIC's, and mechanism of action and resistance are summarized in **Table I.1**. [6], [28], [29]

WHO has defined multidrug-resistant tuberculosis (MDR-TB) as TB resistant to at least isoniazid and rifampicin, when DS-TB therapy becomes unlikely to cure the disease and a switch in the therapeutical regimen is recommended. MDR-TB risk factors include exposure to anti-TB drugs, intravenous drug users, and individuals at high risk for exposure to or infection with Mtb. [6], [26]

MDR-TB burden has increased in recent years due to lack of patient compliance in DS-TB treatment regimens, inadequate prescription, inefficient therapy due to late identification of drug resistance, or lack of psychosocial and financial support. MDR-TB is mainly distributed by primary transmission, and it is associated with higher mortalities and lower treatment success, fixated in 59% in the most recent WHO data, following a slow increasing trend; and in 2020, over 150 000 patients were diagnosed with MDR-TB and began therapeutic regimens. MDR-TB is currently a main barrier on a successful TB control, due to the reduced efficacy and the enhanced duration, toxicity, and costs of MDR-TB treatment. [6], [20], [26], [30]

MDR-TB therapeutic regimens are longer and more complex, require drugs that are more toxic, expensive, and less well-tolerated, and vary according to many factors, such as drug availability, drug susceptibility, and patient's age, medical history, disease severity and preference. Conventional regimens requirements and WHO recommended drugs for MDR-TB treatment are presented in **Figure I.3** and the chemical structure, mechanism of action, MIC's, and mechanism of resistance of said drugs are summarized in **Table I.2**. [26], [28], [31]

Due to MDR-TB therapeutic regimens issues, new approaches are urgently required. Following the approvals of new drugs with high therapeutic potential in the last

Table I.1 | Mechanisms of resistance and therapeutic action of drugs used to treat DS-TB. [27]–[29], [32].

Drug	Rifampicin	Isoniazid	Ethambutol	Pyrazinamide
Discovery Year	1966	1952	1961	1952
Action	Antimycobacterial (in replicant and dormant Mtb)	Antimycobacterial (in replicant and dormant Mtb)	Antimycobacterial (in replicant Mtb); Delays resistance to other regimen drugs	Antimycobacterial (in Mtb in acidic environments, e.g., granulomas)
Structure	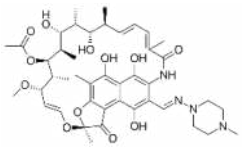	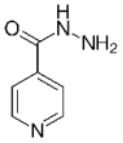	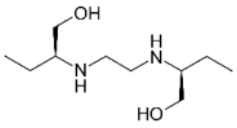	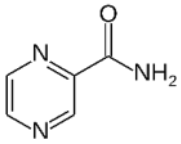
MIC (µg/mL)	0.05 – 1	0.02 – 2	1 – 5	16 – 50
Molecular Target	RNA polymerase β-subunit	NADH-dependent enoyl-acyl carrier protein reductase (after activation by catalase-peroxidase)	Arabinosyl transferase	aspartate decarboxylase (after activation by pyrazinamidase)
Mechanism of anti-TB action	RNA synthesis inhibition	Cell wall mycolic acid biosynthesis inhibition	Cell wall arabinogalactan biosynthesis inhibition	Coenzyme A synthesis inhibition Membrane energy depletion
Genes involved with resistance [Mutation Frequency, %]	rpoB [95-96]	katG [50-95] inhA [8-43]	embB [47-65]	pncA [72-99]
Gene product	RNA polymerase β-subunit	Catalase-peroxidase; NADH-dependent enoyl-acyl carrier protein reductase	Mycobacterial arabinosyl transferase	Pyrazinamidase
Cross-resistance[6]	Other rifamycins	Ethionamide	none	Rifampicin
Compensatory mutations[7]	rpoA rpoC	oxyR' ahpC	unknown	unknown

decade, e.g. bedaquiline (BDQ) and delamanid (DLM); MDR-TB therapeutic regimens are expected to become all-oral, and increase their tolerance, compliance, and success rate. [8], [26], [31].

WHO has defined extensively drug-resistant tuberculosis (XDR-TB) as MDR-TB that is also resistant to fluoroquinolones and second-line injectable drugs, indicating the probable failure of the standardized second-line therapeutic regimen. XDR-TB results from failures in the identification and treatment of MDR-TB patients. XDR-TB is mainly distributed by primary transmission, and it is associated with higher mortalities, estimated to be around 60%; and lower treatment success, averaging 14%. [6], [20], [28]

[6] Cross-resistance is a process where an organism develops resistance to several substances that have a similar mechanism of action by exposition to just one of those substances.
[7] Compensatory mutations are mutations that correct a loss of fitness due to earlier mutations. These are essential to reinstall DR-Mtb strain's fitness and their transmissibility.

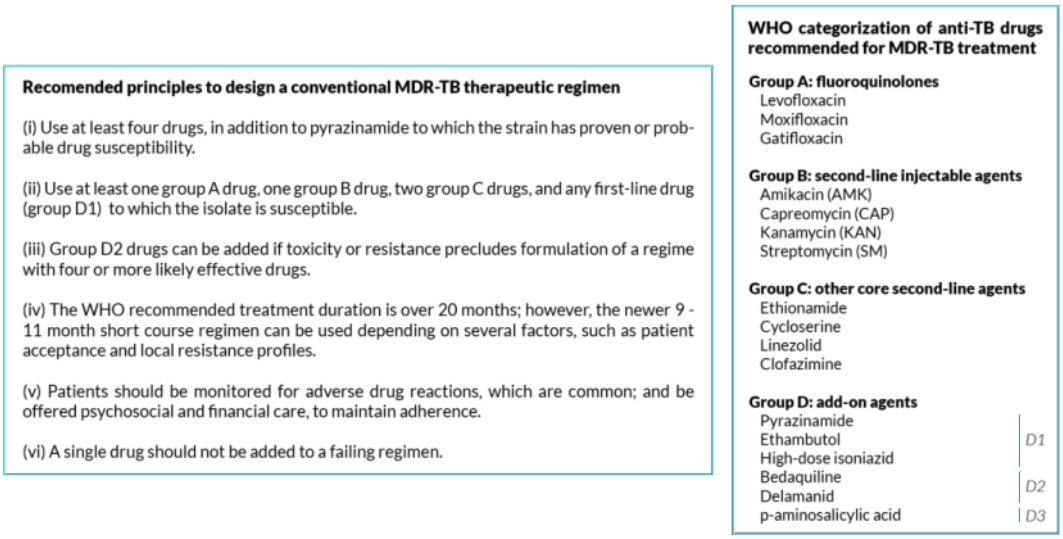

Figure I.3 | **WHO's conventional MDR-TB regimen requirements**
Recommended principals to design a conventional MDR-TB therapeutic regimen (left panel), and WHO categorization of anti-TB drugs recommended for MDR-TB treatment. Adapted from [6], [26]

XDR-TB management requires better resources and enhanced financial support, and XDR-TB patients have limited therapeutic options, with no standard treatment. Therapeutic regimens should include four or more drugs to which the strain has confirmed susceptibility, during 18 to 24 months. XDR-TB therapeutic regimens are linked to high levels of toxic adverse effects; and therefore, these patients should be closely monitored during treatments. [20], [26], [33]

The introduction of new drugs, such as BDQ and DLM (or analogous drugs), and repurposed drugs, such as linezolid, in XDR-TB therapeutic regimens have increased treatment success rates; and a short, all oral therapeutic regimen comprising these drugs is currently being evaluated, showcasing promising results with increased efficiency and decreased toxicity. [26], [27], [33]

Mismanagement during XDR-TB treatment leads to total drug-resistant tuberculosis (TDR-TB), defined as TB resistance to all drugs available for drug susceptibility testing. TDR-TB is virtually incurable, and has a mortality superior to XDR-TB, presenting itself as a serious public health threat. TDR-TB patients do not have efficient therapeutic options, and therefore may benefit from novel drug's clinical trials or surgical interventions (typically elective partial lung resection). [20], [26], [28]

Although anti-TB therapy has shown a marked improvement in the last decades, current anti-TB therapeutic regimens still have long durations, a high pill burden, and long-term cumulative adverse effects that lead to low patient compliance and acceptance, that consequently result on higher levels of treatment failures and emergence of resistance, that ultimately resulted in programmatically incurable forms of TB. Thus, the development of a potent, short, and cheap anti-TB regimen, well-tolerated and efficient in treating all forms of TB, with minimal adverse effects and a low pill burden should be a priority in TB control. To achieve this goal, the development of new drugs active against DR-Mtb strains is urgent, preferably with activity in new, unexplored targets and pathways which are not predisposed to resistance. This will allow the decrease in anti-TB therapeutic regimens' duration and minimize drug resistance emergence. [29], [34]–[38]

Table I.2 | Mechanisms of resistance and therapeutic action of drugs used to treat MDR-TB. [20], [27], [28], [39]

Drug	Bedaquiline	Clofazimine	Cycloserine	Delamanid	Ethionamide	Fluoroquinolones	Linezolid	p-aminosalicylic acid	Second-line injectable agents[8]
Active against	Replicant and dormant Mtb	Replicant and dormant Mtb	Replicant Mtb	Replicant and dormant Mtb	Replicant Mtb	Replicant and dormant Mtb	Replicant Mtb	Replicant Mtb	Replicant Mtb
Structure	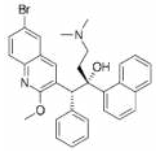	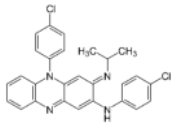	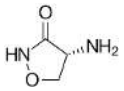	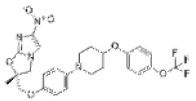	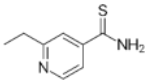	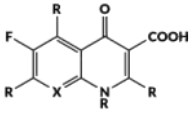	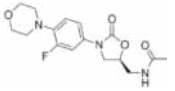	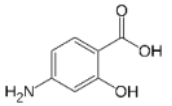	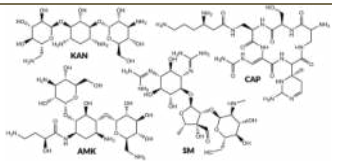
MIC (µg/mL)	0.03 – 1	0.1 – 1.2	8 – 32	0.006 – 0.24	2.5 – 25	0.5 – 2.5	0.25 – 0.5	1 – 8	2 – 8
Molecular Target	ATPsynthase	unknown	unknown	unknown (activated by deazaflavin-dependent-nitro-reductase)	NADH-dependent enoyl-acyl carrier protein reductase (activated by monooxigenase)	DNAgyrase	50S ribosomal L3 protein	Dihydropteroate synthase (activated by dihydrofolate synthase)	16S rRNA ribosomal protein S12
Mechanism of anti-TB action	Cell respiration inhibition	ROS toxicity	Cell wall peptidoglycan biosynthesis inhibition	Cell wall mycolic acid biosynthesis inhibition; Cell respiration inhibition	Cell wall mycolic acid biosynthesis inhibition	Transcription inhibition	Protein synthesis inhibition	Folic acid and thymine metabolism inhibition	Protein synthesis inhibition
Genes involved with resistance [Mutation Frequency, %]	atpE; Rv0678	Rv0678	alrA; cycA	ddn; fgd1	ethR; ethA; inhA	gyrA [90]; gyrB [10-15]	rplC [90]; rrl [1.9-11]	thyA [40]; folC; ribD [90]	rrs [60-70]; rpsL [SM, 6]; tlyA [CAP, 3]
Gene product	ATP synthase sununit C; Transcriptional regulator MmpR5	Transcriptional regulator MmpR5	D-alanine racemase; D-alanine cellular transporter	Deazaflavin-dependent nitro-reductase; F420-dependent glucose-6-phosphate dehydrogenase	ethA transcriptional regulator; Monooxigenase; NADH-dependent enoyl-acyl carrier protein reductase	DNAgyrase	50S ribosomal L3 protein; 23S ribosomal RNA	thymidylate synthase A; dihydrofolate synthase; riboflavin biosynthesis protein	16S rRNA; ribosomal protein S12; rRNA methyltransferase
Cross-resistance	Clofazimine	Bedaquiline	none	none	Isoniazid	Fluoroquinolones	none	none	Second-line injectable agents

[8] Includes kanamycin (KAN), amikacin (AMK), capreomycin (CAP), and streptomycin (SM)

I. 4. 2. Latent Tuberculosis

As stated previously, one of the biggest obstacles in TB eradication is the Mtb's ability to remain in a latent, non-replicative state inside an infected host during multiple decades. Patients with this condition (LTBI) are asymptomatic and have a 10% chance of progressing to ATB. In recent years, despite the progressive decrease in ATB cases, especially in high-income countries, LTBI incidence remained stable. As most new ATB cases result from reactivation of LTBI patients, the intensification of LTBI diagnosis and treatment is currently recognized as an essential requirement to a successful TB control, and to prevent disease transmission. [11], [40], [41]

Most approved anti-TB drugs target cellular processes in replicant cells, as cell wall synthesis and transcription; and thus, these drugs have a low efficiency against LTBI due to the metabolic and physiologic changes the mycobacteria present in this state. Nevertheless, and in the absence of better options, current LTBI treatment is based on prolonged administration of approved anti-TB drugs. For this reason, LTBI therapy is associated with significant adverse effects and as most patients are asymptomatic, treatment conclusion rates are significantly low, not surpassing 30%. [11]

WHO recommends four alternative therapeutic regimens for LTBI: daily isoniazid for 6 to 9 months, daily rifampicin for 4 months, daily isoniazid and rifampicin for 3 months, or weekly isoniazid and rifapentine[9] for 12 weeks. The isoniazid monotherapy is the oldest and most commonly used regimen and has a 90% efficiency in preventing progression from LTBI to ATB. Its main advantages are the considerable clinical experience with isoniazid, and its low cost. Nevertheless, this regimen is associated with high hepatotoxicity, which led to the need to develop alternative regimens. Therapeutic regimens based on rifamycins (rifampicin and rifapentine) have shown identical efficacy to the daily isoniazid regimen. These regimens are associated with lower hepatotoxicity and higher completion rates, and their use have been increasing over the last few years. Recently, the use of fluoroquinolones in patients with resistance to rifamycins have shown to be an effective and low-cost therapeutic regimen; and since then many TB control programs have adopted therapeutic regimens based in fluoroquinolones to treat LTBI with DR-Mtb. [6], [41]–[44]

The efficiency of current LTBI therapeutic regimens is hampered by the low compliance and low completion rates, namely due to the long treatment duration and adverse effects. There is therefore a need to develop alternative regimens that are shorter and safer, in order to achieve better compliance and be more easily widespread. For this reason, new vaccines, immune-based therapies, and new drug regimens for LTBI treatment are currently being evaluated and developed, aiming to simplify and shorten LTBI therapeutic regimens. [41], [42], [45]

Until more effective and safer LTBI therapeutic regimens are developed and implemented, the best strategy to prevent ATB continues to rely on massive testing of the population with high risk of developing TB, such as immunosuppressed patients, children under five, and recent contacts with active pulmonary TB. However, the systematic testing and LTBI treatment require a lot of investments, and are therefore

[9] Rifapentine is a rifamycin derivative with a longer half-life and increased potency.

difficult to implement in most high TB prevalence countries, as most available resources in these countries are used to control ATB cases. [41], [46]

Despite current efforts, around a quarter of the world's population is still estimated to be infected with LTBI, accounting for a huge reservoir of Mtb. Progression from LTBI to ATB constitute the main source of ATB in low-burden regions, and it is clear that is necessary to effectively address LTBI in order to successfully control TB. There is therefore, an urgent need to develop new and enhanced LTBI treatments, including functional treatments for patients infected with DR-Mtb strains. [29], [43]

I. 5. Electron Transport Chain

Mtb is an obligate aerobe, and thus, relies on oxidative phosphorylation (OxPhos) via the electron transport chain (ETC) to produce energy for growth and division. However, and unlike most bacteria, Mtb cannot use substrate-level phosphorylation to grow, probably due to the lack of a lactate dehydrogenase which limits an efficient fermentation process. Thereby, Mtb is dependent upon OxPhos for its viability. [47]–[51]

OxPhos is a bioenergetic pathway that generates ATP from the phosphorylation of ADP. During the OxPhos process, electrons are transferred from electron donors produced in the central metabolic pathways to molecular oxygen through the ETC. The energy released in this process is conserved by proton-pumping transmembrane proteins that establish a proton gradient and thus generate an electrochemical gradient, called proton motive force (PMF). [51]–[54]

The Mtb ETC is a highly conserved collection of membrane-bound and membrane-associated enzymes and co-factors. It is comprised by five main primary dehydrogenases, which fuel the ETC as electron donors; two main terminal oxidoreductases, which catalyse the transfer of electrons to terminal electron acceptor; and an ATPsynthase, that produces ATP through the dissipation of the PMF. In **Figure I.4**, a schematic representation of the Mtb ETC is presented. [47]–[49]

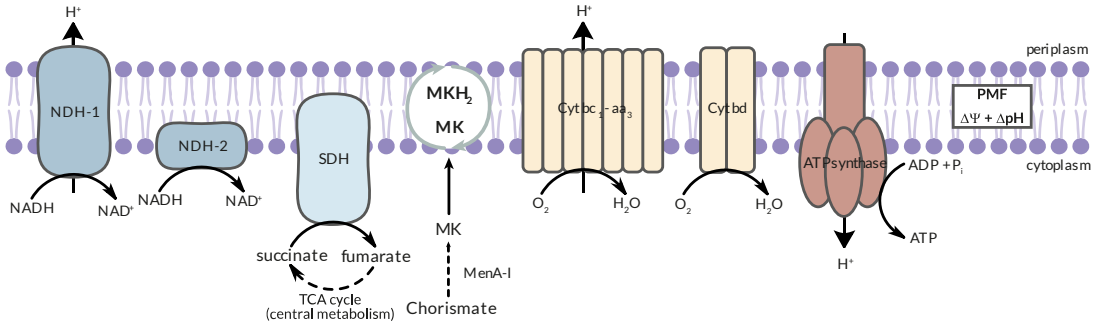

Figure I.4 | Schematic representation of the Mtb ETC

Within the Mtb ETC, membrane bound NADH dehydrogenases (NDHs) and succinate dehydrogenase (SDH) act as the primary electron feeders. Mtb has three NDHs: a proton-pumping type I NDH and two non-pumping type II NDHs. These three enzymes oxidize the NADH co-factor into NAD^+, using menaquinone (MK) as an electron acceptor. Mtb also contain two isoforms of SDH, SDH-1 and SDH-2. SDH oxidizes succinate to fumarate in the cytoplasm, using MK as an electron acceptor. Thus, SDH couples the tricarboxylic acid (TCA) cycle, part of the central metabolic pathway, with the ETC. [48], [54]–[56]

MK exists in a MK / menaquinol (MKH_2) redox pool, serving as an intermediary electron carrier to transport electrons from the primary dehydrogenases to the terminal oxidoreductases. MK is a membrane soluble lipoquinone synthesized from chorismate via a series of enzymes, MenA-I, and it is the sole electron transporter in the Mtb ETC. [49], [55]

The pool of reduced MKH_2 is oxidized by the terminal oxidases that transfer the electrons to oxygen molecules, reducing them to water. The Mtb ETC is branched, and thus MKH_2 electrons can be transferred to two aerobic terminal oxidases: the cyt bc_1-aa_3

complex and cyt bd. The cyt bc_1-aa_3 complex is active in normoxia conditions and it is energetically more efficient due to its proton-pumping capabilities, while the cyt bd is active in hypoxic and stress-inducing conditions and it is energetically less favourable. [48], [50], [57], [58]

The movement of electrons is coupled with proton pumping into the periplasm and use of protons from the cytoplasm, thus generating the proton and electrochemical gradient (PMF). The ATPsynthase then utilizes the PMF as a source of energy to drive the phosphorylation of ADP to ATP. [51], [55]–[57]

I. 5. 1. Cytochrome bc_1-aa_3

The Cytochrome bc_1-aa_3 supercomplex is an energy-efficient terminal oxidase that transfer electrons from MKH_2 to molecular oxygen, in the Mtb ETC. Cyt bc_1-aa_3 has proton-pumper activity, pumping four protons to the periplasm for every two electrons transferred from MKH_2. Moreover, for each two electrons used in the reduction of molecular oxygen to water, the enzyme consumes two cytoplasmatic protons and releases two protons to the periplasm. Additionally, the bc_1-aa_3 supercomplex is able to slowly degrade nitric oxide (NO). Cyt bc_1-aa_3 is a key enzyme to the generation and maintenance of the PMF, and to the consequent energy production. [48], [51], [53], [59], [60]

The Mtb Cyt bc_1-aa_3 supercomplex is comprised by two tightly associated protein complexes: a menaquinol-cytochrome c oxidoreductase, or cyt bc_1, analogous to the mitochondrial complex III, and an aa_3 oxidase, or cyt aa_3, analogous to the mitochondrial complex IV. This supercomplex precludes the necessity of a soluble or membrane-bound cyt C, and thus, instead, the Mtb cyt bc_1 has a QcrC subunit that functionally replaces cyt C in canonical ETC. The bc_1 complex has the proton-pumping activity and transfer the MKH_2 electrons to the cyt aa_3. The complex has two conformations: one in which has a direct electronic link to cyt aa_3 and another where interrupts the connection. Cyt aa_3 uses the electrons to reduce the oxygen molecules to water. [48], [51], [60], [61]

The bc_1-aa_3 supercomplex is energetically more favourable and thus, under normoxia and during exponential growth, acts as the primary terminal oxidase in Mtb. Unsurprisingly, this supercomplex is essential for mycobacterial growth and its inhibition results in growth arrest. Cyt bc_1-aa_3 has a tightly controlled expression and is inhibited by acidic mediums and lack of oxygen. However, cyt bc_1-aa_3 is not essential for cell survival and as long as the alternate cyt bd is expressed, bc_1-aa_3 inhibitors do not induce bactericidal effects. [48], [49], [54], [62], [63]

The central role of the bc_1-aa_3 complex in the ETC and the significant differences to the mammalian counterpart make the supercomplex a good therapeutical target. Moreover, cyt bc_1-aa_3 appears to be a promiscuous drug target and through high throughput screenings, many small molecules have been identified as cyt bc_1-aa_3 inhibitors, the majority targeting QcrB, a cyt bc_1 key component. QcrB inhibitors are typically high affinity antagonists, with very low toxicity. Cyt bc_1-aa_3 inhibition reduces proton pumping and consequently disrupt ATP production, increases the cytoplasmatic proton concentration, and blocks mycobacterial growth. Additionally, it upregulates Cyt bd oxidase, and increases oxygen consumption and respiration rates. [47], [49], [51], [64], [65]

Usually, cyt bc_1-aa_3 inhibitors target the catalytic domain and have structures analogous to MK or MKH_2. Imidazopyridine derivatives are prime examples that have shown to be particularly potent, the most prominent example being Q203 [discussed in **I. 6. 4**], an imidazopyridine amide which is currently in phase II clinical trials. Structurally similar to the imidazopyridines, a pyrazolopyridine carboxamide series were designed through a scaffold strategy, with the lead compound, TB-47 [discussed in **I. 6. 4**], currently in early-stage development. [48], [49], [51], [55]

Lansoprazole, a gastric proton-pump inhibitor, was found to be a potent hit compound in a screen of FDA-approved drugs. Lansoprazole acts as prodrug and is converted *in vivo* into lansoprazole sulphide, that was identified to be a QcrB inhibitor on a distinct site from the one targeted by imidazopyridines. Several other QcrB inhibitors drug classes have been reported and are reviewed elsewhere [49], [54]. In **Figure I.5**, the structure and MICs for selected QcrB inhibitors are presented. [47]–[51], [54], [64]

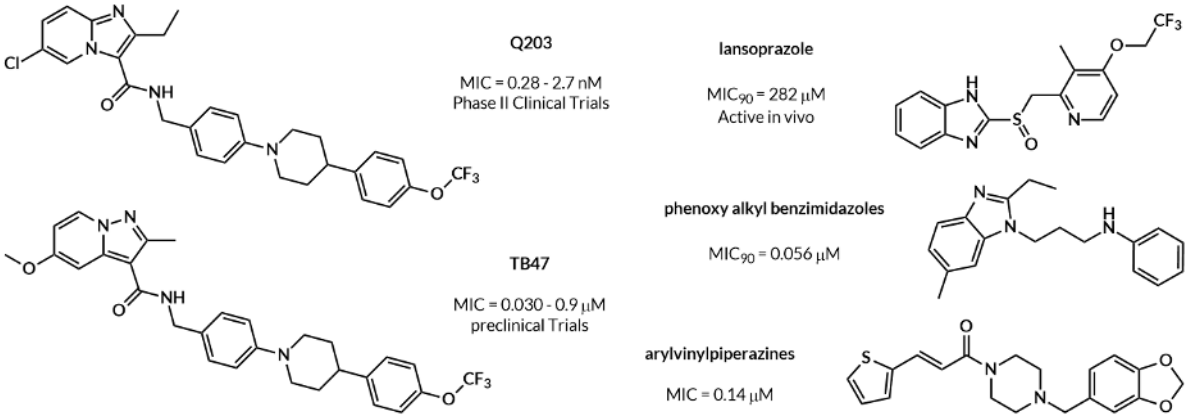

Figure I.5 | **Representative QcrB inhibitors** [49], [51], [64]

I. 5. 2. Cytochrome bd

Cytochrome bd-type menaquinol oxidase, or cyt bd, is a non-proton pumping, less energetically efficient terminal oxidase that transfer electrons from MKH_2 to molecular oxygen, in the Mtb ETC. Curiously, cyt bd catalyses the reaction without generating ROS species or protons. Instead, cyt bd generates PMF solely by transmembrane charge separation, by releasing the two protons from the MKH_2 oxidation into the periplasm and uptaking the two protons required to form a water molecule from the cytoplasm. Cyt bd is exclusive to prokaryotic ETC and unlike cyt bc_1-aa_3, the enzyme is more versatile, with multiple functions reported. [48], [51], [59], [66]

Cyt bd has a high affinity for oxygen, a quick dissociation rate with NO, and a peroxidase activity. The terminal oxidase is capable of detoxifying ROS and antibacterials, and protects the bacilli against hypoxia, cyanides, hydrogen peroxides, ammonia, nitrites, sulphides, chromates, NO, and antimycobacterials. Additionally, cyt bd has an oxygen-scavenger role. Cyt bd's expression is essential for growth under nitrosative, oxidative, and hypoxic stresses, where the enzyme is capable of compensating the inactivation of Cyt bc_1-aa_3. Cyt bd may also play a role into the Mtb's natural drug tolerance, namely to drugs that directly target the ETC. [47], [48], [59], [66]

Cyt bd was reported to be essential to resist the adaptive immune response, by being overexpressed and functioning as an alternative oxidase in conditions where cyt

bc_1-aa_3 is inhibited, such as during the acidification of the phagosome, in antibiotic-induced stresses, or in the chronic phase of infection, when the host immune system creates oxidative and nitrosative stresses to eliminate pathogens. Thus, cyt bd contributes to Mtb virulence, and since the enzyme is not encoded in animal genomes, it can serve as an attractive promising therapeutical target for new, selective anti-TB drugs. [49], [50], [56], [66], [67]

Sole inhibition of cyt bd does not have any antimycobacterial effects. However, cyt bd inhibitors have synergetic effects with isoniazid, quicken the bactericidal activity of ATPsynthase inhibitors, and turn QcrB inhibitors bactericidal. Thus, cyt bd inhibitors appear to be particularly attractive in combination therapy, namely in combination with cyt bc_1-aa_3 inhibitors, as the simultaneous inhibition of both terminal oxidases is highly bactericidal in a short period of time, and successful at killing both active and latent bacilli. The non-essentiality of cyt bd represents a challenge to identify its inhibitors, and thus not many cyt bd inhibitors are known. To this date, only few inhibitors were identified and only one, aurachin D, is characterized. In **Figure I.6,** aurachin D's chemical structure and MIC is presented. Aurachins are isoprenoid quinoline alkaloids, originally extracted from myxobacteria. Further development of aurachin D is complicated by its toxicity and lack of selectivity, but optimized derivatives of aurachin D have great potential as anti-TB drugs. [47]–[51], [55], [56], [66]–[68]

Aurachin D
(MIC_{90} = 85 μM)

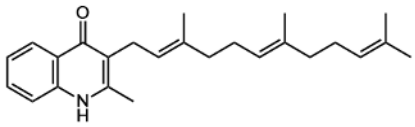

Figure I.6 | **Cyt bd inhibitors** [49], [51]**.**

I. 6. Targeting the ETC to control TB

Mycobacteria have adapted to rescue themselves under unfavourable conditions, such as normoxia, nutrient scarceness, and exposure to drugs, by reformulating their metabolism to conserve energy and evade the effects of drug treatments. A fundamental characteristic for this adaptation is the Mtb respiratory flexibility, that allows the bacilli to vary the ETC enzyme composition in response to environmental conditions. Adding the existence of human homologs to most ETC enzymes that hamper the development of selective inhibitors, and the presence of alternative enzymes that allow Mtb to reroute the electron flow and escape of inhibition, there was a lot of scepticism in the utility of targeting the ETC. [51], [52], [59]

Nevertheless, all living cells require a structure to maintain their integrity and the ability to generate energy to support growth and division. Hence, it is unsurprising that these systems must function efficiently for Mtb to be viable, thus making them vulnerable targets for the development of novel drugs. Additionally, the redundancy across the ETC is not universal and neither ATPsynthase nor the enzymes involved in the MK biosynthesis have any known homologues. With the discovery of BDQ, a selective ATPsynthase inhibitor, it became clear it was possible to specifically target mycobacterial components without affecting their mitochondrial counterparts, despite the high degree of conservation in the ETC. Furthermore, BDQ showed bactericidal activity against latent bacilli, where the existent, traditional chemotherapeutics could not. [47], [52], [57], [68]

After the success of BDQ, several research groups focused on targeting OxPhos for the discovery of novel anti-TB drugs and since then, the collection of OxPhos inhibitors expanded drastically. Currently, more than 30% of all new antimycobacterial drugs in clinical trials target the OxPhos, and more than 65% of Phase III trial regimens include a OxPhos inhibitor. **Table I.3** summarizes the structure, MIC, and molecular target for all OxPhos inhibitors currently approved and/or in clinical trials. [47], [51], [69]

The capability of several small molecules to specifically target energy production in Mtb has validated OxPhos as a viable drug target. This pathway is particularly promising for several reasons. First, since a sustained PMF and ATP homeostasis are essential for the viability of both active and latent Mtb bacilli, and as TB control requires the elimination of both replicant and non-replicant Mtb forms, drugs that target both latent and replicant bacilli are desirable as they allow the treatment of both ATB and LTBI. [47], [49], [51], [70]–[72]

Furthermore, the current anti-TB drugs limited efficiency against latent bacilli results on the need for current ATB therapeutic regimens to have long durations, which results in high adverse effects, low compliance, low completion rate, and emergence of resistance that hamper TB control. As the ATP intracellular concentration is five to six times lower in latent bacilli compared to active cells, latent bacteria are extremely sensitive to the further ATP depletion and thus, OxPhos inhibitors appear to be specifically active against these subpopulations. The development of specific anti-TB drugs that target latent bacilli is expected to reduce ATB treatment duration, avoid resistance emergence, and reduce LTBI treatment duration, which will further remove a great impair in the implementation of strategies that avoid the development of the active form of the disease. [72]–[75]

Table I.3 | Target and clinical statue of OxPhos inhibitors currently in clinical settings. [47], [49], [51], [57], [64]**.**

Drug	Drug Class	MIC	Target	Clinical Statue	Structure
Bedaquiline	diarylquinoline	MIC_{90} = 7.2– 24 nM	ATPsynthase PMF	Approved / Phase III	**Figure I.7**
TBAJ-587	diarylquinoline	MIC = 4.9 nM	ATPsynthase	Phase I	**Figure I.7**
TBAJ-876	diarylquinoline	MIC_{90} = 6.0 nM	ATPsynthase	Phase I	**Figure I.7**
squaramide derivative		MIC_{90} = 0.5 μM	ATPsynthase	Pre-clinical	**Figure I.7**
Pyrazinamide	carboxamide	MIC = 0.13 – 0.4 mM	Coenzyme A synthesis PMF	Approved	**Figure I.8**
SQ109	ethylenediamine	MIC_{90} = 2.4 μM	cell wall biosynthesis menaquinone synthesis, PMF	Phase IIb/III	**Figure I.8**
Nitazoxanide	thiazolide	MIC_{90} = 9.8 μM	Host immune response PMF	Phase II	**Figure I.8**
Clofazimine	riminophenazine	MIC = 0.5 μM	ROS toxicity (via NDH-2)	Approved / Phase III	**Figure I.9**
TBI-166	riminophenazine	MIC = 0.12 μM	ROS toxicity (via NDH-2)	Phase I	**Figure I.9**
Q203	imidazopyridine	MIC = 0.28 – 2.7 nM	cyt bc_1-aa_3	Phase II	**Figure I.5**
TB47	pyrazolopyridine	MIC = 0.03 – 0.9 μM	cyt bc_1-aa_3	Pre-clinical	**Figure I.5**
Delamanid	nitroimidazole	MIC = 0.9 - 5.6 nM	mycolic acid synthesis NO toxicity	Approved / Phase III	**Figure I.10**
Pretomanid	nitroimidazole	MIC = 0.042 - 0.7 μM	mycolic acid synthesis NO toxicity	Approved / Phase III	**Figure I.10**

Additionally, as drug efflux pumps depend on chemical energy to actively transport drugs out of the bacterial cell, perturbations on the PMF and ATP levels should also interfere with their function. As efflux pumps remove xenobiotics from the cell, they play a significant role in the development of resistance and thus, the OxPhos inhibition may also indirectly aid in overcoming efflux-pump mediated drug resistance. [49], [70]–[72]

Simultaneous administration of several drugs is the cornerstone of TB treatment. Combination strategies increase efficacy and reduce treatment timelines and thus improve patient compliance, limit side-effects, reduce costs, delay the emergence of resistance, and enhance cure rates. Thus, when developing novel anti-TB, it is essential to evaluate their effects when administration in combination with existent drugs. Bioenergetic inhibitors are synergetic with each other and expectably, targeting multiple steps of the OxPhos pathway has proven to be a better strategy for tackling both DS- and DR-TB. [47], [51], [68], [69]

I. 6. 1. Targeting the ATPsynthase: BDQ and derivatives

Bedaquiline [**Figure I.7**] is the prototypical inhibitor of OxPhos by inhibition of the ATPsynthase. BDQ is a first-in-line diarylquinoline that was discovered by chemical optimization of a hit compound identified from a screening of over 70 000 compounds against *M. smegmatis*, and it was approved by the FDA in 2012, becoming the first approved drug specifically for TB in more than 40 years. Currently, BDQ is conditionally administrated for the MDR-TB treatment. [47], [55], [76]

BDQ is a potent bactericidal, efficacious against MDR- and latent Mtb bacilli. In clinical trials, BDQ demonstrated accelerated sterilizing activity, being able to reduce DS-TB treatment in two months. Additionally, when added to standard combination therapy, BDQ has shown to reduce treatment time, decrease mortality, and prevent further resistance of MDR-TB. BDQ is now a component of multiple regimens in phase II and III clinical trials and the most represented drug in novel therapeutic regimens. [47], [55], [76]

BDQ activity is proposed to work through binding to two subunits on the ATPsynthase, thus inhibiting ATP synthesis. Additionally, BDQ is capable of acting as a protonophore [discussed further in **I. 6. 2**], leading to the uncoupling of the ETC via collapse of the PMF. Inhibition by BDQ depletes intracellular ATP levels, activates respiration, and induces a metabolic remodelling that upregulates ATPsynthase, NDH-2 and cyt bd. Moreover, through a broken feedback loop to try to maintain ATP levels, BDQ accelerates the central metabolism and downregulates efflux pump expression and biomass generating processes, leading to an increased $NADH/NAD^+$ ratio. Interestingly, the bacterial activity of BDQ is delayed, i.e., does not occur immediately upon the ATP depletion, explained by the metabolic remodelling Mtb experiences upon BDQ exposure [47], [51], [56], [76]

Not only BDQ is highly efficacious, it is also suggested to be more effective in latent bacteria than in replicant ones. Additionally, BDQ is highly selective with a MIC_{50} ratio between the mitochondrial and mycobacterial ATPsynthase higher than 20 000, validating the ATPsynthase as a target for the development of selective anti-TB drugs. BDQ was also shown to be synergistic with anti-TB drugs that target the cell wall biosynthesis inhibitors, probably due to increased cellular penetration, and OxPhos, due to a more efficient bioenergetics inhibition. [51], [76]

Despite all, BDQ's use is limited by some pharmacological and toxicological liabilities, such as its poor aqueous solubility (< 5 mg/mL) and it being extensively protein bound (>99.9%). Moreover, BDQ is exceptionally lipophilic (cLogP = 7.25), which contributes to its long terminal half-life (24h) due to accumulation within tissues. Additionally, BDQ interacts with cyt P450 inhibitors and inducers and has cardiac toxicity, raising concerns regarding co-administration of BDQ with other anti-TB drugs, e.g. fluoroquinolones. [55], [76]

The toxicity associated with BDQ and the emergence of BDQ-resistant Mtb strains restrain the use of BDQ to MDR- and XDR-TB patients. Thus, to address its shortcomings, a medicinal chemistry approach was conducted to study the chemical space of diarylquinolines to find the next generation equivalents with superior safety profiles. In this context, two 3,5-diakoxy-4-pyridyl derivatives, TBAJ-587 and TBAJ-876 [**Figure I.7**], showed to be particularly interesting and are currently in Phase I clinical trials. [49], [51], [54], [55], [76]

These second-generation diarylquinolines shown to inhibit the ATP synthesis by binding to ATPsynthase in the same sites than BDQ. Additionally, this compounds showed a reduction in lipophilicity, higher clearence, less cardiotoxicity, and retention of BDQ's potent activity. Interestingly, these compounds do not have uncoupler abilities, suggesting this property may not be essential for BDQ's activity. [49], [54], [76]

Additionally, a number of recent studies have identified new ATPsynthase inhibitors with novel mechanisms of action. A family of squaramide derivatives showed to be particularly interesting, with its lead compound [**Figure I.7**] currently being evaluated on pre-clinical trials. These compounds target ATPsynthase through a different binding site, meaning they do not show cross-resistance to BDQ, and have shown to be active against BDQ-resistant strains. [47], [51], [56]

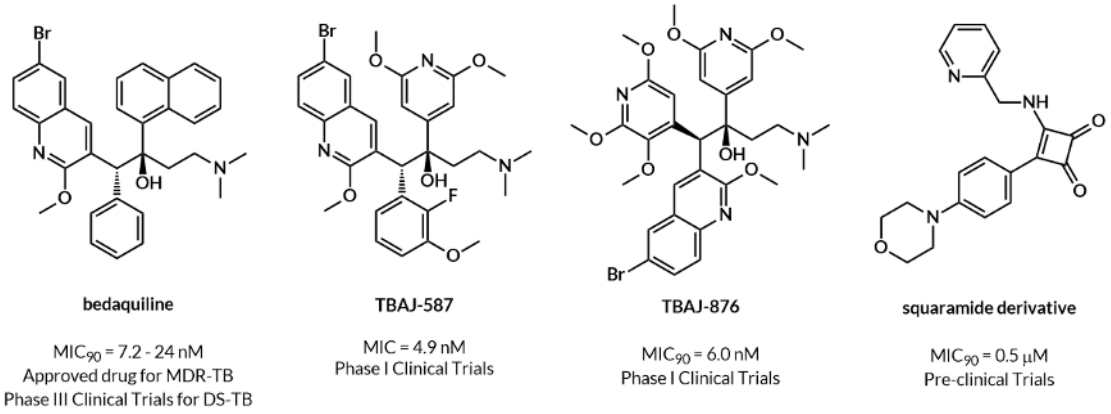

Figure I.7 | **ATPsynthase inhibitors currently in clinical settings** [49], [51]**.**

I. 6. 2. Targeting the PMF: PZA, SQ109 and NTZ

The PMF consists of an electrical potential due to charge separation across the membrane and a chemical potential of protons. The generation and maintenance of a PMF is essential for the Mtb energy production and consequent bacterial growth and survival, in every metabolic state. The importance of PMF as a drug target is further validated by the observation that dissipation of the PMF leads to death in hypoxic conditions, and the dependence of efflux pumps in PMF [49], [51], [57]

PMF uncouplers generally act as protonophores and uncouple OxPhos from the ETC, thus inhibit ATP synthesis, leading to cell death. Protonophores are generally lipophilic weak acids that transport protons through the membrane, thus balancing the proton and electric gradient that constitute the PMF. Their lipophilic nature makes their movement across the cellular membrane easy, and their weak acidity allows them to partake in a repeating cycle of protonation in the periplasm and deprotonation on the cytoplasm. This activity dissipates the PMF uncoupled from ATP synthesis, which is lethal in Mtb. [53]

Generally, PMF uncouplers are not sufficiently selective to be used as antimycobacterial agents and thus, the development of specific PMF uncouplers remains an area of interest. However, there are some examples of anti-TB drugs in clinical use that act as PMF uncouplers in addition to an alternative mode of action, such as BDQ [**Figure I.7**], PZA, SQ109 and nitazoxanide (NTZ), showcased in **Figure I.8**. [51], [53]

Pyrazinamide is a pro-drug discovered in the early 1940s, and currently used as a first-line anti-TB drug. PZA is hydrolysed in acidic conditions by pyrazinamidase to pyrazinoic acid, the drug's active form. Although PZA's mechanism of action is not still fully understood, current knowledge is that PZA acts as a multitarget drug that dissipates

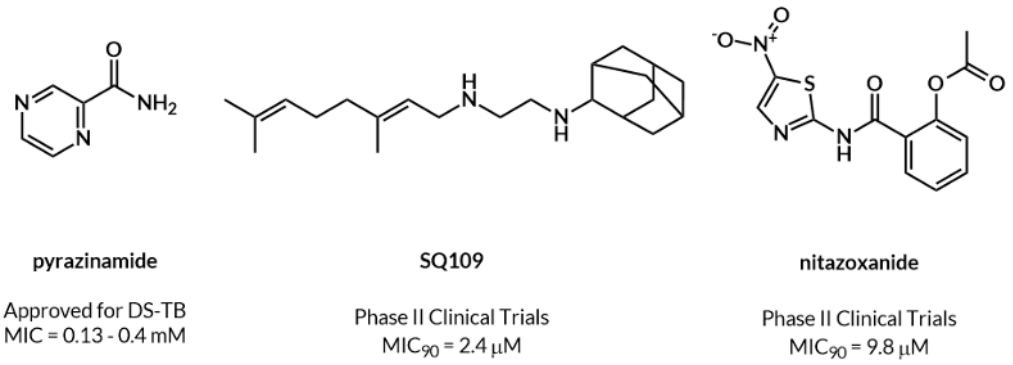

Figure I.8 | **PMF uncouplers currently in clinical settings** [49], [51], [64]

the PMF, inhibits ATP synthesis, inhibits membrane transport, and reduces the activity of other proteins, such as aspartate decarboxylase, a protein involved in the Coenzyme A biosynthetic pathway. Evidence of PZA's uncoupling activity first arise with its ability to target latent bacilli, contrary to all other first-line anti-TB drugs that target biomass producing pathways. Moreover, PZA has shown to be more active in latent bacilli than in active bacilli, and as PZA requires acidic pH for its activity, it is more active in the granuloma acidic environment. Additionally, PZA showed to synergize with other PMF uncouplers to deplete ATP depletion and enhance mycobacterial killing, implying its anti-TB activity relies substantially on its uncoupling activity. [49], [51]

SQ109 is an adamantane-based anti-TB drug, structurally related to the first-line drug ethambutol. It has successfully completed phase II clinical trials, and is active against DS-, MDR-, and XDR-TB. Furthermore, its activity is only mildly attenuated under hypoxic or nutrient-starved conditions. Initially, SQ109 was reported to interfere with the assembly of mycolic acids in the mycobacterial cell wall through inhibition of membrane transporter MmpL3, but it is currently considered that this is not the primary target of SQ109. Recently, it was demonstrated that SQ109 interferes with respiration, through inhibition of MK biosynthetic pathway enzymes, MenA and MenG, and the ability to act as protonophore and dissipate the PMF. Although SQ109 monotherapy for 14 days does not reduce bacteria burden, addition of SQ109 to the combinations regimens highly increases their efficiency. Notably, SQ109 shows synergy with BDQ and clofazimine (CFZ), further suggesting the OxPhos is a SQ109's important target. and does not have any observed resistant mutants, likely due to its ability to inhibit multiple targets. [47], [51], [55]

Nitazoxanide is an FDA-approved repurposed drug with broad-spectrum antiparasitic and antiviral activity. NTZ is a pro-drug that is deacetylated in the gastrointestinal tract to tizoxanide, which is believed to be the active form. NTZ has an associated low cost and an excellent safety profile, and is available as an oral drug, making it an attractive and easily accessible treatment. NTZ is proposed to promote Mtb killing by enhancing autophagy through the inhibition of the human mTORC1, and additionally disrupt the PMF, through activity as a protonophore. Furthermore, the nitro group was shown to be essential for the drug activity, suggesting a mechanism of NO toxicity, but further studies are required. NTZ inhibits potently both active and latent Mtb bacilli but has poor pharmacokinetic and pharmacodynamic proprieties. Thus, there is some interest in the development of NTZ derivatives with improved bioavailability. [47], [77], [78]

I. 6. 3. ROS toxicity: CFZ and TBI-166

Clofazimine [**Figure I.9**] is a riminophenazine pro-drug, originally approved as anti-leprosy agent, and later repurposed for the treatment of MDR-TB. CFZ decreases central carbon metabolism, inhibits respiration, collapses the PMF, and generates ROS intracellularly. Furthermore, CFZ is capable of killing both active and latent bacilli, and both DS- and MDR- Mtb strains. The use of CFZ in MDR-TB treatment regimens results in shorter treatment durations and higher cure rates and expectedly, CFZ is an integral part of most MDR-TB therapeutic regimens. [47], [54]

Although the CFZ exact mechanism of action is still uncertain, the OxPhos is its presumed target. CFZ does not inhibit NDH-2, but instead is proposed to act as a pro-drug that competes with MK for NDH-2 reduction. The reduced form of CFZ is highly unstable, and generates ROS *in vivo* through a spontaneous, non-enzymatic re-oxidation by oxygen. This reaction restores clofazimine and thus, under aerobic conditions, clofazimine can partake continuous redox cycles, continuously generating ROS, eventually leading to cell death. CFZ is metabolized slowly and has an associated low frequency of resistance. Additionally, CFZ is shown to shorten treatment duration of first-line treatment regimes, and it synergizes with other OxPhos inhibitors such as BDQ and Q203. [47], [51], [54], [56]

Despite all, CFZ use has been restricted due to concerns regarding its side effects, namely orange discoloration of the skin. Thus, significant efforts are ongoing to develop derivatives with better pharmacokinetic and safety profiles. The most promising analogue is TBI-166 [**Figure I.9**], which is more potent than CFZ *in vitro*, and at least as potent *in vivo*, with lesser skin discoloration. TBI-166 is believed to share CFZ's mode of action, and is currently in Phase I clinical trials [47], [49], [55]

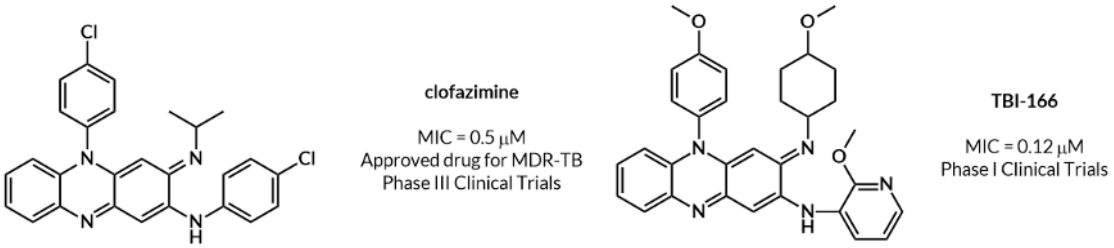

Figure I.9 | **ROS generators currently in clinical settings.** [49], [51], [64]

I. 6. 4. Targeting terminal oxidases: Q203 and TB-47

Q203 [**Figure I.5**] is an imidazopyridine amide derivative with nanomolar antimycobacterial activity. Q203 is currently in Phase II clinical trials, and is capable of inhibiting DS-, MDR- and XDR-Mtb strains. Moreover, it is well tolerated and has a high selectivity, low toxicity, and promising pharmacokinetics. Q203 potently inhibits cyt bc_1-aa_3 by binding to the QcrB subunit and thus, forces Mtb to use the alternative cyt bd. As this terminal oxidase is energetically less efficient, Q203 results on reduced ATP levels, enhanced oxygen consumption, increased NADH production, and upregulated central carbon metabolism cyt bd expression. [47], [56], [69]

Due to the Mtb's ETC plasticity, Q203 is only bacteriostatic despite its potent inhibition and thus, Q203 does not result in cell death. However, Q203 is a potent companion drug, increasing the bactericidal activity of several OxPhos inhibitors.

Particularly, the 3-drug combination of Q203, BDQ and CFZ is highly synergistic, resulting on a rapid and potent bactericidal activity with complete sterilization within 5 days. The synergetic effect is thought to arise from Q203 and BDQ's ability to increase NADH levels that in turn potentiate CFZ's ROS-producing activity. [51], [54], [55]

Unsurprisingly, under simultaneous genetic or chemical inhibition of cyt bd, Q203 has a rapid and potent bactericidal activity in both active and latent bacteria. These findings indicate that simultaneous targeting of both terminal oxidases may represent a particularly promising strategy to kill Mtb. Additionally, cyt bd can detoxify ROS, which is suggested to protect Mtb against drugs dependent on ROS production, such as CFZ and BDQ, and protects the cell from NO, that could increase the cell toleration against drugs dependent on NO toxicity, such as NTZ, DLM and pretomanid (PTM). Thus, cyt bd is emerging as one of the most important targets in anti-TB drug development. [47], [49], [56], [66]

Structurally similar to Q203, a series of pyrazolopyridine carboxamide series were designed through a scaffold hopping strategy. The lead compound, TB-47, is currently in pre-clinical studies and is active against DS- and DR-Mtb strains and both active and latent bacilli. Furthermore, TB-47 has high selectivity, is well-tolerated, has ideal pharmacokinetic properties, and has an excellent safety profile. TB-47 shares the mechanism of action with Q203 and thus, it only has bacteriostatic activity in Mtb. However, just like Q203, TB-47 can be powerful in combination therapies, and shows synergy with many anti-TB drugs, such as PZA, rifampicin, CFZ. [49], [79], [80]

I. 6. 5. NO toxicity: delamanid and pretomanid

The production of reactive nitrogen species (RNS) is a key component in the host's innate immune response to defend itself from invading pathogens such as Mtb. NO is the main RNS produced by the host and the main source for the generating other RNS. During infection, the Mtb bacilli resides predominantly in the lung macrophages, which produce NO. NO and other RNS create a hostile environment that impairs the mycobacterial growth, by inhibition of DNA replication and bacterial respiration, through inhibition of the terminal oxidases. [60], [81]

It is currently thought that cyt bd is involved in the Mtb tolerance against NO and furthermore, has a crucial role in host colonization, where the nitrosative stress inhibits cyt bc_1-aa_3. The Mtb cyt bd does not have a measurable NO reductase and thus, cyt bd NO tolerance relies on its capability of reversibly sequestering NO, serving as a NO deposit that protects the cyt bc_1-aa_3, which is susceptible to irreversible inhibition by NO. Cyt bd is more resistant to NO inhibition than cyt bc_1-aa_3, due to its higher dissociation rate, but is still rapidly inhibited *in vivo*. [60]

Delamanid and pretomanid are two structurally related nitroimidazoles recently approved for the treatment of MDR-TB. Recently, an all-oral, six month, 3-drug combination comprising BDQ, PTM and linezolid, was approved for the treatment of XDR-TB. In **Figure I.10**, the structures of PTM and DLM are presented. [47], [56], [76]

DLM and PTM were found to inhibit the biosynthesis of mycolic acid, which are an essential component of the cell wall. However, the observance that these drugs were bactericidal against both active and latent bacilli suggested an alternative mechanism of action, as mycolic acid biosynthesis is downregulated in latency. Both DLM and PTM are

pro-drugs that require activation by an F420 nitroreductase, an enzyme which produces des-nitro metabolites, with the release of NO. The putative additional mechanism of action is that the intracellular release of NO poisons the cytochrome oxidases, resulting in respiration arrest, and consequent cell death. DLM and PTM treatment results on a quick decrease in intracellular ATP levels, an increased MKH_2/MK ratio, and upregulation of cyt bd and nitrate reductase, which further support the terminal oxidases as a target of these nitroimidazoles. [47], [48], [69]

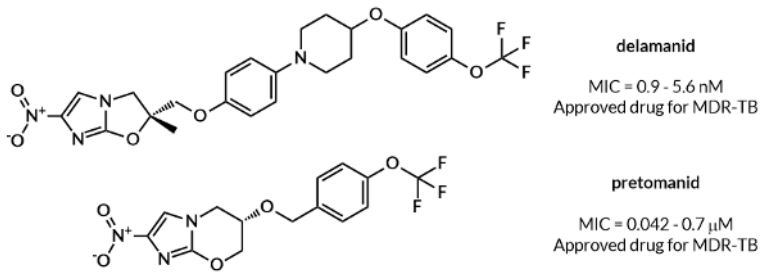

Figure I.10 | **Nitroimidazoles currently in clinical settings.** [49], [51], [64]

I. 7. Dissertation Aims

TB remains a deadly epidemic, still globally prevalent mainly due to poverty, a general societal neglect on a country scale, and to low compliance and low therapy completion rates, on a patient scale. Although there are currently available therapeutic regimens that can effectively cure DS-TB, MDR-TB, and XDR-TB, regimens are lengthy, to guarantee elimination of the latent bacilli. Consequently, TB therapy is associated with high adverse effects, which leads to the observed low completion rates and emergence of drug resistance.

A diversified portfolio of drugs offers the best hope in long-term success to control TB. However, development of anti-TB drugs is a complicated task, as the new drugs should not only be effective against both DS- and DR-Mtb strains and active and latent bacilli; but also should optimally be cheap, compatible with current drugs and anti-retroviral therapy, be preferably administered by oral route, have low toxicity, have a new mechanism of action, and be easily used in global contexts. Moreover, the development of new anti-TB drugs is hampered by a lack of investment, regulatory delays, and a difficulty to implement new drugs into treatment regimens.

Combination therapy is the base of current anti-TB treatment, as combination regimens have the benefit of limiting the emergence of drug resistance, and additionally counteract the Mtb respiratory flexibility and tolerance networks. Recently, after the approval of BDQ, DLM and PTM, the ETC emerged as a promising target for anti-TB control. ETC inhibitors show potent bactericidal activity in both active and latent bacilli, a particularly attractive quality for anti-TB drugs, as it leads to decreased treatment duration, reduced prevalence of latent infections, and delayed resistance emergence. Additionally, ETC inhibitors work synergistically with each other and thus potentiate their activity in combination regimens. Thereby, drug regimens comprising drugs that target multiple ETC components are considered to be a particularly effective strategy to potentially control TB.

Naturally, multi-targeting drugs, i.e., drugs capable of acting on different targets at the same time, are also emerging as attractive tools to control TB, as these drugs can minimize drug resistance, reduce pill burden and drug-drug interactions, and improve patient adherence. Several ETC inhibitors are multi-targeting drugs [e.g., BDQ, PZA, SQ109, and NTZ]. but DLM and PTM are the most prominent examples. The two nitroimidazoles are hybrid drugs, i.e., drugs that combine two distinct pharmacophores that independently target different pathways, connected by covalent bonds. Hybrid drugs can produce a synergetic effect and thus, potentiate a pharmacological effect bigger than the sum of the effect of each pharmacophore.

This master thesis project aims the development of hybrid compounds that effectively inhibit the Mtb ETC through the inhibition of both terminal oxidases, which as was stated in the previous chapter, is considered to be a particularly promising strategy to kill Mtb. The hybrid compounds' general structure is presented in **Figure I.11**.

A set of hit compounds sharing the pyrroloquinolone (PYQ) scaffold emerged from a screening of the iMed.ULisboa compound library against the Mtb H37Rv strain. These hit compounds have shown promising results as antimalarial agents through the

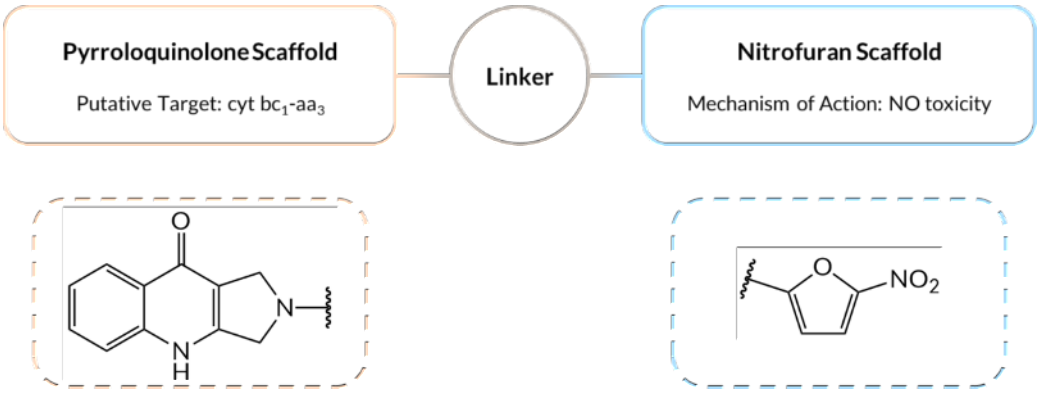

Figure I.11 | Hybrid compounds general structure.

inhibition of the mitochondrial ETC of the *Plasmodium falciparum*, the malaria parasite, through inhibition of the mitochondrial complex III.

The *P. falciparum* mitochondrial complex III has a high homology with the Mtb cyt bc_1, and recently, Chong et al. [82] reported that a quinolone derivative with significant antimalarial activity through the inhibition of the mitochondrial complex III was effective against mycobacteria. Through molecular docking studies, it was revealed that the quinolone derivative bind to the MKH_2-binding site of the Mtb cyt bc_1, which is structurally close to its plasmodium counterpart.

The nitrofuran scaffold comprises a nitro group in a heteroaromatic ring and thus, similarly to DLM and PTM, it can be rapidly reduced *in vivo* by the Mtb intracellular nitroreductases, with the release of NO. Recently, Zeng et al [81] reported the combination of cyt bc_1 inhibitors with NO donors potently inhibit the Mtb respiration and have strong bactericidal activity, despite that individually neither agent is bactericidal. The putative mechanism of action is that the chemical inhibition of the cyt bc_1-aa_3 pathway sensitizes the bacilli to the NO toxicity and thus even a slight inhibition of cyt bd by NO leads to the blockage of the ETC.

Thus, these hybrid compounds are proposed to multitarget the Mtb, through the chemical inhibition of cyt bc_1-aa_3 with a simultaneous release of NO that targets cyt bd, thus inhibiting both terminal oxidases and effectively inhibiting the Mtb ETC.

I. 8. Dissertation Objectives

This master thesis project aims to develop hybrid compounds that target the Mtb ETC. In order to achieve the proposed aim, three main objectives have been defined:

1. To develop and synthesize a small library of hybrid compounds through a medicinal chemistry approach, by performing several structure variations on a base scaffold (PYQ), in order to perform a structure–activity relationship analysis. All synthesized compounds will be characterized through structural elucidation techniques (^{1}H NMR, ^{13}C NMR, MS).
2. To evaluate the physicochemical parameters and pharmacokinetic properties of the hybrid compounds *in vitro*, including solubility, stability (in phosphate buffer saline [PBS] and human plasm), and metabolic (in mice microsomes) assays.
3. To evaluate the biological activity against Mtb *in vitro* and the hybrid compounds' cytotoxicity using HEK 293 cells.

Chapter II

Library Synthesis

Chapter II – Library Synthesis

This chapter describes the synthesis of a small library of hybrid compounds, including both final and intermediate compounds. As stated prior, this library comprises compounds containing the two moieties with expected pharmacological activity against Mtb [the pyrroloquinolone (PYQ) scaffold and the nitric oxide releasing moiety], connected by a variable linker with either amide or imine bonds. Detailed information regarding the experimental synthetic procedures is given in **Chapter VI**.

Figure II.1 describes the general synthetic route used to obtain the compounds. The library was created using a divergent synthesis approach, by derivatization of compound **4** (the PYQ scaffold), as divergent synthesis strategies allow the quick creation of small libraries, thus being useful in chemical synthesis.

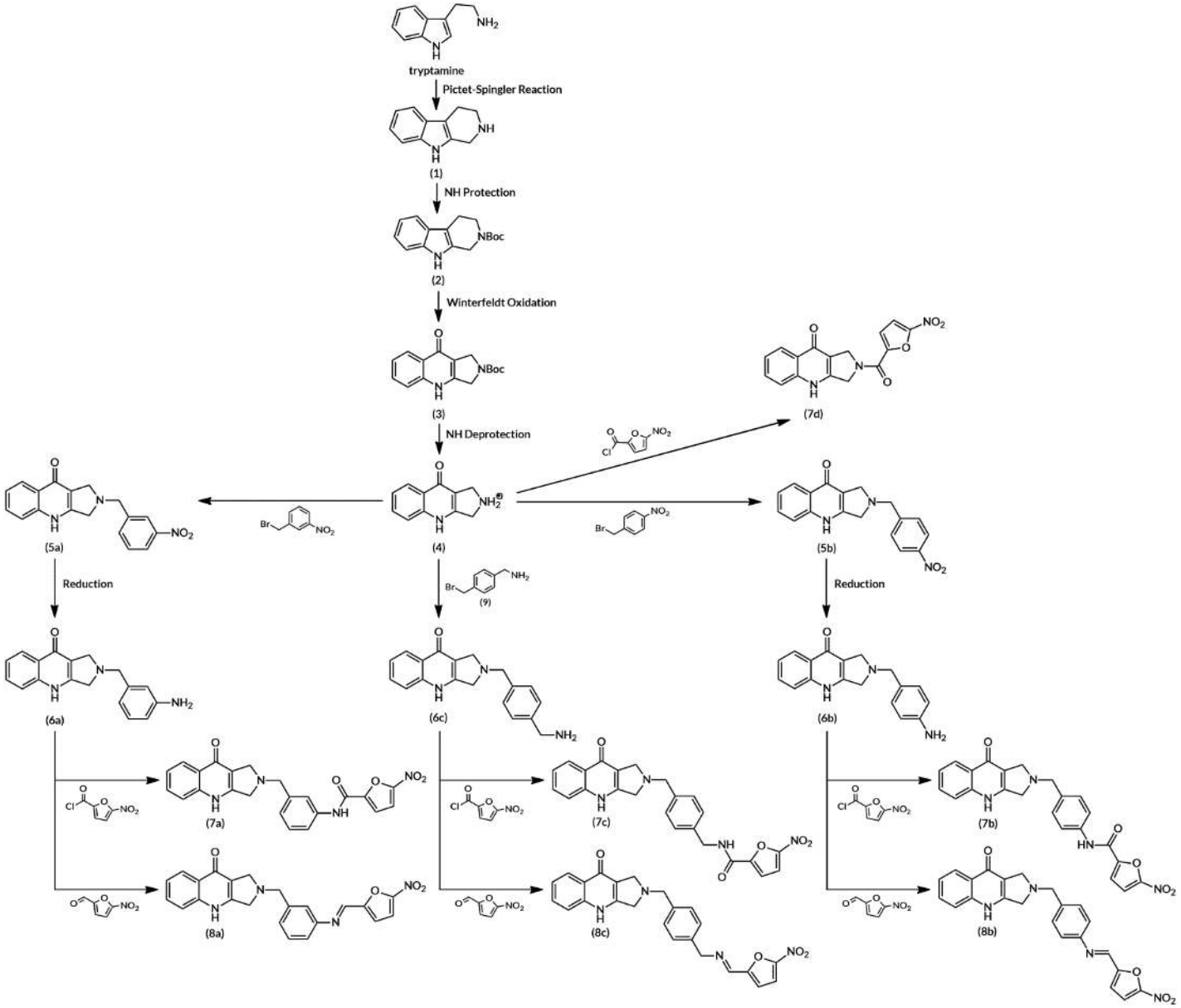

Figure II.1 | General synthetic route used for the library synthesis.

II. 1. Pyrroloquinolone Scaffold Synthesis

The synthesis of the PYQ scaffold **(4)**, the starting compound in the divergent library synthesis, is the first step to obtain the hybrid compounds. This synthesis was already optimized in the research group and is described in **Figure II.2**

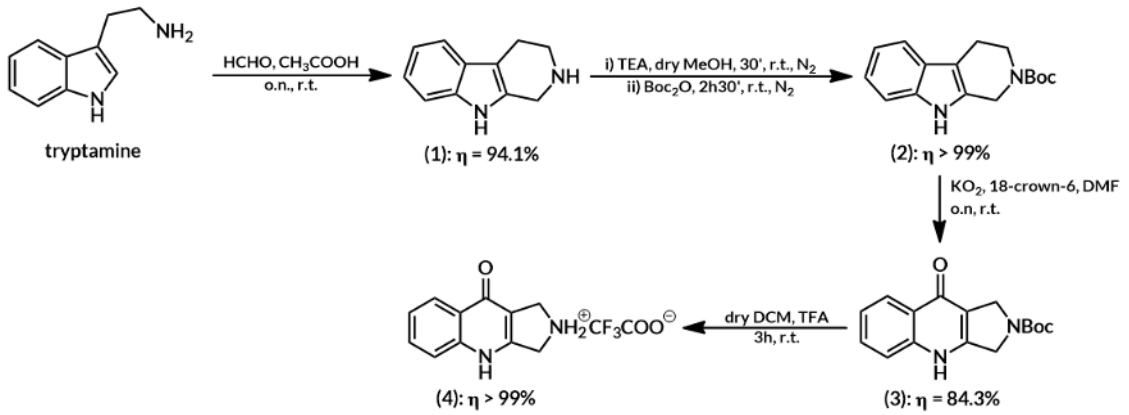

Figure II.2 | Synthetic route for the synthesis of the PYQ scaffold. [compound 4]

The first synthetic step is a Pictet-Spengler reaction, where a tryptamine molecule is condensed with a formaldehyde molecule, followed by an intramolecular cyclization to obtain compound **1**. The aliphatic amine is then protected with a *tert*-butyloxycarbonyl group (Boc) to obtain compound **2**. The next step is a Winterfeldt oxidation, originating compound **3**, and lastly, the amine in compound **3** is deprotected via acidic hydrolysis to obtain compound **4.**

The Pictet-Spengler reaction was first discovered in 1911 by Amé Pictet and Theodor Spengler, and more than a century later, the reaction is still used as one of the most direct, efficient, and versatile method for the synthesis of complex natural products and other polyheterocyclic scaffolds. This reaction was originally reported in the synthesis of tetrahydro-isoquinolines in the total synthesis of complex alkaloids but since then had its uses expanded. In 1928, Tatsui described the extension of the Pictet-Spengler reaction to tryptamine, to obtain tetrahydro-β-carbolines. [83], [84] **Figure II.3** describes the reactional mechanism for the conversion of tryptamine in compound **1**.

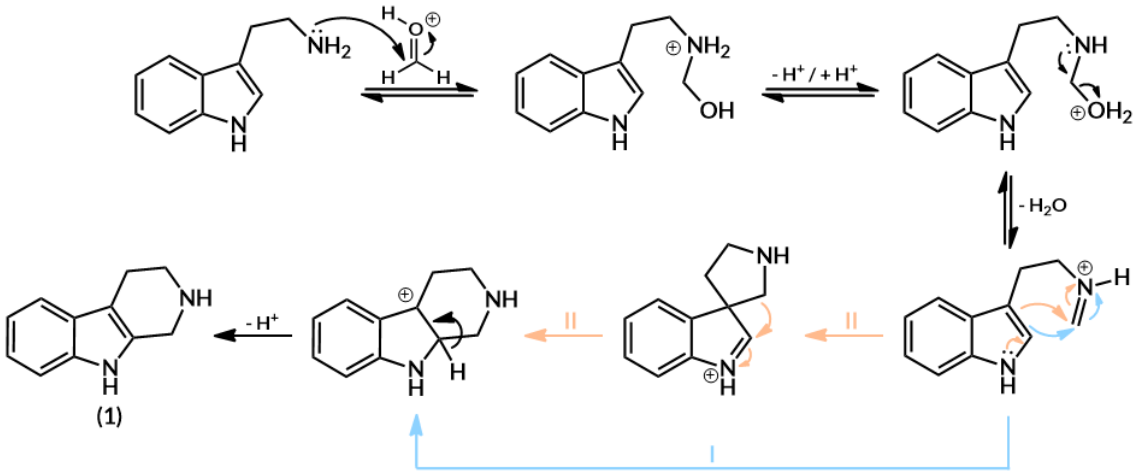

Figure II.3 | Reaction mechanism for compound 1 synthesis. [Pictet-Spengler reaction]

In acidic medium, formaldehyde molecules shift between a deprotonated and protonated state, in an acid-base equilibrium. The reaction mechanism begins with the attack of the tryptamine's nucleophilic aliphatic amine to the formaldehyde's electrophilic carbonylic carbon, after acidic activation. The nucleophilic addition forms a carbinolamine. The obtained molecule is unstable and eliminates a water molecule after an acid-base tautomerism, originating an electrophilic iminium ion. The reaction can then proceed by two alternative pathways. On one hand, the double bond can act as a nucleophile and attack the electrophilic iminium ion (electrophilic addition), in a cyclization that results on the formation of a tricyclic carbocation with a new six-member ring [classical Pictet-Spengler, pathway I (blue)]. On the other hand, the nitrogen lone electron pair can assist the electrophilic addition through the delocalizing of its electrons, in a cyclization that originates a tricyclic cation with a new five-member ring (spiroindolenine) [Pictet-Spengler mechanism specific to indoles, pathway II (orange)]. The spiroindolenine intermediate then suffers an intramolecular aliphatic rearrangement, favoured by the decrease of ring strain, consequence of the ring expansion from a five- to a six-member ring, and the shift from the positive charge from the more electronegative nitrogen atom to a less electronegative carbon atom. This rearrangement originates the aforementioned tricyclic carbocation with a new six-member ring, that loses a proton to eliminate the carbocation and restores the double bond, leading to compound **1**.

Compound **2** results from the protection of compound **1**'s aliphatic amine with a Boc group, in a nucleophilic addition of the amine to the Boc anhydride. **Figure II.4** describes the reactional mechanism for compound **2** synthesis.

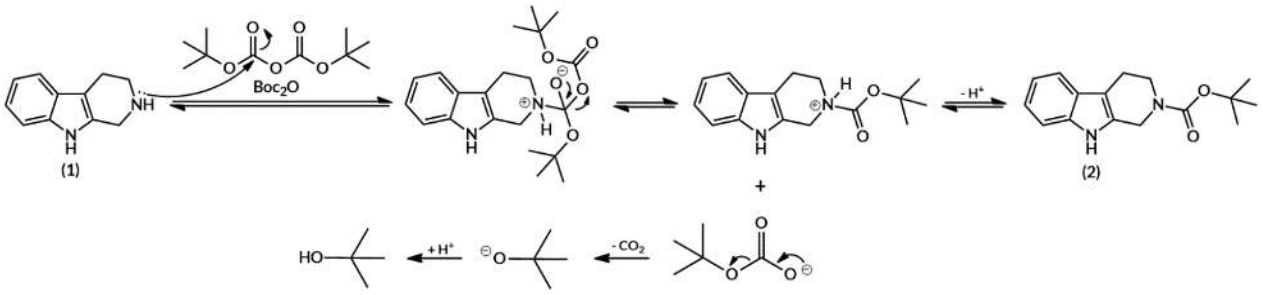

Figure II.4 | Reaction mechanism for compound 2 synthesis.

The reaction mechanism begins with the nucleophilic attack of compound **1**'s aliphatic amine to one of the dicarbonate's carbonylic carbon, with delocalization of the double bond electrons to the oxygen and formation a tetrahedral intermediate. The negatively charged oxygen can then delocalize its electrons to restore the double bond and eliminate the best leaving group, the *tert*-butyl carbonate. The compound, with a newly formed carbamate bond, is deprotonated by the strong, non-nucleophilic base [triethylamine (TEA)] present in the medium, originating compound **2.** The released *tert*-butyl carbonate is unstable, and through an electron delocalization eliminates carbon dioxide, which makes the reaction irreversible, and the released *tert*-butoxide captures a proton from the protonated TEA.

Compound **3** results from the oxidation of compound **2** via Winterfeldt oxidation. The Winterfeldt oxidation is a convenient reaction that rearranges indoles into their corresponding quinolones. The reaction, first described in the 1970s, is a one pot

sequence of a Witkop oxidation[1] and a Camps cyclization[2], using molecular oxygen (O_2) and a strong base (sodium hydride or potassium *tert*-butoxide). Thus, the reaction does not work well for substrates with functional groups sensitive to strong bases, which is one of its main limitations. To overcome these limitations, Spier introduced an alternative oxidation reagent, potassium superoxide (KO_2). KO_2 is used in synthesis as a useful oxygen nucleophile, and it is a much weaker base that can be used in many cases where the Winterfeldt oxidation fails. The KO_2 oxidation of indoles to quinolones derivatives in dimethylformamide (DMF) in the presence of a phase transfer reagent, such as 18-crown-6, shows to be mild and efficient. The 18-crown-6 functions as a ligand for cations, especially potassium cations. Thus, the phase transfer catalysts traps the potassium superoxide's cations, and consequently releases the reactive species, the superoxide ion ($O_2^{\cdot -}$), in the reaction medium [85]–[87]. **Figure II.5** describes the reactional mechanism for the oxidation of compound **2** in compound **3**.

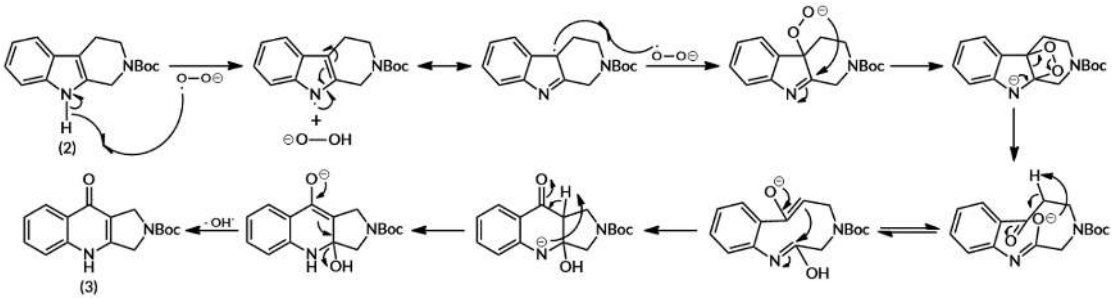

Figure II.5 | Reaction mechanism for compound 3 synthesis. [Winterfeldt Oxidation]

The reaction mechanism begins with the capture of the indole hydrogen atom by the radicalar $O_2^{\cdot -}$ ion, releasing a hydrogen peroxide anion. The newly formed radical is stabilized by ressonance and can react with another $O_2^{\cdot -}$ ion. Thus, the molecule incorporates an $O_2^{\cdot -}$ ion and forms a new carbon-oxygen bond. The negatively charged oxygen works as a nucleophile and attacks the Schiff base in an intramolecular cyclization, forming a four-membered cyclic peroxide. The molecule then suffers a rearrangement driven by the lone pair of electrons in the negatively charged nitrogen, with a break of the peroxide bond and a ring opening. The newly formed ketone moiety can then be converted in the respective enolate by a keto-enol tautomerism, that can act as a nucleophile and add to the restored Schiff base in another intramolecular cyclization. Thus, the pyrroloquinolone ring system is formed, and through an E1cB reaction a hydroxide ion is eliminated to obtain compound **3**.

Compound **4** results from the deprotection of compound **3**'s Boc group through acidic hydrolysis. **Figure II.6** describes the reactional mechanism for compound **4** synthesis.

The reaction mechanism begins with compound **3** activation by the carbamate's oxygen protonation in the acidic medium. Through an E1 reaction, the quaternary carbon eliminates the carbamate in two steps. First the C-O bond is slowly cleaved, releasing a stable *tert*-butyl carbocation, that loses proton to eliminate the carbocation, forming a

[1] The Witkop oxidation is a chemical reaction that converts indoles in o-acylamidoacetophenones, through an oxidative cleavage of the indole double bond.
[2] The Camps cyclization is an intramolecular chemical reaction that converts o-acylamidoacetophenones into quinolones, using hydroxide ion.

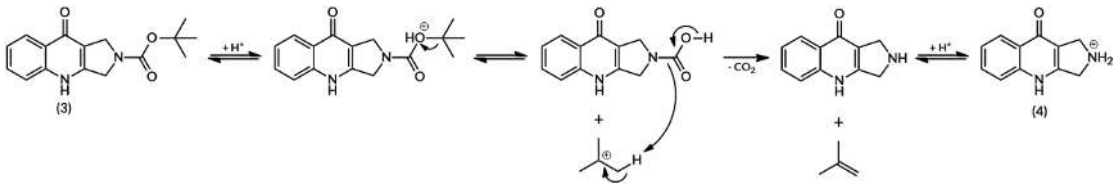

Figure II.6 | Reaction mechanism for compound 4 synthesis.

double bond. The conjugate base in the medium captures a proton from the primary carbamate, and through an electron delocalization, a carbon dioxide molecule is eliminated. Due to the formation of two gaseous molecules (carbon dioxide and butylene), that are released from the reactional media, the reaction is irreversible. Compound **4** is obtained in a protonated state due to the reaction acidic medium.

II. 2. Linker Addition

As previously stated, this library comprises compounds containing two moieties with expected pharmacological activity against Mtb, connected by a variable linker with either an amide or an imine bond. Therefore, the linker addition, the second step in the library synthesis, starts the divergent synthesis and thus, multiple commercial and synthesized linkers were added to the PYQ scaffold, as described in **Figure II.7**

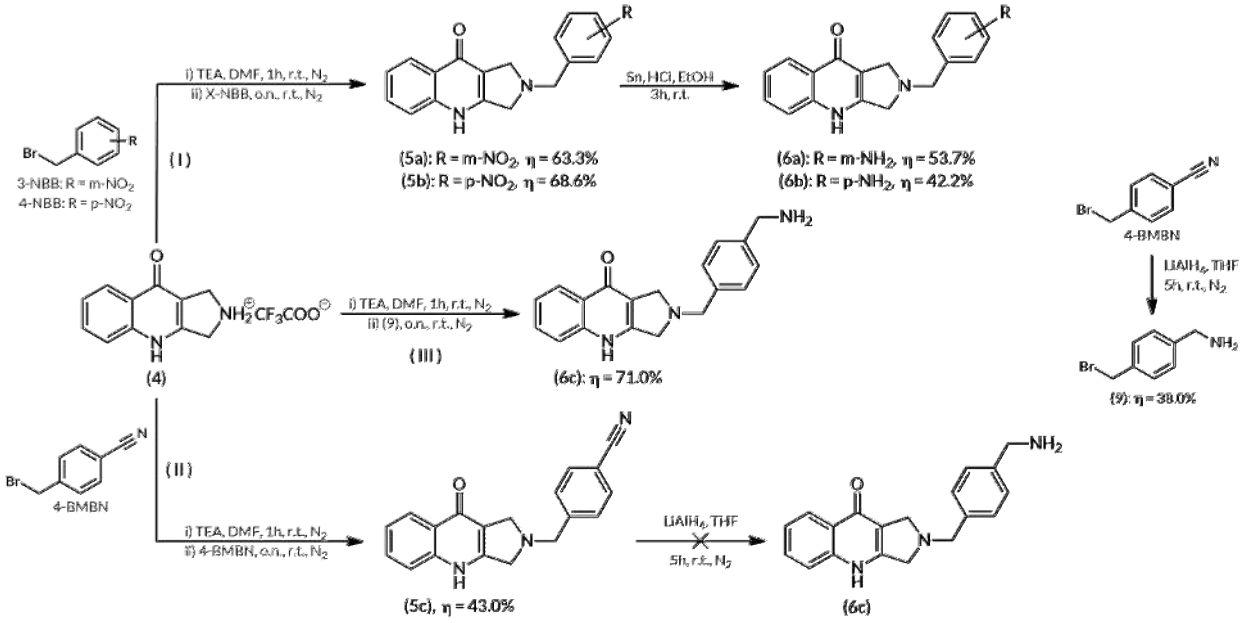

Figure II.7 | Synthetic route for linker additions.

In **pathway (I)**, the first synthetic step is a bimolecular nucleophilic substitution (S_N2), where two different nitrobenzyl bromides (NBB) are added to compound **4** to obtain compounds **5a** and **5b**. Compounds **6a** and **6b** are obtained by reducing the nitro groups into amine groups, in order to allow the formation of the imine and amide bond. In **pathway (II)**, the first synthetic step is also a S_N2 reaction, where a 4-(bromomethyl)-benzonitrile (4-BMBN) molecule is added to compound **4** to obtain compound **5c**. Compound **6c** would then be obtained by reducing the nitrile group into an amine group, but the reaction did not work. Thus, an alternative synthetic route was used, described in **pathway (III)**, where first the nitrile group in the 4-BMBN molecule was reduced to an amine group to obtain compound **9**. Then compound **9** was added to compound **4** through an S_N2 reaction to obtain compound **6c**. **Pathways (I) and (II)** were designed to avoid the formation of aminobenzyl bromides intermediates and thus avoid possible polymerization in basic medium, but the alternative **pathway (III)** shown to be able to synthesize compound **6c** without detection of any polymerization side-products.

Compounds **5a, 5b** and **5c** result from a S_N2 reaction, where compound **4**'s aliphatic amine acts as a nucleophile, and the benzyl halide acts as the electrophile. The conditions for this reaction were already optimized in the research group, and the reactional mechanism is described in **Figure II.8.**

In the activation phase, the compound **4**'s amine group can shift between a protonated and a deprotonated state, in an acid-base equilibrium with the strong base (TEA) present in the reactional medium. With the addition of the benzyl halide linker, the

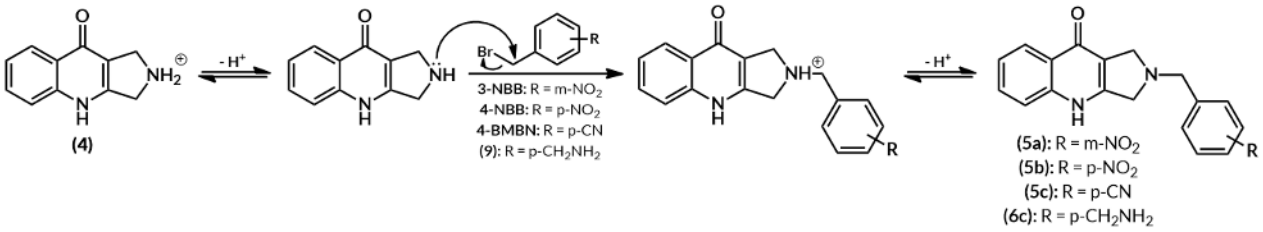

Figure II.8 | Reaction mechanism for compounds 5a, 5b, 5c, and 6c synthesis.

more nucleophilic deprotonated compound **4** attacks the electrophilic benzyl halide. As the new carbon-nitrogen bond is formed, the carbon-bromine bond is broken synchronously, and a bromide ion is released. Finally, the compound's amine is once again deprotonated by TEA, to obtain compounds **5a, 5b,** and **5c**.

As the bromide ion is a very good leaving group, benzyl bromides can eliminate the bromide ion and generate a stable carbocation, stabilised by resonance. Thus, the aforementioned synthesis could also occur simultaneously by a unimolecular nucleophilic substitution (S_N1), to obtain the same end product. Nevertheless, as the linker is a primary benzyl bromide, and a polar aprotic solvent (DMF) is used, the S_N2 reaction should be the primary reactional mechanism.

Compounds **6a** and **6b** result from the reduction of the aromatic nitro group (oxidizing agent), in acidic medium, using a solid metal as the electron source (reducing agent). The reactional and purification conditions for this reaction needed to be optimized, and the attempted conditions are presented in **Table II.1.** The reactional mechanism is described in **Figure II.9.**

The reaction was first tried using the procedure described by Klövekorn et al. [88], but no product formation was observed. An alteration in the used reducing agent, from Fe^0 to Zn^0, led to the formation of the desired product, but with a very low yield [2.5%, compound **6a**]. Thus, an alternative procedure, used in the research group was tried, with Sn^0 as the reducing agent and a more acidic medium. The desired product was obtained, with a slightly better yield [3.5%, compound **6a**]. After an increase on the reaction time, to ensure the complete consumption of the starting material; an increase on the pH on the basification step, to ensure the complete compound deprotonation and thus increased solubility in organic solvents; and the addition of a filtration step, inspired by the previous procedure, to remove excess metal that hamper the separation of phases in the extraction process; the desired compound was obtained with an increased yield. [21.4%, compound **6a**]. As the presence of ethanol (EtOH) (reaction solvent) hampered the phase separation in the extraction process, two new steps were added to the purification method to remove the EtOH before the extractions. These alterations led to a further yield increase. [35.3%, compound **6a**; 22.2%, compound **6b**]. Finally, a methodological simplification was done, which led to a further yield increase [53.7%, compound **6a**; 42.2%, compound **6b**].

In acidic medium, the nitro group in compounds **5a** and **5b** can altern between a deprotonated and a protonated state, in an acid-base equilibrium. The protonated, more electrophilic state is more susceptible to receive two electrons from the reducing agent (tin) in the reactional medium. The formed alkoxide group is a strong base, and thus the reduced molecule quickly captures a proton, forming a diol intermediate. In the acidic medium, the diol intermediate can altern between a deprotonated and a protonated

Table II.1 | Compounds 6a and 6b synthesis optimization
The shaded rows indicate original procedures, while the white rows indicate attempts consisting in alterations of the original procedures. The alterations are marked as bold and underlined.

Reactional conditions	Key purification steps	Observations	Yield [Compound]
Fe^0, HCl, EtOH 80 ºC, react until Fe^0 complete consumption	Vacuum filtration	Solvent was added (t = 3h), as precipitate formation was observed More Fe^0 was added (t = 24h), as no reaction was observed	no observed reaction (t = 28h) **[6a]**
Zn^0, HCl, EtOH 80 ºC, react until **Zn^0** complete consumption	Vacuum filtration	Solvent was added (t = 20h), as precipitate formation was observed	2.5% **[6a]**
Sn^0, HCl, EtOH, r.t., 1h	Basification until pH 5 Extraction with DCM	The mixture was filtrated, as the excess solid metal hampered the separation of phases in the extraction	3.3% **[6a]**
Sn^0, HCl, EtOH, r.t., **3h**	**Vacuum filtration** Basification until **pH 8** Extraction with DCM	A poor separation of phases in the extraction is observed	21.4% **[6a]**
Sn^0, HCl, EtOH, r.t., 3h	Vacuum filtration **Solvent evaporation** **Dissolution in H_2O** Basification until pH 8 Extraction with DCM	-	35.3 % **[6a]** 22. 2% **[6b]**
Sn^0, HCl, EtOH, r.t., 3h	Vacuum filtration Solvent evaporation **Dissolution in sat. $NaHCO_3$ (pH 8)** Extraction with DCM	-	53.7 % **[6a]** 42.2% **[6b]**

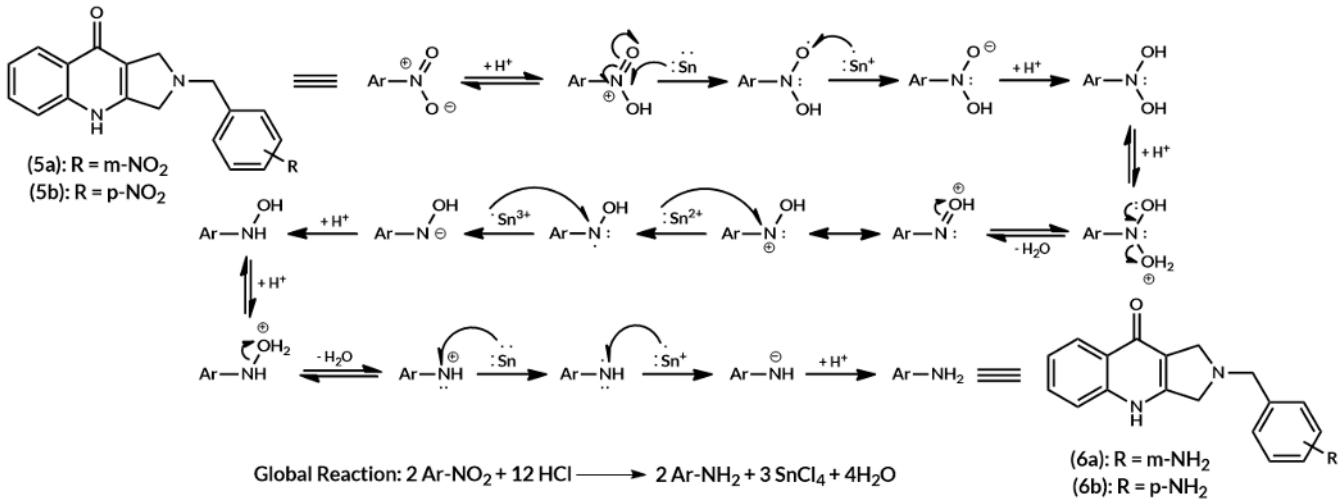

Figure II.9 | **Reaction mechanism for compounds 6a and 6b synthesis.**

state, in an acid-base equilibrium. In the protonated state, the molecule can expel a water molecule, driven by the lone electron pair of the adjacent hydroxide group, to form a protonated nitroso group. After an electron rearrangement, the nitrogen atom can once again be reduced, by receiving two more electrons from the reducing agent, to form an hydroxyamide group. This strong base quickly captures a proton to form a hydroxylamine. Once again, in the acidic medium, the hydroxylamine intermediate can alter between a deprotonated and a protonated state, in an acid-base equilibrium. In the protonated state, the molecule can expel another water molecule; and then, the nitrogen atom can once again be reduced, by receiving two more electrons from the reducing agent, to form a strongly basic nitrenium ion. Finally, the nitrenium ion quickly captures a proton, to form an amine group, originating compounds **6a** and **6b**. As tin (II) is a stronger reducing agent than tin (0), the global reaction oxidizes tin (0) to tin (IV), as it is described in the global reaction equation.

Compound **6c** would result from the reduction of compound **5c**'s nitrile group to a primary amine, using a hydride donor ($LiAlH_4$) as the reducing agent. However, for unknown reasons this reaction did not work. The reaction was followed by thin layer chromatography (TLC), and the complete consumption of compound **5c** was observed, but the desired compound was not obtained after the purification process. Thus, a new approach was designed, where the order of the reduction and linker addition was switched.

Compound **9** results from the reduction of the commercial 4-BMBN linker's nitrile group to an amine, using a hydride donor ($LiAlH_4$) as the reducing agent. The reactional and purification conditions were based on a procedure described by Aksenov et al. [89]. The reactional mechanism is described in **Figure II.10.**

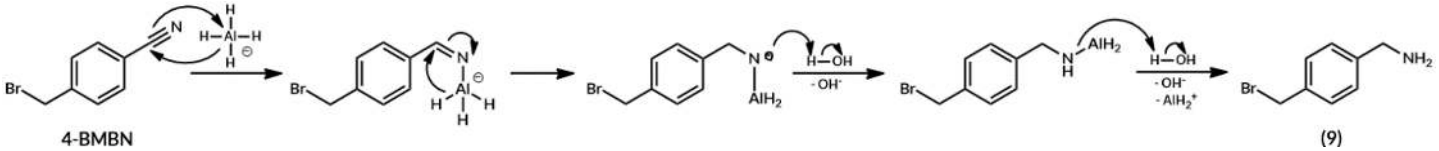

Figure II.10 | **Reaction mechanism for compound 9 synthesis.**

The reactional mechanism is initiated by the hydride transfer from the $LiAlH_4$ to the polar nitrile bond. The nucleophilic hydride ion attacks the electrophilic nitrile carbon, with delocalization of the π-electrons to capture the aluminium hydride, to form an imine intermediate. Through an intramolecular nucleophilic attack, another hydride ion is transferred from the aluminium hydride to the imine's electrophilic carbon, with delocalization of the π-electrons to form an amide ion. Finally, in the workup phase, the amide ion captures a proton, to form an amine intermediate. Then, the amine captures another proton, releasing the aluminium hydride cation, to form the primary amine group present in compound **9**.

Finally, compound **6c** was synthesized through a S_N2 reaction, where compound **4**'s aliphatic amine acts as the nucleophile, and compound **9** acts as the electrophile. The conditions for this reaction were already optimized in the research group, and the reactional mechanism is described in **Figure II.8.**

II. 3. Nitrofuran Scaffold Addition

After the addition of the variable linker moiety to the pyrroloquinolone scaffold, the last step in the hybrid compound synthesis is the addition of the nitrofuran scaffold, described in **Figure II.11.** To obtain compounds with either an amide or an imine bonds, two different commercial nitrofurans were added to the synthesized compounds **6a**, **6b**, and **6c**. Additionally, to assess the influence of the linker in our hybrid compounds, a compound without linker was synthesized through the addition of the commercial nitrofuran to compound **4.**

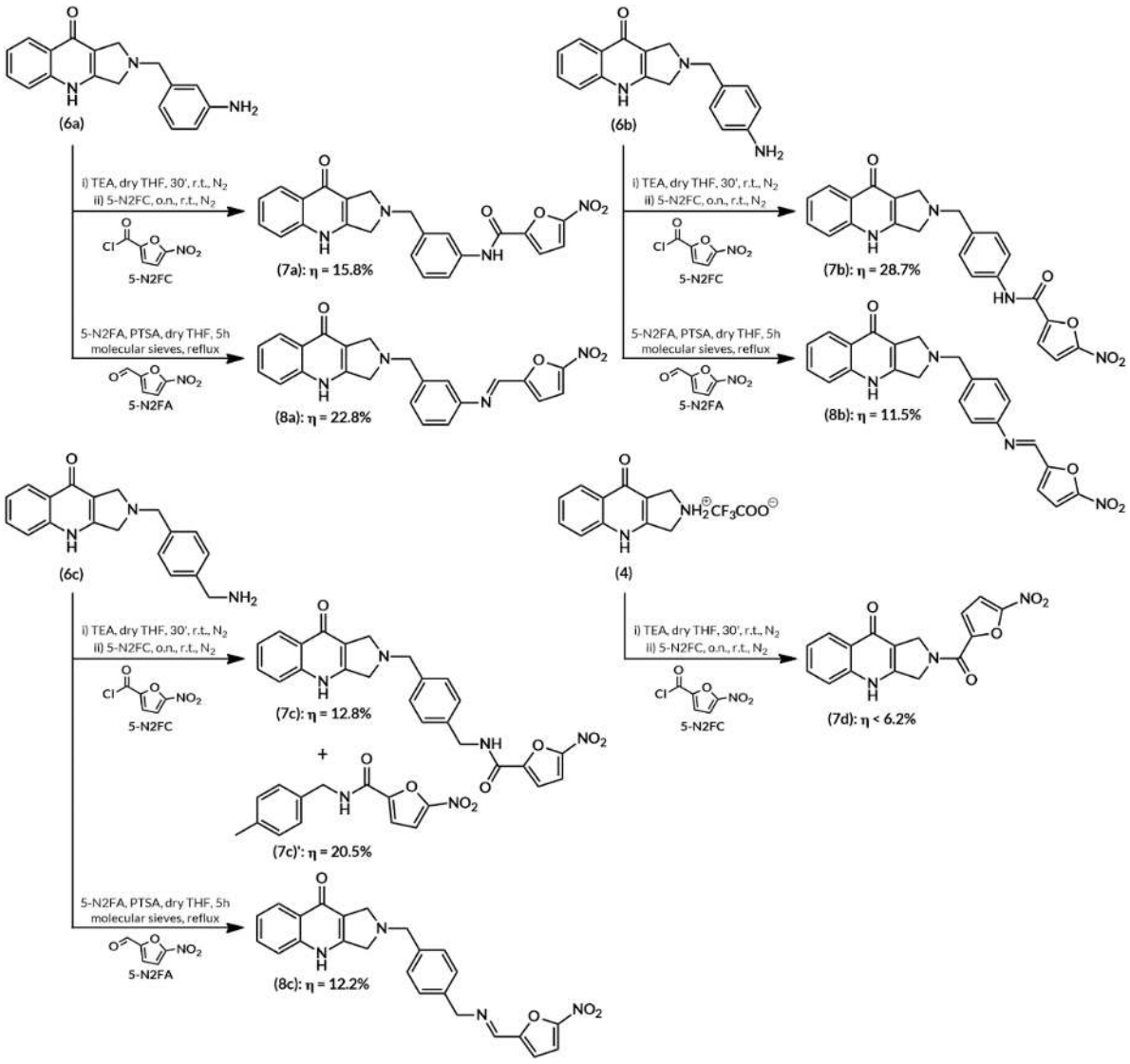

Figure II.11 | Synthetic route for nitrofuran scaffold addition.

In the top pathways, compounds **7a**, **7b**, **7c,** and **7d** are obtained through the condensation between a furoyl chloride and the amine in compounds **6a**, **6b**, **6c,** and **4**, respectively, with formation of an amide bond. Additionally, compound **7c'**, a degradation product of compound **7c** was also obtained. In the bottom pathways, compounds **8a**, **8b**, and **8c** are obtained through the condensation between a furaldehyde and the amine in compounds **6a**, **6b**, and **6c**, respectively, with formation of an imine bond.

Compounds **7a, 7b,** and **7c** result from a nucleophilic acyl substitution, where the primary amine group in compounds **6a, 6b,** and **6c** serve as a nucleophile that displaces the leaving group in the furoyl chloride. **Figure II.12** describes the reactional mechanism for compounds **7a, 7b,** and **7c** synthesis.

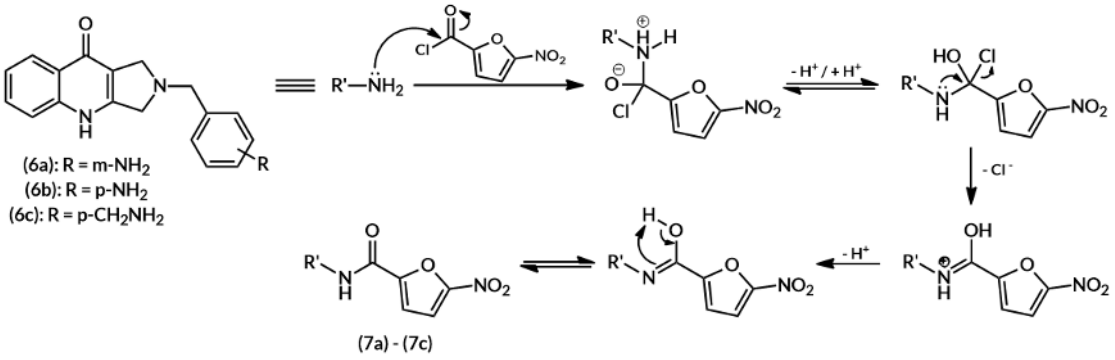

Figure II.12 | Reaction mechanism for compounds 7a, 7b, and 7c synthesis.

The reaction mechanism begins with the nucleophilic attack of the primary amine group in compounds **6a, 6b,** and **6c** to the furoyl chloride's carbonylic carbon, with delocalization of the double bond electrons to the oxygen, and formation of a tetrahedral intermediate. Through acid-base equilibriums, the protonated amine can be deprotonated by the non-nucleophilic base (TEA) in the medium and the negatively charged oxygen can capture a proton from the formed conjugated acid. A chloride ion (good leaving group) is expelled, driven by the delocalization of the lone pair of electrons in the nitrogen atom, with the formation of a double bond. Finally, the TEA in the medium can capture a proton to form an imidic acid intermediate, that can then tautomerize to the corresponding amide, originating compounds **7a, 7b,** and **7c**.

While compounds **7a** and **7b** were obtained from the aforementioned conditions, synthesis of compound **7c** was not initially successful, and instead a degradation product, compound **7c'** was obtained. As the compounds had no exposition to high temperatures, photodegradation seemed to be the most probable degradation process. Thus, synthesis of compound **7c** was repeated, using the same conditions, but taking all measures to protect the compound from light. Using these conditions, compound **7c** synthesis was successful, which supported the hypothesis that compound **7c'** was a result of photodegradation. Nonetheless, further studies would be required to confirm this hypothesis. Unfortunately, compound **7c** was not obtained in time to be used on the remaining assays. Alternatively, compound **7c'** was used, despite not having the pyrroloquinolone scaffold, as it allows an assessment of the influence of the pyrroloquinolone scaffold on the compound properties.

Compound **7d** results from a nucleophilic acyl substitution, where the secondary amine group in compound **4** serve as a nucleophile that displaces the leaving group in the furoyl chloride, in a very similar reaction to the synthesis of compound **7a, 7b,** and **7c**. **Figure II.13** describes the reactional mechanism for compound **7d**.

In the activation phase, the compound **4**'s amine group can shift between a protonated and a deprotonated state, in an acid-base equilibrium with the strong base (TEA) present in the reactional medium. With the addition of the furoyl chloride, the more nucleophilic deprotonated compound **4** attacks the furoyl chloride's carbonylic carbon,

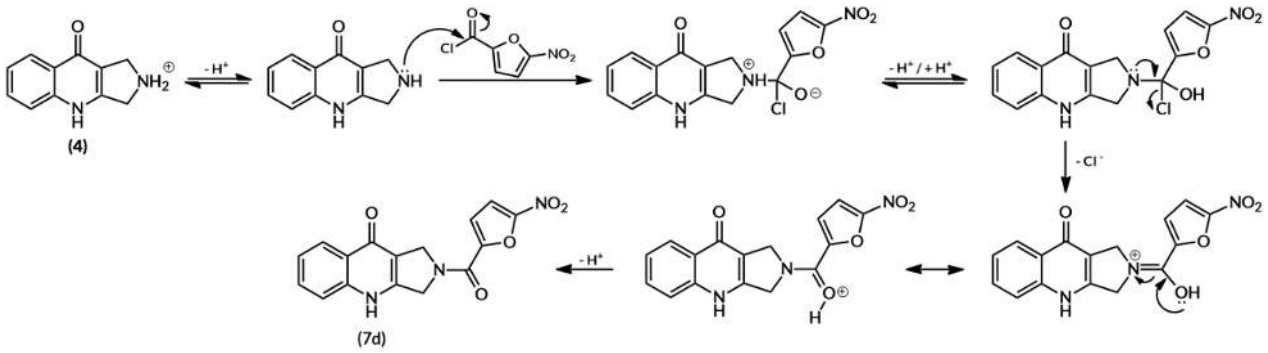

Figure II.13 | **Reaction mechanism for compound 7d synthesis.**
Figure generated with PerkinElmer's ChemDraw® Ultra, version 12.0.2.1076.

with delocalization of the double bond electrons to the oxygen atom, and formation of a tetrahedral intermediate. Through acid-base equilibriums, the protonated amine can be deprotonated by the TEA in the medium and the negatively charged oxygen can capture a proton from the formed conjugated acid. A chloride ion (good leaving group) is expelled, driven by the delocalization of the lone pair of electrons in the nitrogen atom, with the formation of a double bond. The formed protonated imidic acid intermediate can then tautomerize to the corresponding amide, that can be deprotonated by the TEA in the medium, originating compound **7d**.

As secondary amines are less reactive than primary ones, synthesis of compound **7d** was expected to be more challenging than synthesis of compounds **7a, 7b,** and **7c**, and unsurprisingly, compound **7d** was obtained with a smaller yield. However, and despite being purified by column chromatography, compound **7d** was never obtained pure. Due to time constraints, the synthesis was not repeated, and due to the obtained compound low quantity, more purification steps were unviable. Thus, compound **7d** was not used on the remaining assays.

Compounds **8a, 8b,** and **8c** result from a nucleophilic addition of the primary amine group in compounds **6a, 6b,** and **6c** to the furaldehyde, followed by elimination of a water molecule. The imine synthesis is reversible, and usually favours the carbonyl and amine. Thus, a dehydrating agent (molecular sieves) was used to remove the eliminated water molecules, and thereby shift the reaction equilibrium to favour the imine formation. **Figure II.14** describes the reactional mechanism for compounds **8a, 8b,** and **8c** synthesis.

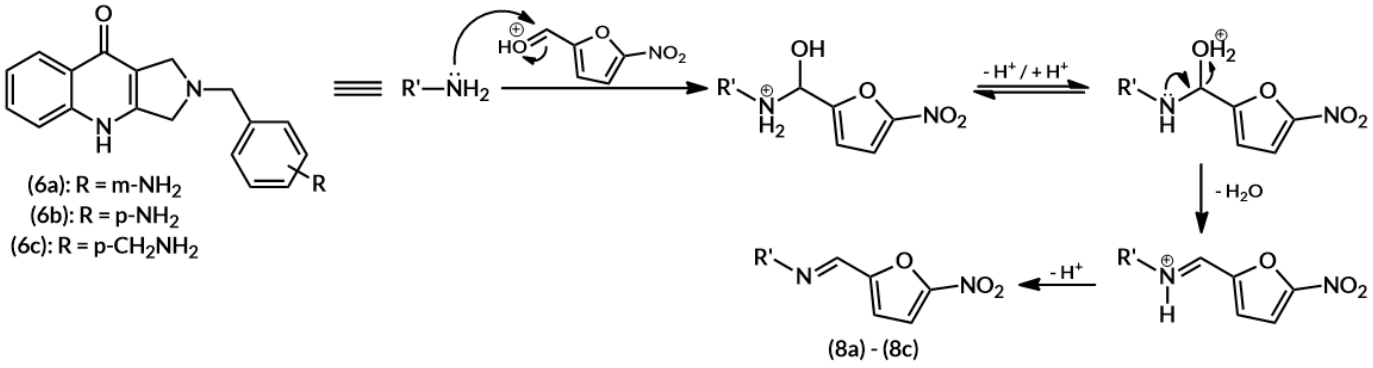

Figure II.14 | **Reaction mechanism for compounds 8a, 8b, and 8c synthesis.**

The reaction mechanism begins with the activation of the furaldehyde's carbonylic carbon, by capturing the acidic proton of the catalytic acid [p-toluenesulfonic acid (PTSA)] in the medium. The activated aldehyde is then susceptible to a nucleophilic attack of the primary amine group in compounds **6a, 6b,** and **6c**, with delocalization of the double bond electrons to the oxygen, and formation of a tetrahedral intermediate. Through acid-base equilibriums, the protonated amine can be deprotonated by the formed PTSA conjugated base in the medium and the alcohol group can capture a proton from the restored PTSA. A water molecule (good leaving group) is then expelled, driven by the delocalization of the lone pair of electrons in the nitrogen atom, with the formation of a double bond. As the molecular sieves remove the generated water molecules from the reactional medium, this step is irreversible. Finally, the formed PTSA conjugated base in the medium can capture a proton to form the imine, originating compounds **8a, 8b,** and **8c**, and restoring the catalytic acid.

II. 4. Structural Characterization

The synthesized compounds were characterized by NMR (^{1}H and ^{13}C), and ESI-MS. In **Chapter VI,** a description of all structural characterizations is presented, and in **Annex 2 – Structural Characterization Spectra,** all compound spectra are presented. In this subchapter, compound **7c'** structural characterization is reported as an illustration of the analysis performed.

Mass spectrometry is a highly sensible analytical technique commonly used in structural elucidation due to its ability to identify unknown compounds in complex mixtures. MS determines molecular masses after ionization on gaseous phase and subsequent ion separation according to their mass to charge ratio. In **Figure II.15,** compound **7c'** mass spectrum is presented, and some adducts are identified.

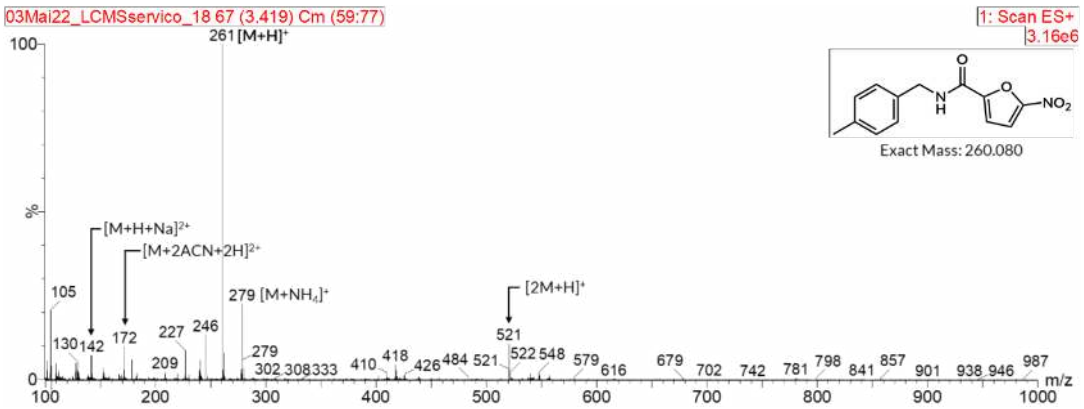

Figure II.15 | Compound 7c' mass spectrum

In compound **7c'** mass spectrum, the base peak (m/z = 261) corresponds to the molecular ion $[M+H]^+$. The presence of a peak corresponding to the molecular ion in a mass spectra is an important indicator to confirm the desired compound is in the tested sample. Besides the molecular ion peak, and according to compound stability, peaks corresponding to molecular fragments and peaks corresponding to adducts can be observed in the mass spectra. For compound **7c'**, four adduct peaks were identified in the mass spectrum: $[2M+H]^+$ (m/z = 521), $[M+NH_4]^+$ (m/z = 279), $[M+2ACN+2H]^{2+}$ (m/z = 172), and $[M+H+Na]^{2+}$ (m/z = 142).

As the mass spectrum was performed in a low-resolution mass spectrometer, the molecule cannot be identified by mass spectrometry alone, as the technique would not distinguish molecules with the same exact mass (rounded to units). Nonetheless, the presence of the base and the adduct peaks are a very strong indicator to confirm compound **7c'** presence.

Nuclear Magnetic Ressonance spectrometry is currently used in organic chemistry as the definitive method to identify monomolecular organic compounds. NMR spectrometry observes the local magnetic fields around atomic nuclei, and as the fields are highly characteristic to individual compounds, NMR spectra are unique, and often highly predictable for small molecules. The most common types of NMR are ^{1}H and ^{13}C – NMR, but the technique is applicable to any nuclei possessing spin. In the subsequent figures, compound **7c'** NMR spectra are presented [^{1}H NMR: **Figure II.16,** COSY: **Figure II.18,** ^{13}C NMR: **Figure II.19,** ^{1}H-^{13}C HSQC: **Figure II.20,** and ^{1}H-^{13}C HSQC: **Figure II.21**]

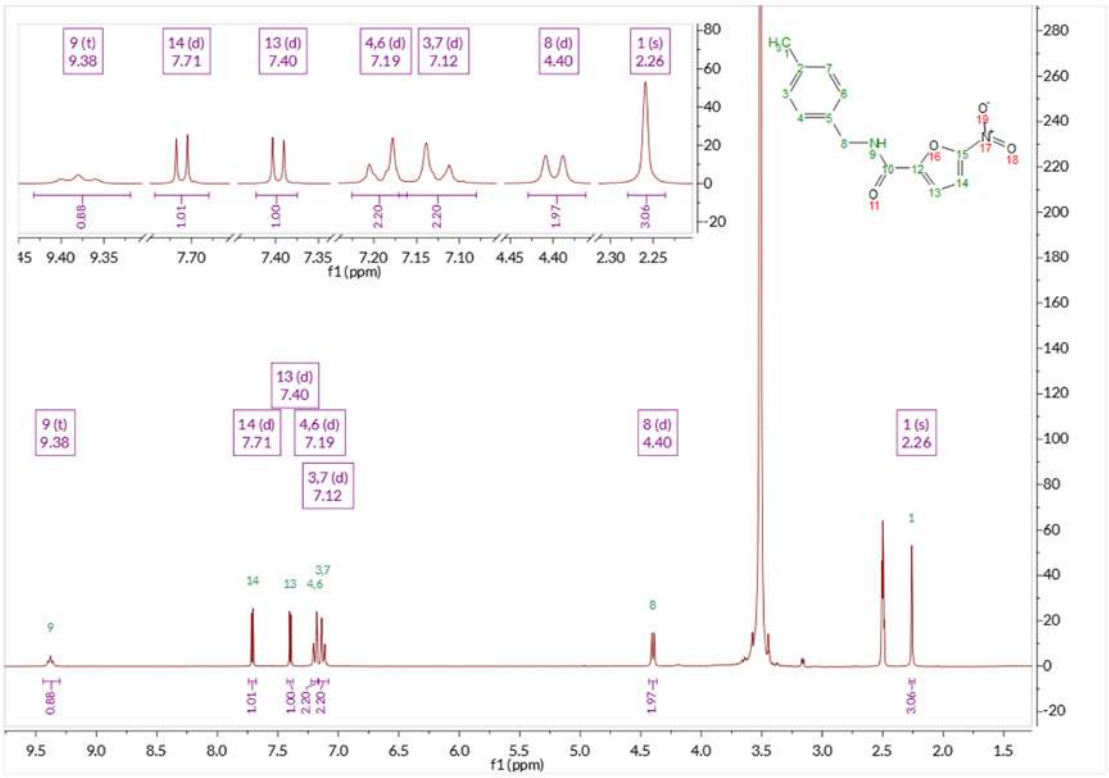

Figure II.16 | Compound 7c' ^{1}H NMR spectrum

Besides the two solvent signals (DMSO and H_2O), the compound **7c'** ^{1}H NMR spectrum displayed 7 signals, integrated for a total of 12 hydrogens. As molecule **7c'** has 12 hydrogens in 7 chemically different environments, the spectrum is according to the structure of the molecule. For each chemically different environment, considering the number of equivalent hydrogens, the number of neighbouring hydrogens and the chemical environment, the NMR signal can be predicted. Considering this, the signal at δ = 2.26 ppm can be straightforwardly assigned to the methyl group **(1).** Similarly, the signals at δ = 7.10 ppm and δ = 7.19 ppm can be straightforwardly assigned to hydrogens **(3)** and **(7)**, and hydrogens **(4)** and **(6)**, although to do a specific assignment between the two pairs of equivalent hydrogens, a bidimensional technique is required.

Despite being more deshielded than the typical range for their functional groups, the methylene group **(8)** can be assigned to the signal at δ = 4.40 ppm and the amide NH **(9)** to the signal at δ = 9.38 ppm. The difference on the chemical shift can be explained by the presence of the electron withdrawing nitro group that is in ressonance with the amide, and thus further deshields the amide NH and, to a lesser extent, the methylene group.

Hydrogens **(13)** and **(14)** can be straightforwardly to the signals at δ = 7.40 ppm and δ = 7.71 ppm. A specific assignment between the hydrogens can be made, by drawing the key ressonance structures for compound **7c'** [**Figure II.17**], where it becomes clear that hydrogen **(14)** is more deshielded than hydrogen **(13)**, as it is covalently bonded to a more carbon with a partial positive charge that is more electronegative and thus, withdraws more electronic density. Therefore, the signals at δ = 7.40 ppm and δ = 7.71 ppm can be assigned to hydrogen **(13)** and **(14)**, respectively.

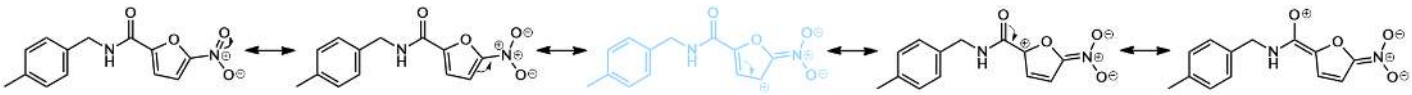

Figure II.17 | Ressonance structures for compound 7c'

Correlation spectroscopy (COSY) is a bi-dimensional $^{1}H - ^{1}H$ NMR technique that allows to observe the couplings between neighbouring hydrogens. In a COSY spectra, the diagonal peaks correspond to the peaks in a ^{1}H NMR, while the cross peaks indicate couplings between pairs of hydrogens. Spin-spin coupling can be seen typically up to three bonds away, and occasionally up to five bonds, generally in allylic and aromatic systems.

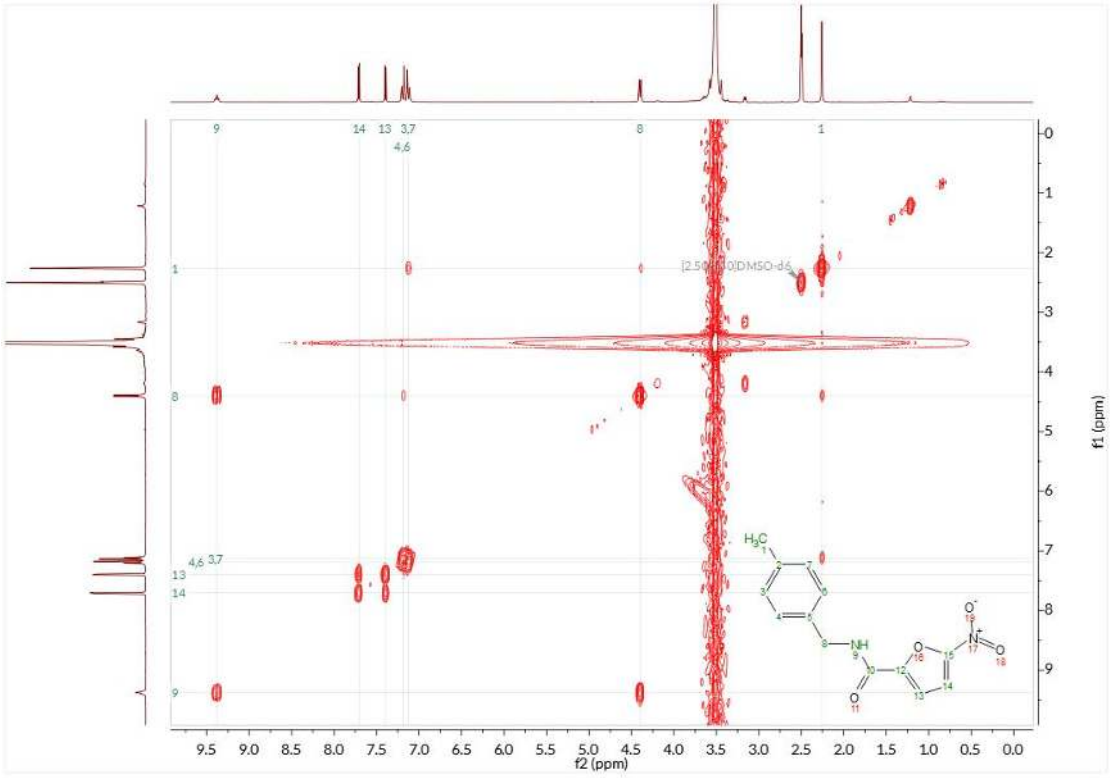

Figure II.18 | Compound 7c' COSY spectrum

By observing the correlations of the signals at δ = 7.10 ppm and δ = 7.19 ppm, the hydrogens **(3)** and **(7)** can be distinguished from hydrogens **(4)** and **(6)**. Besides the cross-peaks between themselves, expected as the aromatic hydrogens are separated by 3 bonds; the signal at δ = 7.10 ppm has a cross-peak with hydrogen **(1)**, while the signal at δ = 7.19 ppm has a cross-peak with hydrogen **(8)**. Hydrogens **(3)** and **(7)** are separated from hydrogen **(1)** by 4 bonds in an aromatic system, while hydrogens **(4)** and **(6)** are separated from hydrogen **(8)** by 4 bonds in an aromatic system. Hence, these groups of hydrogens are expected to couple. Thus, the signal at δ = 7.10 ppm can be attributed to hydrogens **(3)** and **(7)**, and the signal at δ = 7.19 ppm can be attributed to hydrogens **(4)** and **(6)**.

The remaining expected couplings also present cross-peaks in the COSY spectra, confirming the hydrogen attribution. Both the amide NH **(9)** and the methylene group **(8)** and the aromatic hydrogens **(13)** and **(14)** are separated by 3 bonds, and thus are expected to couple, and both present a cross-peak in the COSY spectra.

In a ^{13}C NMR spectrum, similarly to a ^{1}H NMR spectrum, the number of signals indicate the number of chemically different carbons in the molecule, and the chemical shift indicates the carbon's chemical environment. However, in ^{13}C NMR spectrum, signal integration as no significance, and spin-spin coupling is undetected, due to the low natural abundance of ^{13}C, and consequent low probability of two neighbouring ^{13}C in a molecule.

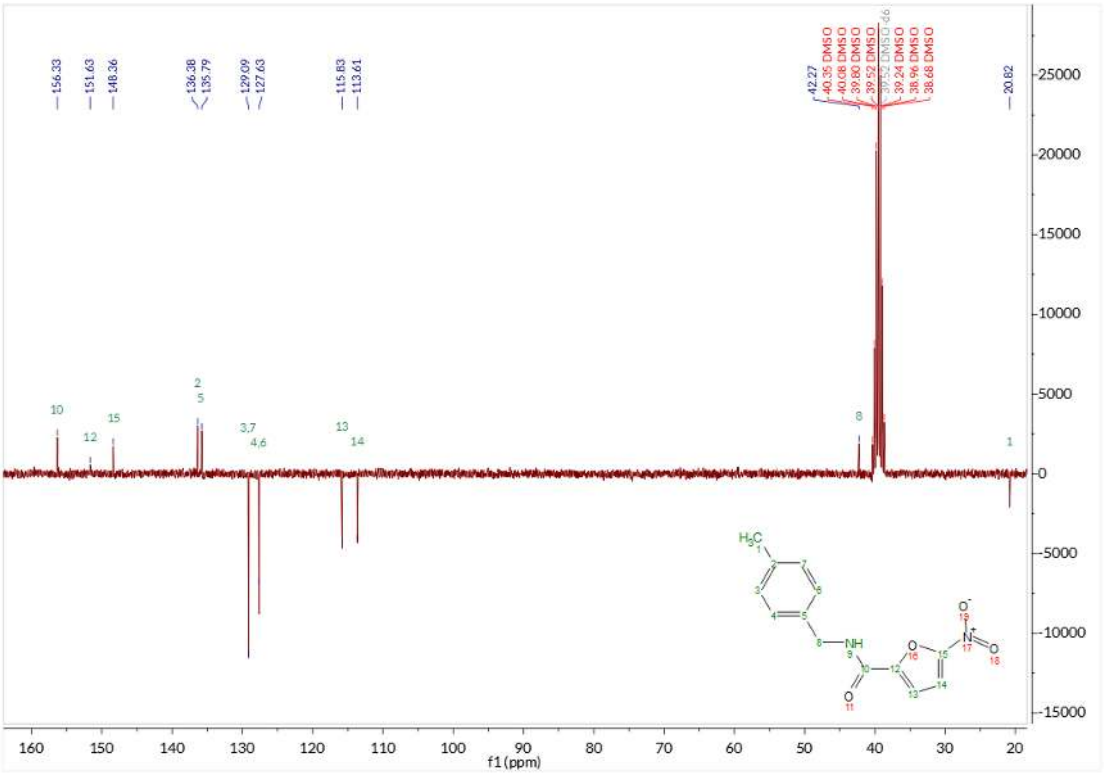

Figure II.19 | Compound 7c' ^{13}C NMR spectrum

Besides the solvent signal (DMSO), the compound **7c'** ^{13}C NMR spectrum displayed 11 signals, correspondent to the 11 chemically different carbons in molecule **7c'**. In a ^{13}C NMR APT experiment, the carbon signals are positive or negative according to the number of carbons attached. In this case, primary and tertiary carbons are yielded negative, while secondary and quaternary carbons are yielded positive. Although some signals in the ^{13}C NMR spectrum could be already attributed based solely on the chemical shift and the number of attached carbons, bidimensional experiences would always be required to attribute all signals.

The heteronuclear single quantum correlation (HSQC) spectroscopy is a bi-dimensional heteronuclear NMR technique, generally ^{1}H – ^{13}C or ^{1}H – ^{15}N, that allows to observe the coupling between hydrogen atoms and heteroatoms separated by one bond. In a HSQC spectra, the peaks correspond to the couplings between the hydrogen and the heteroatom.

The ^{1}H – ^{13}C HSQC spectra has only one peak associated with each ^{1}H and ^{13}C NMR signal, that indicates the hydrogen and carbon are separated by one bond, and thus, are covalently bonded. As molecule **7c'** has all its hydrogens assigned, the ^{1}H – ^{13}C HSQC spectra can be used to directly assign the signals in the ^{13}C NMR spectra to the respective carbons.

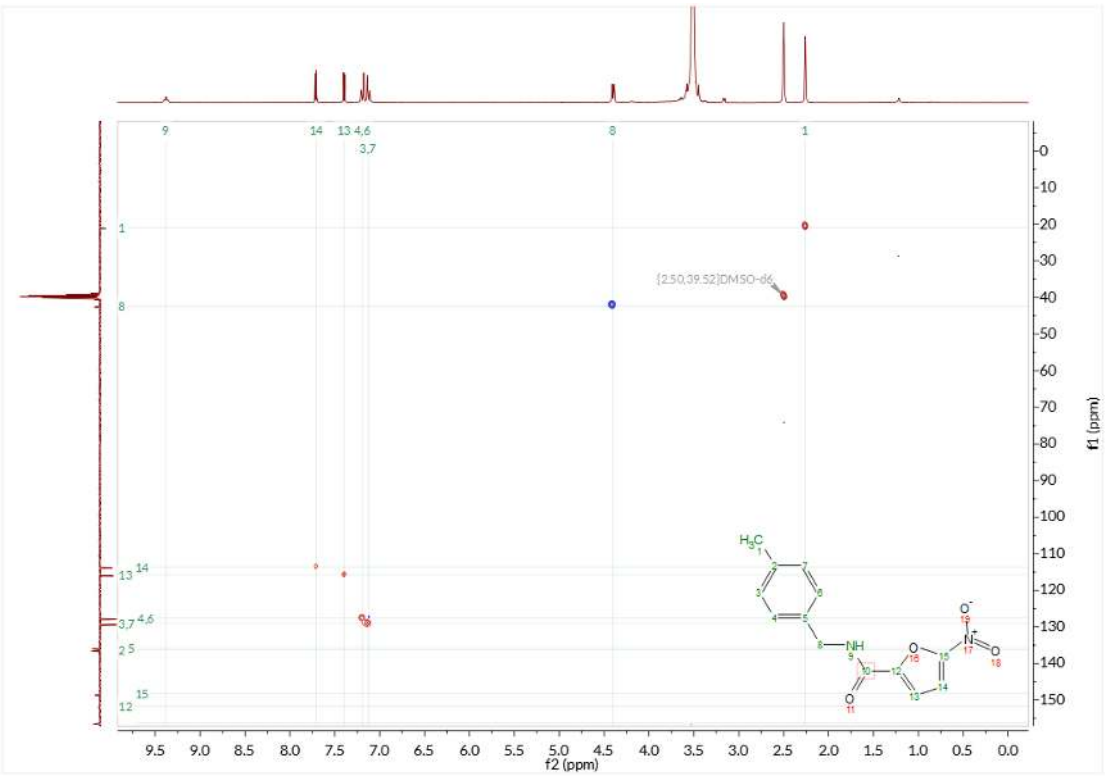

Figure II.20 | Compound 7c' ^{1}H – ^{13}C HSQC spectra

Thus, the signal at δ = 20.8 ppm is assigned to the methyl group **(1)**, the signal at δ = 42.3 ppm is assigned to the methylene group **(8)**, the signal at δ = 113.6 ppm is assigned to the aromatic carbon **(14)**, the signal at δ = 115.8 ppm is assigned to the aromatic carbon **(13)**, the signal at δ = 127.6 ppm is assigned to the chemically equivalent [due to ring symmetry] aromatic carbons **(4)** and **(6)**, and the signal at δ = 129.1 ppm is assigned to the chemically equivalent [due to ring symmetry] aromatic carbons **(3)** and **(7)**. The amide hydrogen **(9)** did not show any coupling, which was expected, as this hydrogen is not bonded to a carbon. Analysing the ^{13}C NMR APT, the signal for secondary carbon **(8)** is yielded positive, while the signals for primary carbon **(1)** and tertiary carbons **(3)**, **(4), (6), (7), (13),** and **(14)** are yielded negative, as expected. Furthermore, all carbon signals are in the usual chemical shift ranges for their functional groups [δ = 20-40 ppm for aliphatic carbons adjacent to aromatic rings, δ = 25-60 ppm for aliphatic carbons adjacent to a nitrogen atom, and δ = 110-160 ppm for aromatic carbons.] The quaternary carbons **(2)**, **(5)**, **(10), (12),** and **(15)** do not show any peak in the ^{1}H – ^{13}C HSQC spectra, as they do not have any hydrogen atom directly bonded.

The heteronuclear multiple-bond correlation (HMBC) spectroscopy is a bi-dimensional heteronuclear NMR technique, generally ^{1}H – ^{13}C, that allows to observe the coupling between hydrogen atoms and heteroatoms separated by two to four bonds. In a HMBC spectra, the peaks correspond to the couplings between the hydrogen and the heteroatom.

By observing the peaks correspondent to the signals at δ = 156.3 ppm, δ = 151.6 ppm, δ = 148.4 ppm, δ = 136.4 ppm, and δ = 135.8 ppm, the carbons **(2)**, **(5)**, **(10), (12),** and **(15)** can be assigned. The signal at δ = 135.8 ppm has a peak with hydrogens **(4), (6),** and **(8)**. Thus, this signal can be assigned to carbon **(5)**, the only carbon that is

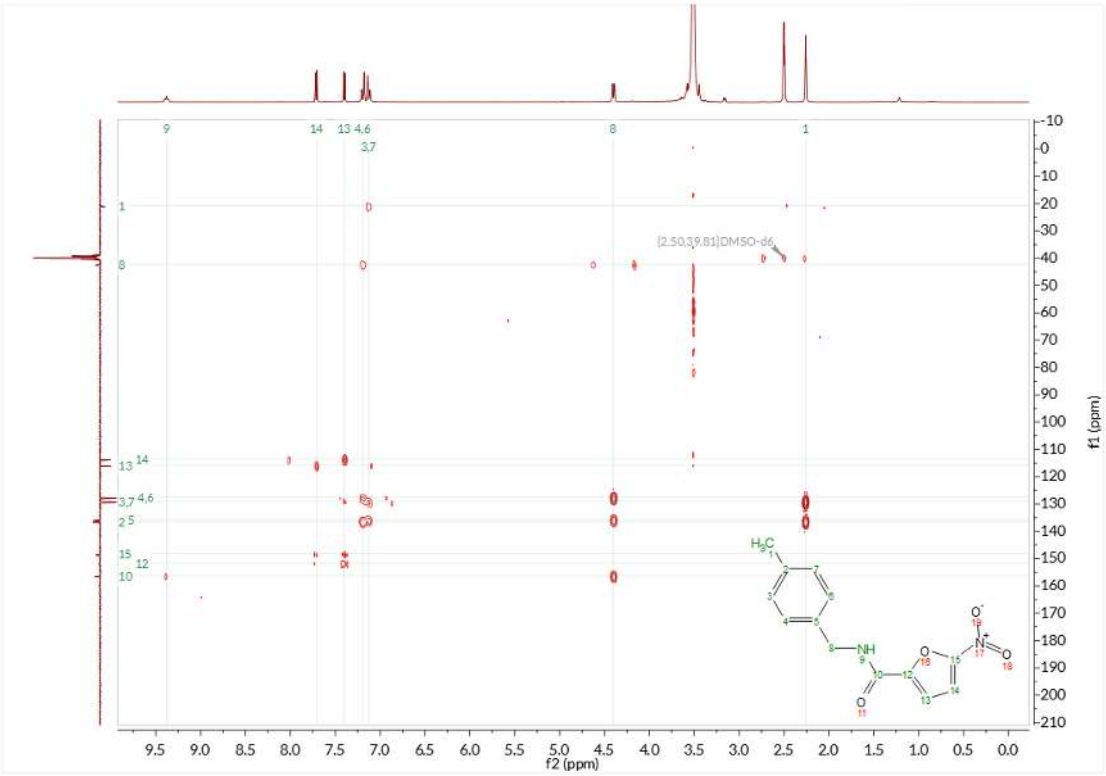

Figure II.21 | Compound 7c' ^{1}H – ^{13}C HMBC spectra

separated by 2 to 4 bonds to those three hydrogens. Using the same logic, the signal at δ = 136.4 ppm, that has a peak with hydrogens **(1), (3),** and **(7),** can be assigned to carbon **(2)**; the signal at δ = 148.4 ppm, that has a peak with hydrogens **(14)** and **(13)**, can be assigned to carbon **(15)**; the signal at δ = 151.6 ppm, that has a peak with hydrogen **(13)**, can be assigned to carbon **(12);** and the signal at δ = 156.3 ppm, that has a peak with hydrogens **(8)** and **(9)** can be assigned to carbon **(10).** Analysing the ^{13}C NMR APT, the signal for all quaternary carbons **(2)**, **(5)**, **(10), (12),** and **(15)** are yielded positive, as expected. Furthermore, all carbon signals are in the usual chemical shift ranges for their functional groups [δ = 110-160 ppm for aromatic carbons and δ = 150-175 ppm for amides].

Other expected couplings can also be observed in the HMBC spectra, confirming the hydrogen and carbon attribution. Carbon **(1)** couples with hydrogens **(3)** and **(7)** (separated by 3 bonds), carbon **(8)** couples with hydrogens **(4)** and **(6)** (separated by 3 bonds), carbon **(14)** couples with hydrogen **(13)** (separated by 2 bonds), carbon **(13)** couples with hydrogen **(14)** (separated by 2 bonds), carbons **(4)** and **(6)** couple with hydrogens **(3), (7)** and **(8)** (separated by 2, 2, and 3 bonds, respectively), and carbons **(3)** and **(7)** couple with hydrogens **(1), (4)** and **(6)** (separated by 3, 2, and 2 bonds, respectively).

Chapter III

Evaluation of physicochemical and pharmacokinetic properties

Chapter III – Evaluation of physicochemical and pharmacokinetic properties

The evaluation of physicochemical and pharmacokinetic properties is an essential task in drug design and drug development, and it is necessary for regulatory approval. A drug physicochemical and pharmacokinetic properties underlie all aspects of its action and can impact its safety, efficacy, and toxicity. [90]

III. 1. Solubility Assessment

Aqueous solubility is an important parameter in drug development. The lack of aqueous solubility is correlated with poor absorption and subsequently low bioavailability. Thus, drugs with low solubility frequently require to be administrated in higher doses to assure the therapeutical plasma concentration. Additionally, compounds with low aqueous solubility are difficult to evaluate on *in vitro* and *in vivo* biological assays, as the precipitation of these compounds leads to an alteration of the compound concentration, originating erratic and erroneous results. [91], [92] So, given the importance of aqueous solubility in drug development, this parameter was determined using a method previously developed in our group [93], using HPLC analysis.

Initially, to establish an adequate wavelength for the HPLC analysis, UV spectra were recorded for compounds **7a, 7b, 7c', 8a, 8b,** and **8c**. Unfortunately, during this experiment, compounds **7a, 7b, 8a,** and **8b** were found to be degraded both in solution and solid samples. The compounds presented additional spots in the TLC and multiple peaks in the HPLC chromatogram. Unfortunately, due to time constrains, it was not possible to repeat the synthesis of these compounds and thus, further analyses were only performed in compounds **7c'** and **8c**. In **Figure III.1,** the UV spectra of compounds **7c'** and **8c** are presented.

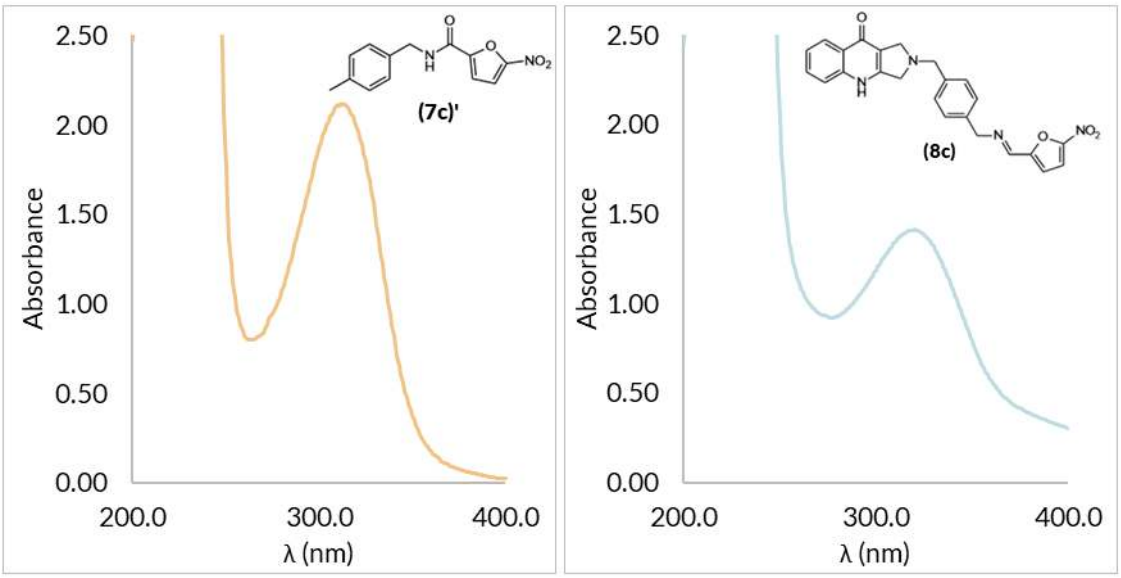

Figure III.1 | UV spectra of compounds 7c' and 8c.

In order to quantify the compounds' aqueous solubility, a calibration curve was first plotted to confirm the linear relation between the compound concentration and the area of the peak observed in the HPLC chromatogram. The calibration curves were plotted using solutions with different concentrations of each compound in dimethyl sulfoxide (DMSO) and are presented in **Annex 1 – Calibration Curves.**

To determine the aqueous solubility, a solution of each compound in PBS was used. PBS is an isotonic pH buffer (pH ~7.4) that matches the osmolarity and ion concentration found on the human body and is commonly used in biological research. In order to validate the method, salicylic acid was used as an external standard, due to its high aqueous solubility. The values obtained in the assay are presented in **Table III.1,** together with calculated physicochemical properties.

Table III.1 | Physicochemical properties and solubility of compounds 7c' and 8c.
Physicochemical properties were calculated using the Molinspiration Property Calculation Service [© Molinspiration Cheminformatics 2022], available on https://www.molinspiration.com/. Aqueous solubility was measured at 37 ºC.

Compound	(7c')	(8c)	Salicylic Acid
Structure	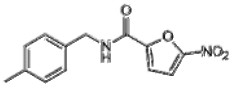	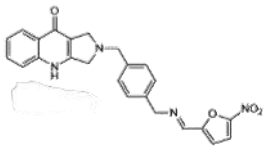	
Physicochemical Properties	MW = 260.25 Da log P = 2.32 TPSA = 86.25 Å^2 HBA = 6 HBD = 1	MM = 428.45 Da log P = 2.45 TPSA = 107.43 Å^2 HBA = 8 HBD = 1	-
Solubility (μM)	>200	193.3	>200

Ordinarily, a drug candidate should have an aqueous solubility higher than 10 μM to simplify preclinical trials. [91] Both compound **7c'** and **8c** have shown significantly higher aqueous solubility, with compound **7c'** showing an aqueous solubility higher than the method's limit (200 μM). Thus, further development of these compounds is not expected to be hampered by solubility issues.

Additionally, both compounds have no violations of the Lipinski's rule of five[1], and thus are expected to have a good oral bioavailability, a key indicator of drug absorption. Moreover, both compounds have a total polar surface area (TPSA) inferior to 140 Å^2, and thus are expected to be able to permeate cell membranes. Together with the high aqueous solubility, it is expected that these compounds will be well absorbed and be able to reach their pharmacological concentration in the systemic circulation and their cellular targets.

[1] The Lipinski's rule of five states that, in general, an orally active drug has no more than one violation of the following criteria: no more than 5 hydrogen bond doners (HBD), no more than 10 hydrogen bond acceptors (HBA), a molecular mass (MM) less than 500 Daltons, and a calculated octanol-water partition coefficient (log P) that does not exceed 5.

III. 2. Stability in Physiological Conditions

Chemical stability is an important property of drug candidates and impacts greatly the drug discovery and drug development processes. Chemical degradation can significantly lower the drug's intended dose and thus, lead to poor bioavailability due to pre-systemic loss of the active pharmaceutical ingredient, and consequently result in insufficient therapeutic efficacy. Furthermore, drug decomposition can generate toxic metabolites that cause adverse side effects. [94]

Due to the associated financial and temporal costs on discovering instability problems in late drug development process, stability studies are generally performed during drug discovery and early drug development stages. In drug discovery, stability of the active pharmaceutical ingredient in solution state is the main focus, typically in short term, in hours or days. [94] Given the importance of drug stability in drug discovery, the stability in physiological conditions was determined using a method optimized in our group, via HPLC analysis.

To evaluate the physiological stability, compounds were incubated in PBS buffer at 37 ºC (conditions that simulate physiological conditions), and samples were periodically taken and analysed by HPLC. The peak area of the HPLC chromatogram was already demonstrated to be linearly correlated with the drug concentration (see **Annex 1 – Calibration Curves.**) and thus, observed alterations in peak areas over time correlate with an alteration in drug concentration.

In a simplified degradation model, as the one presented in **Figure III.2**, the degradation process follows a pseudo-first order kinetic, where the active compound molecule is converted in one or more degradation products. In this scenario, the disappearance rate of the compound is given by equation **(1)**, where k is the pseudo-first order constant. By rearranging the former equation, the relation between concentration of active compound and time can be expressed (equation **(2)**). Finally, the half-life ($t_{1/2}$), i.e., the time required for a quantity to reduce to half of its initial value, can be calculated using equation **(3)**, derived from the application of the half-life definition in equation **(2)**.

$$\mathbf{A \rightarrow Degradation\ Products}$$

$$(\mathbf{1}) \; -\frac{d[A]}{dt} = \; v = k \times [A]$$

$$(\mathbf{2}) \; \ln[A] = \; \ln[A]_0 - k \times t \; \Leftrightarrow [A] = \; [A]_0 \times e^{-k\,t}$$

$$(\mathbf{3}) \; \text{By definition, when } t = \; t_{1/2}, \text{then } [A] = \frac{1}{2}\,[A]_0 \; \Rightarrow \; t_{1/2} = \frac{\ln(2)}{k}$$

Figure III.2 | Simplified degradation kinetic model with respective relevant equations.

In **Figure III.3,** the graphic representation of the relation between the HPLC chromatogram peak area and incubation times are presented for compounds **7c'** and **8c.** As the peak areas are linearly proportional to the compound concentration, the relation between peak areas and incubation time is equivalent to the relation between compound concentration and incubation time.

Until 96 hours of incubation in PBS, compound **7c'** maintained a stable peak area, with the observed variation being attributed to method errors. Thus, it can be inferred that its concentration is stable during this period, and the compound is stable in

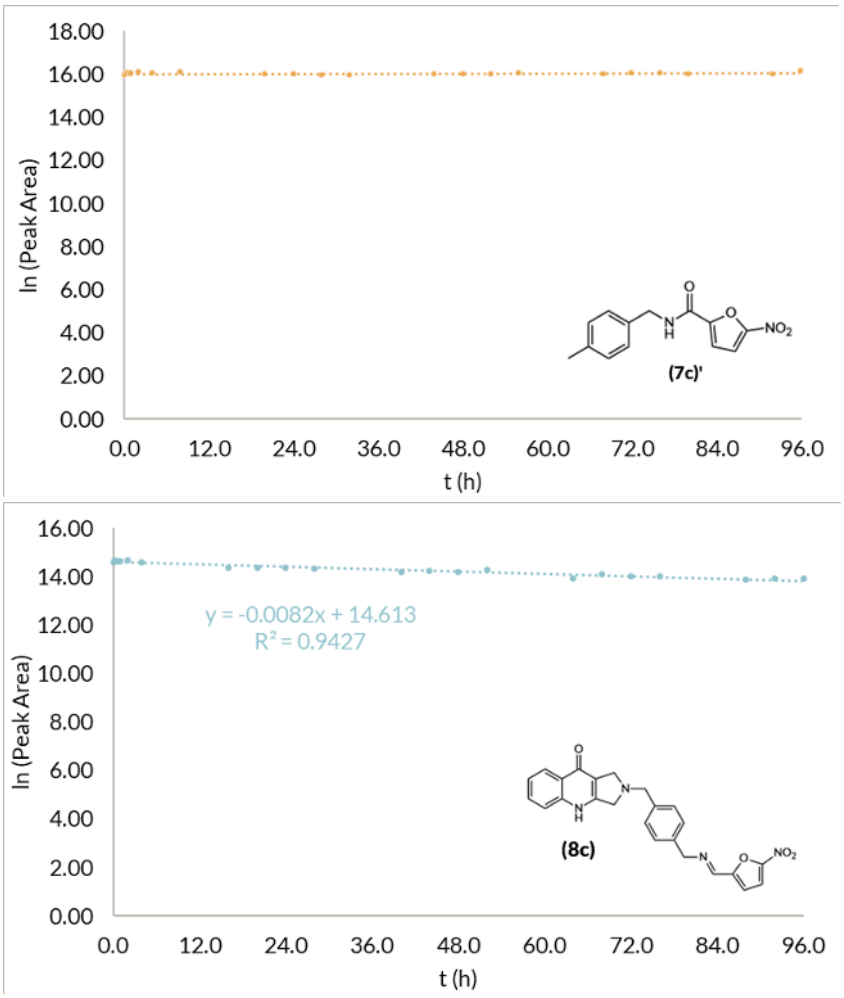

Figure III.3 | **Graphic representation of compound stability in PBS.**
The graphs portray the relation between the natural logarithm of the HPLC chromatogram peak areas and the sample incubation time, in hours.

PBS. In turn, compound **8c** showed a slow decrease in the peak area. Thus, it can be deduced that its concentration has also slowly decreased during the incubation time. Through the equations presented in **Figure III.2**, one can determine the observed disappearance rate (k_{obs}) and the half-life, 0.0082 h^{-1} and 84.3h, respectively. The most common degradation pathways involve hydrolysis, hydration, oxidation, intramolecular cyclization, photolysis, and racemization. As imines are more susceptible to hydrolysis than amides, it was not surprising that the imine **8c** showed to be less stable than the amide **7c'**.

Most drugs reach their highest concentration in blood after one or two hours if administrated by oral route and seconds to minutes if administrated by intravenous route; and are eliminated from the organism to untraceable levels in 1 to 3 days. As both compounds **7c'** and **8c** have half-lives higher than 3 days, further development of these compounds is not expected to be hampered by issues regarding poor chemical stability.

III. 3. Stability in Human Plasma

Once a drug enters into the systemic circulation, either by absorption (oral route) or direct administration (intravenous route), it must be distributed through the organism to its target cells. Drug distribution is mediated by blood and thus, drug stability in plasma has an important role in drug discovery and drug development. [95]

Human plasma contains a high number of hydrolytic enzymes and therefore, compounds with functional groups such as esters, amides, lactones, lactams, carbamides, sulphonamides, and peptidomimetics, are more susceptible to degrade in plasma through hydrolysis. Aside prodrugs, where a rapid conversion to the active drug in plasma is desirable, drugs that rapidly degrade in plasma generally have a rapid clearance and short half-life, resulting in poor *in vivo* efficacy, as the minimal pharmacologically active dose may not be attained, or the drug may not be able to reach its pharmacological target. Additionally, drugs that bind to plasma proteins also have their efficiency compromised, as the less bound a drug is, the more efficiently it can traverse or diffuse through cell membranes. Plasma stability assays have multiple applications in drug discovery, such as prioritize compounds for *in vivo* studies, screen pro-drugs, and alert investigation teams to labile structural motifs. [95] Given the importance of plasma stability in drug discovery, the drug stability in human plasma was determined via HPLC analysis.

To evaluate the plasma stability, compounds were incubated in human plasma [80% (v/v) in PBS] at 37 ºC, and samples were periodically taken and analysed by HPLC. As stated in the previous subchapter, the drug degradation process can be modelled by a pseudo-first order kinetic model, as the one presented in **Figure III.2.** In **Figure III.4**, the graphic representation of the relation between the HPLC chromatogram peak area and incubation times are presented for compounds **7c'** and **8c**.

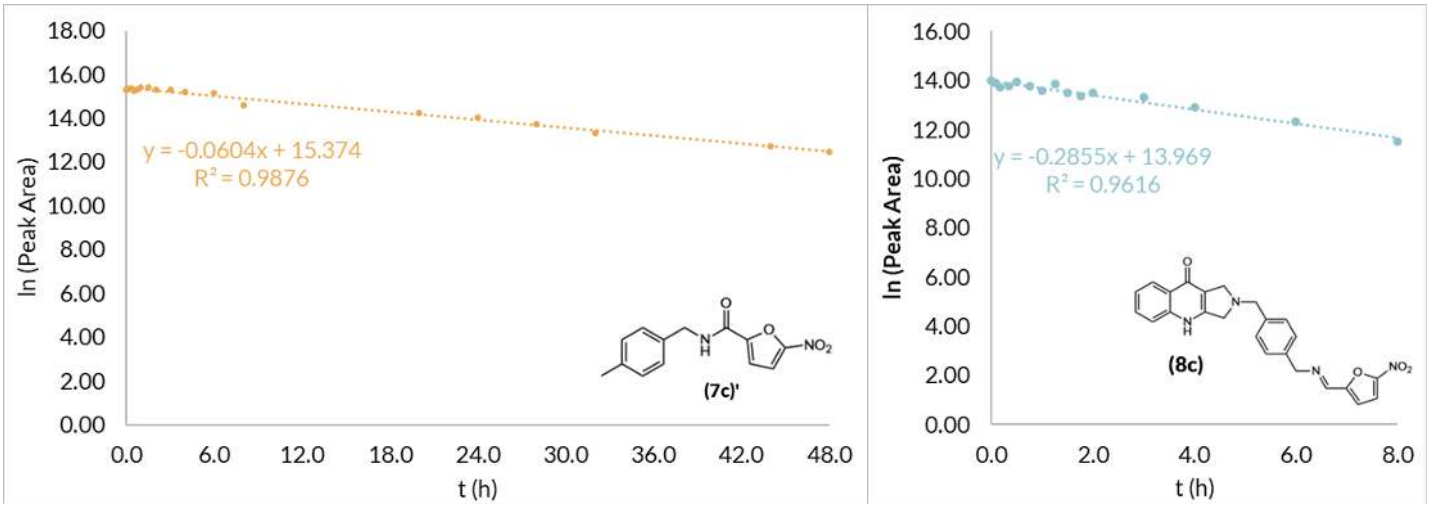

Figure III.4 | Graphic representation of compound stability in human plasma.
The graphs portray the relation between the natural logarithm of the HPLC chromatogram areas and the sample incubation time, in hours.

Both compounds **7c'** and **8c** showed a continuous decrease in the chromatogram peak areas. Through the equations presented in **Figure III.2**, the observed disappearance rate and the half-lives for both compounds can be determined: 0.0604 h^{-1} and 11.5h for compound **7c'** and 0.2855 h^{-1} and 2.43h for compound **8c**, respectively.

Both compounds show significantly lower half-lives in plasma compared to the PBS buffer and thus, it can be inferred that both compounds are degraded by plasma enzymes. This result is expected as human plasma contains amidases and non-specific esterases capable of hydrolysing amides, and dehydrogenases capable of reducing imines [95], [96].

As previously stated, most drugs reach their highest concentration in blood after one or two hours if administrated by oral route and seconds to minutes if administrated by intravenous route. Although the average circulation time of blood is 1 minute, as drugs penetrate different tissues at different speeds, depending on the drug's ability to cross membranes, drugs can remain in blood circulation for several days until they are eliminated. Although there are some approved orally administered drugs with active pharmaceutical ingredients with *in plasma* half-lives of around a hour, an in plasma half-time of 1.5 hours is recommended to ensure traceable compound quantities in the typical drug discovery studies (6 hours studies). [95] Thus, as both compounds **7c'** and **8c** have half-lives higher than the recommended threshold, further development of these compounds is also not expected to be hampered by issues regarding poor in plasma stability.

III. 4. Metabolic Assays

As soon as a drug enters into the systemic circulation, it begins to be eliminated either by excretion, metabolism, or most commonly, a combination of both. When the rate of these processes surpasses the rate of absorption, the drug plasmatic concentration decreases, and the drug enters its elimination phase. Understanding the drug routes of clearence is a key aspect in drug development, as clearance is a determinant of every pharmacokinetic parameter, such as drug half-time, oral bioavailability and efficacious dose. [97]

Drugs are typically subjected to a variety of biotransformation reactions to form one or more active or inactive metabolites. The formed metabolites can present pharmacological activity and/or toxicity and thus, it is essential not only to assess the extent of metabolism (metabolic stability), but also understand and characterize the principal metabolizing routes (metabolite identification). Given the importance of metabolic stability in drug discovery, the metabolic stability was determined via HPLC analysis.

To evaluate the metabolic stability, compounds were incubated in a mice liver microsomes solution at 37 ºC, and samples were periodically taken and analysed by HPLC. Liver microsomes are vesicles of the hepatocyte endoplasmic reticulum and contain membrane phase I enzymes, such as cytochromes P450, flavine-containing monooxygenases, esterases, amidases, and epoxide hydrolases, and also phase II enzymes, such as glucuronosyltransferases. Thus, liver microsomes can be used to assess the principal phase I and phase II metabolic pathways and are the model of choice for drug metabolism and drug interaction studies.

As stated previously, the drug degradation process can be modelled by a pseudo-first order kinetic model [**Figure III.2.**]. In **Figure III.5**, the graphic representation of the relation between the HPLC chromatogram peak area and incubation times are presented for compounds **7c'** and **8c**.

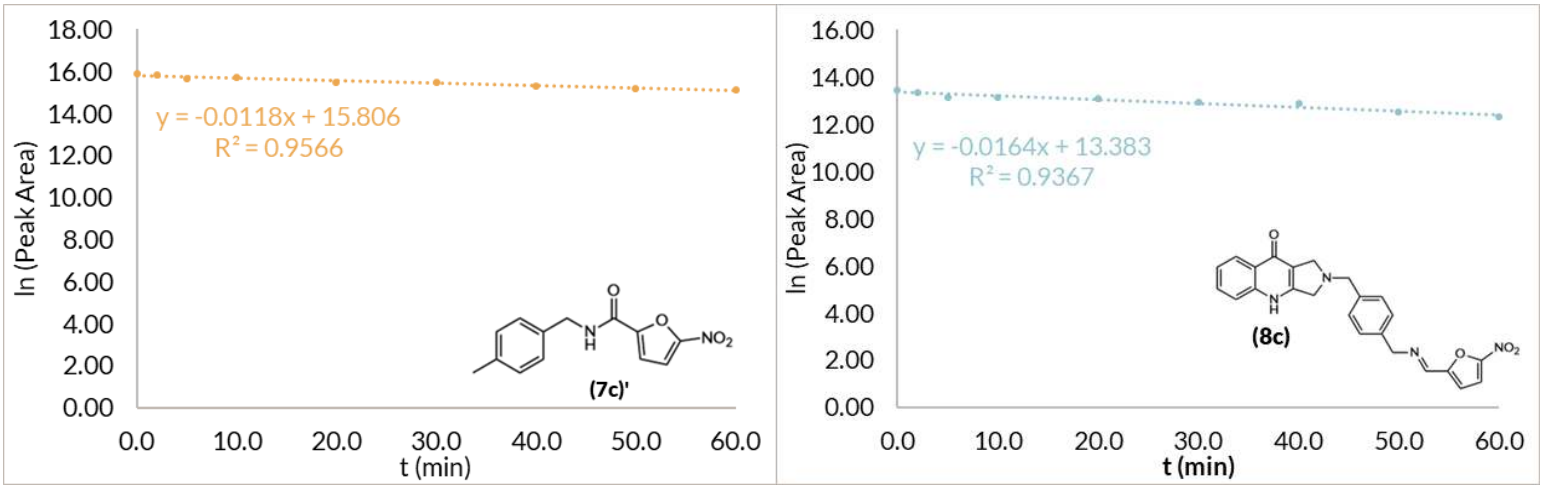

Figure III.5 | Graphic representation of compound metabolic stability.
The graphs portray the relation between the natural logarithm of the HPLC chromatogram areas and the sample incubation time, in minutes.

Both compounds **7c'** and **8c** showed a continuous decrease in the chromatogram peak areas. Through the equations presented in **Figure III.2**, the observed disappearance rate, the half-lives, and the compound reminiscent percentage after 30 min can be determined for both compounds: 0.0118 min^{-1}, 59 min, and 70% for compound **7c'** and 0.0164 h^{-1}, 42 min, and 61% for compound **8c**, respectively.

Both compounds show significantly lower half-lives in the liver microsomes compared to the PBS buffer and thus, it can be inferred that both compounds are metabolized in the liver. This was expected, as besides the presence of amidases and dehydrogenases capable of hydrolysing amides and reducing imines, respectively; both compounds **7c'** and **8c** have multiple positions susceptible to cytochrome P450 metabolism [**Figure III.6**]. For instance, compound **7c'** can be susceptible to α-hydroxylation on the carbon adjacent to the amide, with subsequent cleavage of the C-N bond, hydroxylation on the non-sterically hindered methyl group, and aromatic hydroxylation, while compound **8c** can be susceptible to various α-hydroxylations on the carbons adjacent to the amine, with subsequent cleavages of the C-N bond, and aromatic hydroxylation. Nonetheless, a metabolite identification study would be required to identify the formed metabolites. [98]

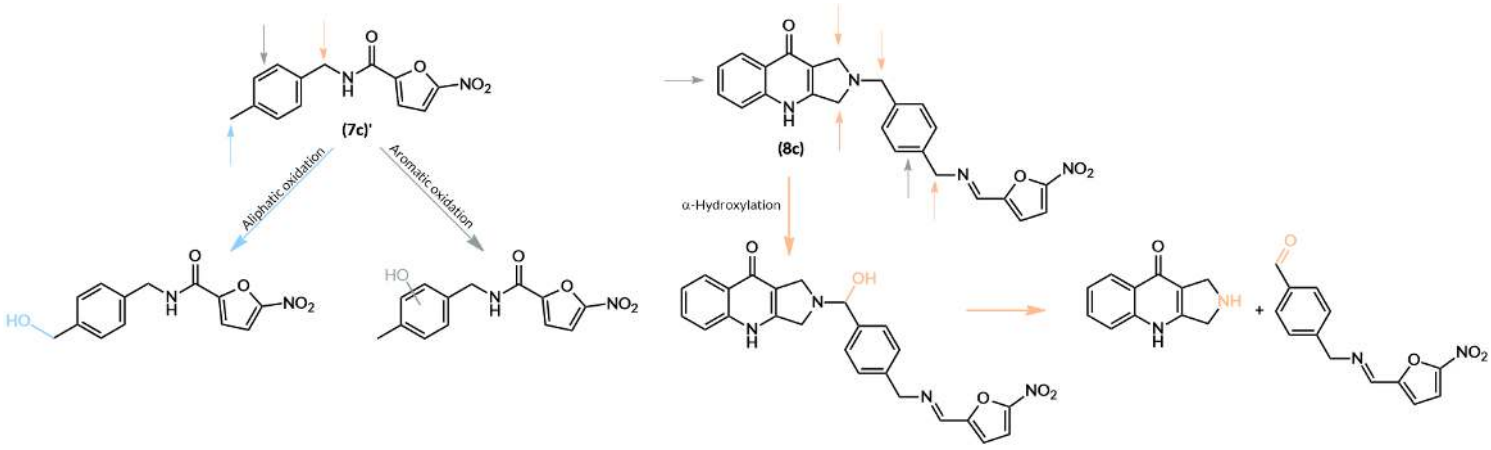

Figure III.6 | Predicted metabolizable positions in compounds 7c' and 8c
Each coloured arrow signals a position susceptible to cytochrome P450 metabolism, with each colour corresponding to a type of metabolization. An example of the predicted metabolites is given for each type of metabolization.

The intrinsic clearence (CL_{int}) is the ability of the liver to remove a drug in the absence of flow limitations and binding of a drug to cells or proteins in the blood. With the exception of pro-drugs, very highly cleared compounds are undesirable, as they are likely to be rapidly cleared *in vivo*, resulting in a short duration of action. The intrinsic clearance can be written in function of the observed metabolic elimination constant, and the concentration of the catalytic enzymes in the incubation solution, as it is described in **Figure III.7**.

$$\mathrm{CL_{int}} = \frac{\text{Incubation Volume}}{\text{Enzyme Mass}} \times \mathrm{k_{obs}}$$

Figure III.7 | Relation between Intrinsic Clearance, elimination constant and enzyme concentration

Through the equation described above, the intrinsic clearance can be determined for both compounds: 23.7 $\mu L min^{-1} mg^{-1}$ for compound **7c'** and 33.0 $\mu L min^{-1} mg^{-1}$ for compound **8c**. Compounds can be characterized into low, medium, or high clearance according to their intrinsic clearance. For rat liver microsomes, drugs are considered to have a high clearance if their intrinsic clearance is superior to 86.1 $\mu L min^{-1} mg^{-1}$ and a low clearance if their intrinsic clearance is inferior to 15.8 $\mu L min^{-1} mg^{-1}$. [99] Thus, both compounds **7c'** and **8c** have medium clearence, meaning further development of these compounds is not expected to be hampered by issues regarding poor metabolic stability.

III. 5. Comparative Analysis

IUPAC defines pharmacokinetics as the "process of the uptake of drugs by the body, the biotransformation they undergo, the distribution of the drugs and their metabolites in the tissues, and the elimination of the drugs and their metabolites from the body over a period of time". The study of pharmacokinetics revolves on determining the fate of an administered substance, involving absorption, distribution, metabolism, and excretion.

Compounds **7c'** and **8c** presented a good pharmacokinetic profile, summarized in **Table III.2**, with compound **7c'** showing to have higher chemical, in plasma, and metabolic stability. Analysing the structures of both compounds, two possible explanations can be proposed based on the compounds key differences: compound **7c'**'s higher stability is due to the higher chemical stability of the amide bond compared to the imine bond; compound **7c'**'s higher stability is due to not having the PYQ scaffold; or compound **7c'**'s higher stability results from a combination of the two aforementioned factors.

In order to evaluate the influence of the PYQ scaffold on the compound stability, the pharmacokinetic properties of compounds **7c'** and **8c** were compared with two hybrid compounds [**Table III.2**] already developed in our research group. [100]

Table III.2 | Physicochemical and pharmacokinetic properties of developed hybrid compounds. Physicochemical properties were calculated using the Molinspiration Property Calculation Service [© Molinspiration Cheminformatics 2022], available on https://www.molinspiration.com/. Compounds with the shaded background had already been developed in our research group and reported [100].

Compound	Physicochemical Properties	$t_{1/2}$	Solubility (μM)
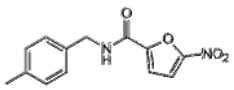	MW = 260.25 Da log P = 2.32 TPSA = 86.25 Å^2 HBA = 6 HBD = 1	stable (PBS) 11.5 h (human plasma) 59 min (liver microsomes)	>200
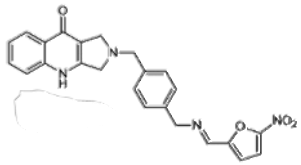	MM = 428.45 Da log P = 2.45 TPSA = 107.43 Å^2 HBA = 8 HBD = 1	84.3 h (PBS) 2.4 h (human plasma) 42 min (liver microsomes)	193
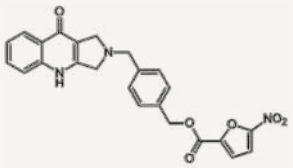	MW = 445.43 Da log P = 2.64 TPSA = 121.37 Å^2 HBA = 9 HBD = 1	70.7 h (PBS) stable (human plasma) 88 min (mice microsomes)	115
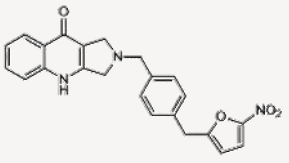	MW = 401.42 Da log P = 3.18 TPSA = 95.06 Å^2 HBA = 7 HBD = 1	stable (PBS) 6.0 h (human plasma) 35 min (mice microsomes)	>200

The three analysed hybrid compounds vary solely on the connection between the nitrofuran scaffold and the benzyl linker: compound **8c** has an imine bond, while the other two compounds have respectively an ester bond and a carbon-carbon bond. Comparing the stability of compound **7c'** with the stability of the hybrid compounds, no correlation can be drawn between the absence of the PYQ scaffold and an increase of stability: while the hybrid compound with a carbon-carbon bond is as chemically stable as compound **7c'**, the hybrid compound with an ester bond showed to have higher in plasma and metabolic stability than compound **7c'**.

Furthermore, all three hybrid compounds presented good pharmacokinetic profiles, with good chemical, in plasma, and metabolic stability, and are expected to have a good bioavailability, as all have no violations of the Lipinski's rule of five, a total polar surface area inferior to 140 $Å^2$, and a high aqueous solubility.

Chapter IV

Biological Evaluation

Chapter IV – Biological Evaluation

The biological evaluation is the most crucial step in drug design and drug development. While activity assays measure the potency of a drug pharmacological activity and are used in most random screenings to begin the drug design process, cytotoxicity assays measure the ability of a compound to cause cell damage or cell death and therefore, their selectivity.

IV. 1. Antimycobacterial Screening

The antimycobacterial screening was performed in the Molecular Mycobacteriology Research Unit (MMRU) at the Faculty of Health Sciences, University of Cape Town, South Africa.

Mtb is a slow-growing bacterium [duplication time: 18 to 24 hours], that can be successfully cultured *in vitro*, using highly nutritious media and aerobic conditions, both in solid and liquid media. In this screening, two different strains were used: *M. tuberculosis* H37Rv pMSp12:GFP and *M. tuberculosis* cydKO pMSp12:GFP, two fully virulent bioreporter mutant strains, resulting from the insertion of a plasmid vector with two reporter genes (*gfp and kan)* in a H37Rv and a cytochrome bd knockout strain, respectively. The *gfp* gene encodes the green fluorescent protein and allows to measure the mycobacterial growth based on the emitted fluorescence, which is proportional to the bacterial concentration. By accounting the minimum and maximum growth control as 100% and 0% inhibition, respectively, a relation between the emitted fluorescence and percentage of inhibition can be made. The *kan* gene encodes resistance to kanamycin. The addition of this antibiotic to the media allows a selective elimination of any mycobacteria that does not have the plasmid vector incorporated. [101], [102]

The antimycobacterial screening was performed using two different media, both containing a Middlebrook 7H9 broth base supplemented with glucose as a carbon source. The first medium was also supplemented with bovine albumin, dextrose, and catalase (ADC), and Tween 80 (Tw). Albumin neutralizes hydrophobic toxins that may form in the mycobacterial growth, dextrose provides another carbon source, catalase promotes the decomposition of hydrogen peroxide, and Tw is a non-ionic detergent that minimizes mycobacterial clumping during growth. The second media was a minimal medium, without albumin. In compounds with high affinity for serum proteins, a high binding to albumin interferes with the result of the assay, and thus, this minimal medium allows for a screening with full compound availability. The minimal medium was supplemented with casitone (CAS), sodium chloride, and tyloxapol (Tx). Casitone is an enrichment supplement with a high content of amino acids and peptides, sodium chloride promotes osmotic balance, and Tx is a non-ionic polymer used as a surfactant with the same function as Tw. [101]

Results were reported at days 7 and 14. Mycobacterial growth increases logarithmically until day 6 and enters a stationary phase afterwards. Results from both timepoints were compared, and when no significant differences were observed, the result from day 14 was considered as the final MIC_{90}. Rifampicin, a first-line drug in anti-TB therapy, was used as a positive control. Results from the antimycobacterial screening are presented in **Table IV.1**.

Table IV.1 | Antimycobacterial activity in two growth media against Mtb H37Rv and Mtb cydKO. Compounds with the yellow shaded background are commercial reagents, the compound with the pink shaded background had already been developed in our research group and reported [100], and the compound with the blue shaded background, rifampicin, was used as a positive control.

		MIC_{90} (µM)			
Compound		***M. tuberculosis* H37Rv**		***M. tuberculosis* cydKO**	
		7H9 CAS GLU Tx	**7H9 ADC GLU Tw**	**7H9 CAS GLU Tx**	**7H9 ADC GLU Tw**
(5a)	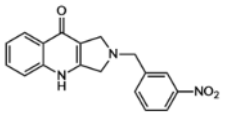	> 125	> 125	62.5	1.887
(5b)	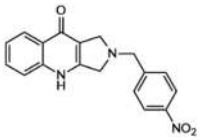	62.5	> 125	0.488	0.974
(6a)	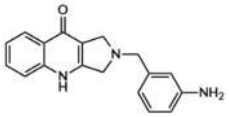	> 125	> 125	22.362	> 125
(6b)	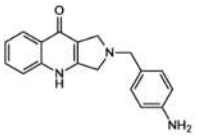	125	> 125	15.625	> 125
(6c)	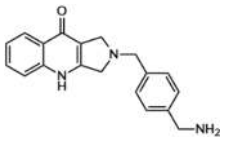	15.135	> 125	62.5	> 125
	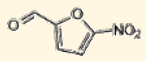	8.216	31.25	not determined	not determined
	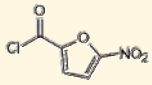	125	> 125	not determined	not determined
(7c')	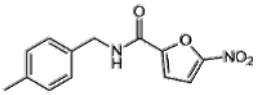	0.343	0.511	< 0.244	0.587
(8c)	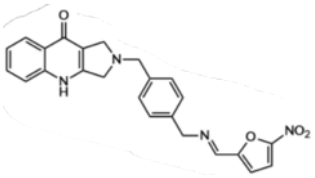	1.922	15.800	1.953	6.171
	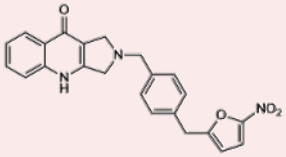	3.385	15.625	2.797	7.845
Rifampicin	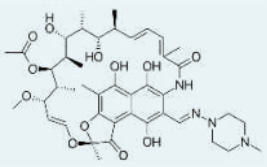	0.015	0.002	0.019	0.001

Despite the reduced number of screened compounds, by analysing the results presented in **Table IV.1**, some interesting conclusions can be drawn. First, by comparing the activity results in both media, a general trend can be observed that compounds show to be more active in the medium without ADC. While in most compounds the difference is not substantial, in some cases [for example, compounds **6a** and **6b** in the Mtb cydKO strain and compound **6c** and **8c** in the Mtb H37Rv strain] the activity is decreased over 5-fold in the medium supplemented with ADC. These differences may be attributed to compound binding to the supplemented bovine albumin, thus decreasing their availability in the media. Human albumin is almost identical to its bovine counterpart, and it is the predominant protein in human plasma. Albumin is known to bind to peptides, proteins, fatty acids, and small organic compounds, through non-covalent binding. As stated previously, drugs that bind extensively to plasma proteins have their efficiency compromised, as the more bound a drug is, the less efficiently it can traverse or diffuse through cell membranes. However, to a certain extent, binding to plasma proteins can increase a drug efficiency, by decreasing their clearance, as the drug fraction bound to the protein is less susceptible to degradation and can be later released as the free fraction diminishes. While compounds **7c'** and **8c** already had their stability in plasma assessed, further studies regarding the protein binding effect would be interesting, focusing on its extension and reversibility. [101], [103]

Second, by comparing compound **5a** with **5b** and compound **6a** with **6b**, a trend can be observed that compounds with a substituent in the *para* position of the aromatic ring are more active that compounds with the same substituent in the *meta* position. These differences may be indicative of the interactions between the compound and the target's active site. A computational approach, like molecular docking, would be an interesting approach to do a preliminary study regarding the interactions between these compounds and the proposed target, and could direct an expansion of the compound library to further develop a structure-activity relation.

Third, intermediate compounds **5a, 5b, 6a,** and **6b** show to be more active in the Mtb cydKO strain, with compound **5b** showing an over 100-fold activity increase comparing with the H37Rv strain. On the contrary, compound **8c**, as well as the other tested hybrid compound, showed very similar activities in both strains. These results were expected and corroborate the proposed hypothesis. The intermediate compounds only possess the PYQ scaffold and thus, were only expected to inhibit cyt bc_1-aa_3. Thus, it was expected that these compounds showed low or no inhibition in the Mtb H37Rv strain, as even with the cyt bc_1-aa_3 inhibited, the bacteria can survive by using cyt bd as the terminal oxidase. However, as the Mtb cydKO strain does not express cyt bd, the inhibition of cyt bc_1-aa_3 in this strain results in an effective disruption of the ETC and thus, the compounds show higher, and in the case of compound **5b** sub-micromolar inhibition. The hybrid compounds possess both scaffolds and thus were expected to inhibit both terminal cytochromes. Thus, it was expected that these compounds showed similar inhibitions for both strains. Nonetheless, and despite these results corroborating the proposed hypothesis, further biological studies, like enzymatic or ATP depletion assays are required to establish the compound target.

Fourth, hybrid compound **8c** showed to be an interesting drug candidate, with a potent, micromolar inhibition, and higher activity than both its parts (compound **6c** and the commercial furaldehyde). Additionally, both hybrid compounds show to be

significantly more active than the nitro intermediates **5a** and **5b** in the Mtb H37Rv strain. This result indicates that the furan ring might be necessary for activity and is concordant with the proposed hypothesis and available literature. As stated previously, the Mtb intracellular nitroreductases rapidly reduce nitro groups in heteroaromatic rings *in vivo*, with the release of NO. Thus, as the nitro group in compounds **5a** and **5b** is not in a heteroaromatic ring, it was expected the Mtb nitroreductases had low or no reductase activity in those compounds and consequently, that those compounds do not present activity through NO toxicity. A nitric oxide assay with these compounds would be an interesting following study, to assess in what extent the nitro groups in compounds **5a** and **5b** are reduced *in vivo*.

Finally, compound **7c'** showed to be our most active compound, with potent, sub-micromolar activity across both tested strains and in both tested media. This result was unexpected, as compound **7c'** does not possess the PYQ scaffold, one of compounds' pharmacophores, hypothesized to be active in cyt bc_1-aa_3. Considering this, it can be hypothesized that compound **7c'** shows activity due to a mechanism of general toxicity. Alternatively, compound **7c'** may show activity due to a novel mechanism of action, which would make it a very interesting lead compound to a novel class of drugs. A toxicity assay would be a crucial following study, to assess the antimycobacterial potential of compound **7c'.**

IV. 2. Cytotoxicity studies

The cytotoxicity studies were performed in the Research Institute for Medicines (iMed.ULisboa), Faculty of Pharmacy, Universidade de Lisboa.

The cytotoxicity of compounds **6c, 7c',** and **8c** was evaluated in HEK293 cells, a human immortalized cell line widely used in cell biology and biotechnology, because of their reliable growth and propensity for transfection. Cell viability was determined through a MTT assay for two different compound concentrations after incubation for 48 hours. Results are expressed as a percentage of viable HEK293 cells and are presented in **Table IV.2**.

Table IV.2 | Compound cytotoxicity in HEK293 cells.
MIC_{90} values are for activity against Mtb H37Rv, in 7H9 CAS GLU Tx media.

Compound		HEK293 cell viability (%)		MIC_{90} (µM)
		20 µM	50 µM	
(6c)	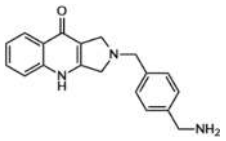	99	92	15.135
(7c')	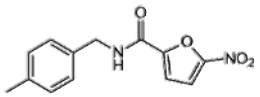	100	92	0.343
(8c)	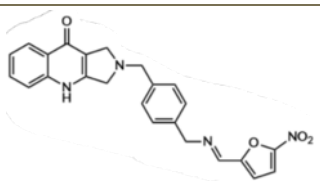	26	22	1.922

While compounds **6c** and **7c'** showed to be non-cytotoxic, compound **8c** displayed some cytotoxicity. This result was surprising, as compound **8c**'s scaffolds are present on either compound **6c** or compound **7c'**, both of them non-cytotoxic, suggesting the cytotoxicity results from the combination of both scaffolds. The 50% cytotoxicity concentration, CC_{50}, was not determined for the compounds and thus, it is not possible to calculate a selectivity index. Nevertheless, by comparing the activity and cytotoxicity of compound **8c**, it is notable that compound **8c** has some selectivity for the Mtb and thus, there may be a pharmacological window. A determination of the CC_{50} would be a crucial following step, in order to determine the selectivity of compound **8c**.

Considering these results, compound **7c'** presents itself as a surprisingly interesting lead molecule. The compound presented sub-micromolar antimycobacterial activity, no cytotoxicity, and a good pharmacokinetic and physicochemical profile. Furthermore, the compound is a small molecule expectedly easy to synthesize, from just one reactional step between commercial reagents (4-methylbenzylamine and 5-nitro-2-furoyl chloride), with the possibility of adding different moieties for activity optimization, without an expected loss of their physicochemical properties.

Chapter V

Conclusions and Future Perspectives

Chapter V – Conclusions and Future Perspectives

Anti-TB therapeutical regimens are ineffective against latent bacilli and thus require long durations and a high pill burden, with consequent long-term cumulative adverse effects, to ensure complete elimination of latent Mtb bacilli and avoid relapses. Consequently, anti-TB therapy has a low patient compliance and acceptance, that results on the emergence of DR-TB, which has a higher lethality and lower treatment success.

Therefore, to control tuberculosis, it is essential to develop a potent and short anti-TB regimen efficient in treating all forms of the disease. To achieve this, it is crucial to develop new drugs active against drug resistant strains with activity in new, unexplored targets and pathways and drugs that effectively address latency.

This thesis reports the synthesis, *in vitro* pharmacokinetic and biological evaluation of hybrid compounds, developed to effectively target the mycobacterial bioenergetics, by inhibiting both Mtb cyt bc1-aa3 and cyt bd. In this project, a small library of hybrid compounds was synthesized, and the synthetic route was optimized. Compounds were characterized through structural elucidation techniques (^{1}H NMR, ^{13}C NMR, MS).

Hybrid compound **8c** presented a good pharmacokinetic profile, with high chemical, plasmatic, and metabolic stability. Furthermore, the compound presented a good aqueous solubility, and its predicted physicochemical properties indicate the compound may have a good bioavailability. Additionally, compound **8c** has low micromolar activity against Mtb, and has some selectivity for the mycobacteria. Thus, and considering previously reported results, compound **8c** and these hybrid compounds in general appear to be promising anti-TB pharmacological agents.

Despite an elucidation of the hybrid compounds' action mechanism was not made, the activity results corroborate the proposed mechanism of action that the hybrid compounds target both Mtb cytochromes and that the nitro group requires an heteroaromatic ring to exert its inhibition.

The nitrofuranylamide **7c'** presented itself has a very interesting lead molecule for anti-TB therapy, with a sub-micromolar MIC value, no cytotoxicity, and a good pharmacokinetic (chemical, plasmatic and metabolic stability) and physicochemical profile. While some nitrofuranylamides have already been reported as promising anti-TB agents, with micromolar or sub-micromolar activities [104], [105], to the best of our knowledge, no report of the nitrofuranylamide **7c'** or the pharmacokinetic profiling of a nitrofuranylamide has been made.

Future steps to continue this project include activity assays in other pathogens to assess selectivity, the pharmacokinetic and biological evaluation of the remaining hybrid compounds, and the extension of the library compound.

Chapter VI

Experimental Procedure

Chapter VI – Experimental Procedure

This chapter describes the experimental work on the synthesis and characterization of all final and intermediate compounds; the evaluation of their molecular properties (lipophilicity and solubility); and the stability, activity, and metabolic studies. Detailed information about the materials and equipment used, experimental procedures, and characterisation techniques are given.

VI. 1. Materials

VI. 1. 1. Reagents and Solvents

All reagents and solvents used in this master thesis were commercial, purchased from Alfa Aesar (www.alfa.com/pt/), Fluorochem (www.fluorochem.co.uk/), Sigma-Aldrich (www.sigmaaldrich.com/PT/en), TCI (www.tcichemicals.com/PT/en), and Thermo Fisher (www.fishersci.pt/), unless stated otherwise. The water used in synthetic, isolation and purification procedures, was distilled and purified using a Direct-Q® 3 UV Water Purification System (Millipore).

For NMR spectra, samples were prepared in commercial deuterated solvents, namely chloroform-d ($CDCl_3$), methanol-d_4 (MeOD), acetone-d_6 and DMSO-d_6, with a purity degree higher than 99%, purchased from Sigma-Aldrich.

For UV experiments and assays that resorted to HPLC experiments, deionized water, acetonitrile [Chem-Lab, HPLC grade (>99.9%)], and methanol [J.T. Baker, HPLC grade (>99.9%)] were used. The water was deionized and purified using a Direct-Q® 3 UV Water Purification System (Millipore).

VI. 1. 2. Equipment

The NMR spectra (mono and bidimensional) were recorded using a Bruker Ultra-Shield 300 MHz or a Bruker 300 MHz Avance II™ NMR spectrometer. The NMR spectrometers are part of the National NMR Network (PTNMR) and are partially supported by Infrastructure Project Nº 022161 (co-financed by FEDER through COMPETE 2020, POCI and PORL and FCT through PIDDAC). Chemical shifts are presented in parts per million relative to tetramethylsilane and coupling constants are expressed in Hertz. Peak multiplicities are given as: singlet (s), doublet (d), doublet of doublets (dd), doublet of triplets (dt), doublet of doublets of doublets (ddd), triplet (t), triplet of doublets (td), multiplet (m).

Mass spectra analysis were performed using an HPLC equipment, model Waters Alliance 2695 Separation Module (Waters®, Ireland), consisting of a quaternary pump system, a degasser, an automatic sampler, and a column oven. The mass spectrometer used was the triple quadrupole mass spectrometer MicroMass Quattromicro® (Waters®, Ireland). Samples were ionized using electrospray ionization technique (ESI), using an electrospray ion source in positive and negative ion mode. For the data acquisition and processing, the MassLynx® software, version 4.1., was used. The mass spectrometer is part of the Portuguese MS Network, LISBOA-01-0145-FEDER-022125, supported by

Lisboa2020, under the Portugal2020 Partnership Agreement, through the European Regional Development Fund

For thin layer chromatography, silica-gel plates with aluminium support were used (Merck TLC Silica gel 60 F_{254} plates) as the stationary phase and a Dual UV Lamp (254 nm and 366nm) (CAMAG®) was used to inspection the thin layer chromatography. For column chromatography, Silica gel 60 (0.040-0.063 mm) was used (Merck).

UV spectra were recorded using a Shimadzu UV-Visible Spectrometer UV-1603. For the data acquisition and processing, the UV-1601PC softwares was used.

HPLC analyses were performed in an Elite LaChrom (VWR Hitachi) system, composed by a L-2130 pump, a L-2400 UV detector, a LiChrospher® 100 RP-18 (5 µm) column, and a Rheodyne® manual sample injector, with a 20 µL sample loop. A Hamilton 100 microliter syringe was used to inject the samples. For the data acquisition and processing, the EZChrome Elite software was used.

The melting points (m.p.) of the synthesized hybrid compounds were determined using a Kofler Bock Monoscop <M>. Throughout this project other various equipment were used including common lab material, rotary evaporators (VWR), analytical balances (Mettler Toledo AG135 and Ohaus Adventurer Pro AV264C), an ultrasonic bath (Bandelin Sonorex TK52), thermostatic baths (Lab Companion BS-06 and Julabo F12), and a centrifuges (Eppendorf 5430r and Beckman and Coulter ™ Microfuge ® 18 Centrifuge).

VI. 2. Synthetic Procedures

This sub-chapter describes the synthetic procedure for the synthesis of all final and intermediate compounds. All spectra mentioned in this section are presented in **Annex 2 – Structural Characterization Spectra.** The chemical structures, synthetic routes, and reaction mechanisms presented in this thesis, were all generated with PerkinElmer's ChemDraw® Ultra, version 12.0.2.1076.

VI. 2. 1. Compound 1 – 2,3,4,9-tetrahydro-1*H*-pyrido[3,4-*b*]indole

Tryptamine (1g, 6.24 mmol) is dissolved in glacial acetic acid (5 mL), and a formaldehyde solution (530 µL, 1.05 eq.) is added. The mixture reacts overnight (o.n.) at room temperature (r.t.). A sodium hydroxide (NaOH) solution (1 M) is added until pH 12, causing the product to precipitate. The product is obtained by vacuum filtration, washed with distilled water, and dried under vacuum. A white powder is obtained. η = 94.1%.

^{1}H NMR (300 MHz, DMSO-d_6): δ 10.61 (s, 1H, H_7), 7.34 (d, J = 7.7 Hz, 1H, H_6), 7.25 (d, J = 7.9 Hz, 1H, H_3), 6.99 (td, J = 8.0, 1.4 Hz, 1H, H_1), 6.92 (td, J = 7.4, 1.3 Hz, 1H, H_2), 3.85 (s, 2H, H_{13}), 2.97 (t, J = 5.6 Hz, 2H, H_{11}), 2.58 (t, J = 5.7 Hz, 2H, H_{10}).

VI. 2. 2. Compound 2 – *tert*-butyl 3,4-dihydro-1*H*-pyrido[3,4-*b*]indole-2(9*H*)-carboxylate

Compound **1** (1g, 5.81 mmol) is dissolved in dry methanol (14 mL), and triethylamine (0.80 mL, 1 eq.) is added. The mixture reacts for 30 min, at r.t., under inert (N_2) atmosphere. Di-*tert*-butyl dicarbonate (1.35 mL, 1 eq.) is added, and the mixture reacts for 2h30min, at r.t., under inert atmosphere. The solvent is evaporated under reduced pressure, and the sample is dried under vacuum. A white powder is obtained. η > 99%.

^{1}H NMR (300 MHz, DMSO-d_6): δ 10.85 (s, 1H, H_7), 7.38 (d, J = 7.7 Hz, 1H, H_6), 7.25 (d, J = 7.8 Hz, 1H, H_3), 7.03 (td, J = 8.1, 1.3 Hz, 1H, H_1), 6.95 (td, J = 8.1, 1.2 Hz, 1H, H_2), 4.55 (s, 2H, H_{13}), 3.66 (t, J = 5.7 Hz, 2H, H_{11}), 2.67 (t, J = 5.7 Hz, 2H, H_{10}), 1.43 (s, 9H, H_{18-20}).

VI. 2. 3. Compound 3 – *tert*-butyl 9-oxo-4,9-dihydro-1*H*-pyrrolo[3,4-*b*]quinoline -2(3*H*)-carboxylate

Compound **2** (750 mg, 2.75 mmol) is dissolved in dimethylformamide (5 mL), under inert (N_2) atmosphere. 18-Crown-6 (727 mg, 1 eq.) and potassium superoxide (KO_2) (782 mg, 4 eq.) are added to the solution. The mixture reacts o.n., at r.t. Distilled water is added to quench the excess KO_2 until no gas formation is observed. A saturated sodium chloride (NaCl) solution (125 mL / 750 mg **(2)**) is added to induce the product to precipitate. The product is obtained by vacuum filtration, washed with distilled water, and dried under vacuum. A pale-yellow powder is obtained. η = 84.3%.

^{1}H NMR (300 MHz, DMSO-d_6): δ 8.08 (d, J = 8.1 Hz, 1H, H_6), 7.46 (d, J = 8.2 Hz, 1H, H_3), 7.37 (t, J = 7.5 Hz, 1H, H_2), 7.07 (t, J = 7.6 Hz, 1H, H_1), 4.45 (d, J = 8.2 Hz, 2H, H_{13}), 4.37 (d, J = 9.2 Hz, 2H, H_{11}), 1.46 (s, 9H, $H_{18\text{-}20}$).

VI. 2. 4. Compound 4 – 9-oxo-2,3,4,9-tetrahydro-1*H*-pyrrolo[3,4-*b*]quinolin-2-ium ion

Compound **3** (400 mg, 1.40 mmol) is dissolved in dry dichloromethane (3 mL), under inert (N_2) atmosphere. A 1:1 dry dichloromethane:trifluoroacetic acid mixture (3 mL / 400 mg **(3)**) is added to the solution, and the mixture reacts for 3h, at r.t. The solvent is evaporated under reduced pressure, and the sample is dried under vacuum to obtain the product in the form of a trifluoroacetate salt. A burgundy solid is obtained. η > 99%.

^{1}H NMR (300 MHz, DMSO-d_6): δ 9.84 (s, 1H, H_{12}), 8.15 (dd, J = 8.1, 1.5 Hz, 1H, H_6), 7.72 (ddd, J = 8.4, 6.9, 1.5 Hz, 1H, H_2), 7.61 (dd, J = 8.5, 1.2 Hz, 1H, H_3), 7.40 (ddd, J = 8.1, 6.9, 1.2 Hz, 1H, H_1), 4.64 (s, 2H, H_{13}), 4.37 (s, 2H, H_{11}).

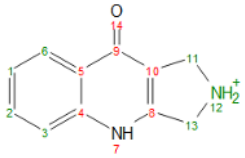

VI. 2. 5. Compound 5a – 2-(3-nitrobenzyl)-2,3-dihydro-1*H*-pyrrolo[3,4-b]quinolin-9(4*H*)-one

Compound **4** (400 mg, 1.33 mmol) is dissolved in dimethylformamide (2 mL), under inert (N_2) atmosphere. Triethylamine (0.60 mL, 3.2 eq.) is added to the solution, under inert atmosphere. The mixture reacts for 1h, at r.t. 3-nitrobenzyl bromide (360 mg, 1.25 eq.) is added to the reaction. The mixture reacts o.n., at r.t., under inert atmosphere. A saturated sodium chloride (NaCl) solution (100 mL / 400 mg **(4)**) is added to induce the product to precipitate. The product is obtained by vacuum filtration, washed with distilled water, and dried under vacuum. A terracotta-coloured powder is obtained. η = 63.3%.

ESI$^+$ – MS m/z (abund.): 322 $[M+H]^+$ (100 %), 187 $[M+H\text{-}CH_2C_6H_4NO_2]^+$ (10%), 643 $[2M+H]^+$ (9%), 363 $[M+ACN+H]^+$ (8%).

^{1}H NMR (300 MHz, DMSO-d_6): δ 8.25 (s, 1H, H_{17}), 8.16 (d, J = 8.5 Hz, 1H, H_{19}), 8.10 (d, J = 7.9 Hz, 1H, H_6), 7.87 (d, J = 7.6 Hz, 1H, H_{21}), 7.73 – 7.56 (m, 2H, $H_{2,20}$), 7.51 (d, J = 8.3 Hz, 1H, H_3), 7.30 (t, J = 7.5 Hz, 1H, H_1), 4.05 (s, 2H, $H_{13,15}$), 3.79 (s, 2H, H_{11}).

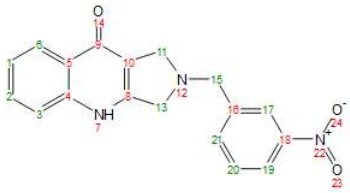

VI. 2. 6. Compound 5b – 2-(4-nitrobenzyl)-2,3-dihydro-1*H*-pyrrolo[3,4-*b*]quinolin-9(4*H*)-one

Compound **4** (400 mg, 1.33 mmol) is dissolved in dimethylformamide (2 mL), under inert (N_2) atmosphere. Triethylamine (0.60 mL, 3.2 eq.) is added to the solution, under inert atmosphere. The mixture reacts for 1h, at r.t. 4-nitrobenzyl bromide (360 mg, 1.25 eq.) is added to the reaction. The mixture reacts o.n., at r.t., under inert atmosphere. A saturated sodium chloride (NaCl) solution (100 mL / 400 mg **(4)**) is added to induce the product to precipitate. The product is obtained by vacuum filtration, washed with

distilled water, and dried under vacuum. A mustard-yellow powder is obtained. η = 68.6%.

^{1}H NMR (300 MHz, DMSO-d_6): δ 12.09 (s, 1H, H_7), 8.24 (d, J = 8.7 Hz, 2H, $H_{18,20}$), 8.10 (dd, J = 8.1, 1.5 Hz, 1H, H_6), 7.69 (d, J = 8.7 Hz, 2H, $H_{17,21}$), 7.61 (ddd, J = 8.6, 6.9, 1.6 Hz, 1H, H_2), 7.50 (d, J = 8.2 Hz, 1H, H_3), 7.29 (ddd, J = 8.1, 6.9, 1.2 Hz, 1H, H_1), 4.08 – 4.00 (m, 2H, $H_{13,15}$), 3.80 (s, 2H, H_{11}).

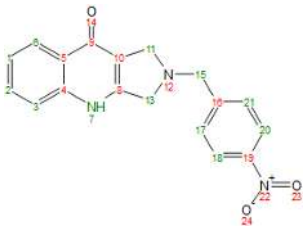

VI. 2. 7. Compound 5c – 4-((9-oxo-1H-pyrrolo[3,4-*b*]quinolin-2(3*H*,4*H*,9*H*)-yl) methyl)benzonitrile

Compound **4** (400 mg, 1.33 mmol) is dissolved in dimethylformamide (2 mL), under inert (N_2) atmosphere. Triethylamine (0.60 mL, 3.2 eq.) is added to the solution, under inert atmosphere. The mixture reacts for 1h, at r.t. 4-(bromomethyl)benzonitrile (327 mg, 1.25 eq.) is added to the reaction. The mixture reacts o.n., at r.t., under inert atmosphere. A saturated sodium chloride (NaCl) solution (100 mL / 400 mg **(4)**) is added to induce the product to precipitate. The product is obtained by vacuum filtration, washed with distilled water, and dried under vacuum. An orange-brown powder is obtained. η = 43.0%.

^{1}H NMR (300 MHz, MeOD): δ 8.31 (dd, J = 8.4, 1.4 Hz, 1H, H_6), 7.83 – 7.64 (m, 5H, $H_{2,17\text{-}18,20\text{-}21}$), 7.59 (d, J = 8.3 Hz, 1H, H_3), 7.45 (ddd, J = 8.2, 6.9, 1.1 Hz, 1H, H_1), 4.13 (t, J = 2.0 Hz, 2H, H_{13}), 4.10 (s, 2H, H_{15}), 4.03 (t, J = 2.0 Hz, 2H, H_{11}).

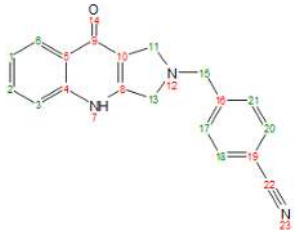

VI. 2. 8. Compound 6a – 2-(3-aminobenzyl)-2,3-dihydro-1*H*-pyrrolo[3,4-*b*]quinolin-9(4*H*)-one

Compound **5a** (150 mg, 0.47 mmol) and tin (Sn^0, 100 mesh) (637 mg, 11.5 eq.) are suspended in ethanol (1.65 mL). An aqueous hydrochloric acid (HCl) solution (0.9 mL HCl / 2.3 mL H_2O) is added to the reactional mixture. The mixture reacts for 3h, at r.t. The solution is filtered under vacuum through celite and washed with ethanol. The filtrate is evaporated under reduced pressure and dried under vacuum. The crude is resolubilized and basified until pH 8 with a saturated sodium bicarbonate ($NaHCO_3$) solution and the product is extracted from the crude with dichloromethane. The organic phase is dried with anhydrous sodium sulphate, filtered, evaporated under reduced pressure, and dried under vacuum. An orange powder is obtained. η = 53.7%.

ESI$^+$ – MS m/z (abund.): 292 $[M+H]^+$ (100 %), 187 $[PYQ+H]^+$ (90%), 314 $[M+Na]^+$ (40%), 158 $[M+H+Na]^{2+}$ (19%), 355 $[M+ACN+H]^+$ (11%),

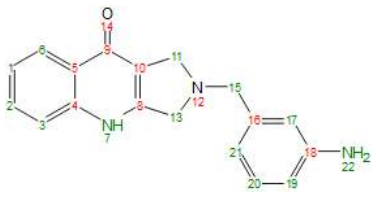

^{1}H NMR (300 MHz, DMSO-d_6): δ 12.04 (s, 1H, H_7), 8.10 (dd, J = 8.1, 1.5 Hz, 1H, H_6), 7.67 – 7.56 (m, 1H, H_2), 7.49 (d, J = 8.3 Hz, 1H, H_3), 7.36 – 7.24 (m, 1H, H_1), 6.98 (t, J = 7.7 Hz, 1H, H_{20}), 6.61 (s, 1H, H_{17}), 6.54 – 6.41 (m, 2H, $H_{19,21}$), 5.05 (s, 2H, H_{22}), 3.94 (s, 2H, H_{13}), 3.73 (s, 4H, $H_{11,15}$).

VI. 2. 9. Compound 6b – 2-(4-aminobenzyl)-2,3-dihydro-1*H*-pyrrolo[3,4-*b*]quinolin-9(4*H*)-one

Compound **5b** (150 mg, 0.47 mmol) and tin (Sn^0, 100 mesh) (637 mg, 11.5 eq.) are suspended in ethanol (1.65 mL). An aqueous hydrochloric acid (HCl) solution (0.9 mL HCl / 2.3 mL H_2O) is added to the solution. The mixture reacts for 3h, at r.t. The solution is filtered under vacuum through celite and washed with ethanol. The filtrate is evaporated under reduced pressure and dried under vacuum. The crude is resolubilized and basified until pH 8 with a saturated sodium bicarbonate ($NaHCO_3$) solution and the product is extracted from the crude with dichloromethane. The organic phase is dried with anhydrous sodium sulphate, filtered, evaporated under reduced pressure, and dried under vacuum. An orange powder is obtained. η = 42.2%.

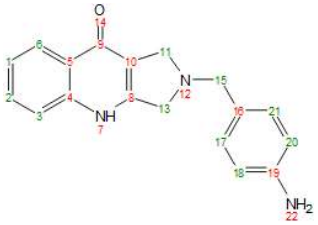

^{1}H NMR (300 MHz, MeOD): δ 8.19 (d, *J* = 8.3 Hz, 1H, H_6), 7.68 – 7.53 (m, 1H, H_2), 7.51 – 7.39 (m, 1H, H_3), 7.39 – 7.25 (m, 1H, H_1), 7.08 (d, *J* = 8.3 Hz, 2H, $H_{17,21}$), 6.66 (d, *J* = 8.3 Hz, 2H, $H_{18,20}$), 3.98 – 3.78 (m, 4H, $H_{13,15}$), 3.71 (s, H_{11}).

VI. 2. 10. Compound 6c – 2-(4-(aminomethyl)benzyl)-2,3-dihydro-1*H*-pyrrolo[3,4-*b*]quinolin-9(4*H*)-one

Compound **4** (200 mg, 0.67 mmol) is dissolved in dry tetrahydrofuran (1 mL), under inert (N_2) atmosphere. Triethylamine (0.30 mL, 3.2 eq.) is added to the solution, under inert atmosphere. The mixture reacts for 1h, at r.t. Compound **9** (180 mg, 1.25 eq.) is added to the reaction. The mixture reacts o.n., at r.t., under inert atmosphere. The solvent is evaporated under reduced pressure and dried under vacuum. The crude is resolubilized in water and the product is extracted from the crude with ethyl acetate. The organic phase is dried with anhydrous sodium sulphate, filtered, evaporated under reduced pressure, and dried under vacuum. An orange paste is obtained. η = 71.0%.

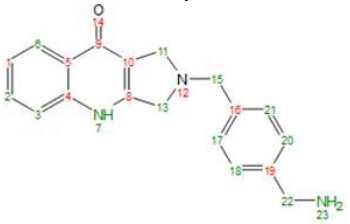

^{1}H NMR (300 MHz, DMSO-d_6): δ 12.42 (s, 1H, H_7), 8.19 – 8.09 (m, 1H, H_6), 7.74 – 7.62 (m, 2H, $H_{18,20}$), 7.62 – 7.52 (m, 2H, $H_{2,3}$), 7.42 – 7.30 (m, 3H, $H_{1,17,21}$), 5.12 (s, 2H, H_{13}), 4.91 (s, 2H, H_{15}), 4.81 (s, 2H, H_{22}), 4.61 (s, 2H, H_{11}), 4.35 (t, *J* = 5.2 Hz, 2H, H_{23}).

VI. 2. 11. Compound 7a – 5-nitro-*N*-(3-((9-oxo-1*H*-pyrrolo[3,4-*b*]quinolin-2(3*H*,4*H*,9*H*)-yl)methyl)phenyl)furan-2-carboxamide

Compound **6a** (100 mg, 0.34 mmol) is dissolved in dimethylformamide (2.5 mL), under inert (N_2) atmosphere. Triethylamine (72 μL, 1.5 eq.) is added to the solution, under inert atmosphere. The mixture reacts for 30 min, at r.t. 5-Nitro-2-furoyl chloride (66 mg, 1.1 eq.) is added to the reaction. The mixture reacts o.n., at r.t., under inert atmosphere. The product is extracted from the reactional mixture with dichloromethane, and the obtained organic phase is extracted with a saturated sodium chloride (NaCl) solution to remove residual solvent. The obtained organic phase is dried with anhydrous sodium sulphate, filtered, evaporated under reduced pressure, and dried under vacuum. The product was purified through liquid chromatography, using a silica gel column and a 9:1 dichloromethane:methanol mixture as the mobile phase. The solvent was evaporated

under reduced pressure and dried under vacuum to obtain an orange powder. m.p.: 59 – 61 ºC. η = 15.8%

ESI$^+$ – MS m/z (abund.): 431 $[M+H]^+$ (100%), 278 $[M+3ACN+2H]^{2+}$ (55%), 292 $[M+H-COC_4H_2ONO_2]^+$ (20%).

^{1}H NMR (300 MHz, $CDCl_3$): δ 7.70 – 7.62 (m, 2H, $H_{6,26}$), 7.60 – 7.51 (m, 1H, H_2), 7.51 – 7.43 (m, 3H, $H_{1,3,27}$), 7.16 – 7.06 (m, 2H, $H_{17,20}$), 6.79 – 6.68 (m, 1H, H_{21}), 6.64 – 6.57 (m, 1H, H_{19}), 3.74 – 3.61 (m, 4H, $H_{13,15}$), 2.96 – 2.81 (m, 2H, H_{11}).

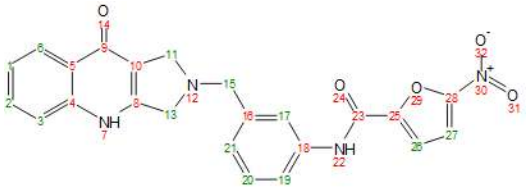

VI. 2. 12. Compound 7b – 5-nitro-*N*-(4-((9-oxo-1*H*-pyrrolo[3,4-*b*]quinolin–2(3*H*,4*H*,9*H*)-yl)methyl)phenyl)furan-2-carboxamide

Compound **6b** (100 mg, 0.34 mmol) is dissolved in dimethylformamide (2.5 mL), under inert (N_2) atmosphere. Triethylamine (72 μL, 1.5 eq.) is added to the solution, under inert atmosphere. The mixture reacts for 30 min, at r.t. 5-Nitro-2-furoyl chloride (66 mg, 1.1 eq.) is added to the reaction. The mixture reacts o.n., at r.t., under inert atmosphere. The product is extracted from the reactional mixture with dichloromethane, and the obtained organic phase is extracted with a saturated sodium chloride (NaCl) solution to remove residual solvent. The obtained organic phase is dried with anhydrous sodium sulphate, filtered, evaporated under reduced pressure, and dried under vacuum. The product is purified through liquid chromatography, using a silica gel column and a 9:1 dichloromethane:methanol mixture as the mobile phase. The solvent is evaporated under reduced pressure and dried under vacuum to obtain an orange powder. m.p.: 63 – 65 ºC. η = 28.7%

ESI$^+$ – MS m/z (abund.): 245 $[C_6H_4NHCOC_4H_2ONO_2+H]^+$ (100%), 187 $[M+H-CH_2C_6H_4NHCOC_4H_2ONO_2]^+$ (68%), 144 $[M+3H]^{3+}$ (50%), 507 $[M+2K-H]^+$ (48%), 431 $[M+H]^+$ (38%), 453 $[M+CH_3OH+H]^+$ (4%).

^{1}H NMR (300 MHz, MeOD): δ 8.31 (dt, *J* = 8.1, 1.7 Hz, 1H, H_6), 7.79 – 7.66 (m, 2H, $H_{26,27}$), 7.62 – 7.52 (m, 3H, $H_{2,17,21}$), 7.50 – 7.38 (m, 3H, $H_{3,18,20}$), 7.30 – 7.19 (m, 1H, H_1), 3.05 – 2.97 (m, 4H, $H_{13,15}$), 2.90 – 2.86 (m, 2H, H_{11}).

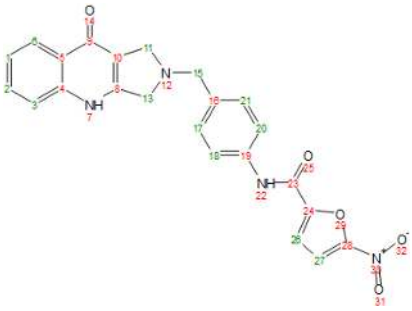

VI. 2. 13. Compound 7c – 5-nitro-*N*-(4-((9-oxo-1*H*-pyrrolo[3,4-*b*]quinolin–2(3*H*,4*H*,9*H*)-yl)methyl)benzyl)furan-2-carboxamide

Compound **6c** (100 mg, 0.33 mmol) is dissolved in dry tetrahydrofuran (2.5 mL), under inert (N_2) atmosphere. Triethylamine (0.18 mL, 4 eq.) is added to the solution, under inert atmosphere. The mixture reacts for 30 min, at r.t., protected from light. 5-Nitro-2-furoyl chloride (63 mg, 1.1 eq.) is added to the reaction. The mixture reacts o.n., at r.t., under inert atmosphere, protected from light. The solvent is evaporated under reduced pressure and dried under vacuum. The product is isolated and purified through liquid chromatography, using a silica gel column and a gradient of hexane:ethyl acetate

and ethyl acetate:methanol mixtures as the mobile phase. The solvent is evaporated under reduced pressure and dried under vacuum to obtain a white powder. m.p.: 67 – 69 ºC. η = 12.8%.

ESI$^+$ – MS m/z (abund.): 283 $[M+3ACN+2H]^{2+}$ (100%), 186 $[M-CH_2C_6H_4CH_2NHCOC_4H_2ONO_2]^+$ (28%), 507 $[M+ACN+Na]^+$ (8%), 463 $[M+NH_4]^+$ (2%).

^{1}H NMR (300 MHz, DMSO-d_6): δ 12.35 (s, 1H, H_7), 12.26 (s, 1H, H_{23}), 8.13 (d, J = 8.1, 2H, $H_{6,28}$), 7.74 – 7.62 (m, 3H, $H_{18,20,27}$), 7.60 – 7.50 (m, 2H, $H_{2,3}$), 7.41 – 7.30 (m, 3H, $H_{1,17,21}$), 5.09 (s, 2H, H_{13}), 4.88 (s, 2H, H_{15}), 4.79 (s, 2H, H_{11}) , 4.59 (s, 2H, H_{22}).

^{13}C NMR (75 MHz, DMSO-d_6): δ 172.4 (C_9), 170.7 (C_{24}), 146.3 (C_8), 145.3 (C_{16}), 140.1 (C_{29}), 131.8 ($C_{18,20,27}$), 125.1 (C_4), 125.0 (C_{26}), 124.8 ($C_{6,28}$), 123.3 (C_1), 123.3 ($C_{17,21}$), 118.4 (C_2), 118.3 (C_3), 117.9 (C_5), 112.8 (C_{10}), 111.6 (C_{19}), 52.4 (C_{15}), 51.3 (C_{22}), 50.7 (C_{13}), 49.9 (C_{11}).

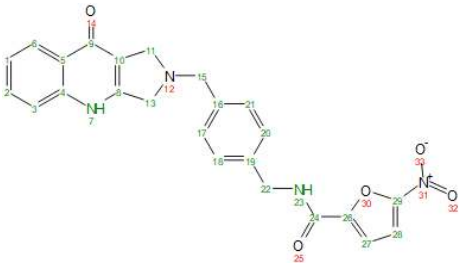

VI. 2. 14. Compound 7c' – N-(4-methylbenzyl)-5-nitrofuran-2-carboxamide

Compound **6c** (100 mg, 0.33 mmol) is dissolved in dimethylformamide (2.5 mL), under inert (N_2) atmosphere. Triethylamine (68 μL, 1.5 eq.) is added to the solution, under inert atmosphere. The mixture reacted for 30 min, at r.t. 5-Nitro-2-furoyl chloride (63 mg, 1.1 eq.) is added to the reaction. The mixture reacted o.n., at r.t., under inert atmosphere. The product is extracted from the reactional mixture with dichloromethane, and the obtained organic phase is extracted with a saturated sodium chloride (NaCl) solution to remove residual solvent. The obtained organic phase is dried with anhydrous sodium sulphate, filtered, evaporated under reduced pressure, and dried under vacuum. The product is purified through liquid chromatography, using a silica gel column and a 7:3 hexane:ethyl acetate mixture as the mobile phase. The solvent is evaporated under reduced pressure and dried under vacuum to obtain a salmon-coloured paste. η = 20.5%

ESI$^+$ – MS m/z (abund.): 261 $[M+H]^+$ (100%), 279 $[M+NH_4]^+$ (22%), 521 $[2M+H]^+$ (11%), 172 $[M+2ACN+2H]^{2+}$ (10%), 142 $[M+H+Na]^{2+}$ (8%).

^{1}H NMR (300 MHz, DMSO-d_6) δ 9.38 (t, J = 6.1 Hz, 1H, H_9), 7.71 (d, J = 3.9 Hz, 1H, H_{14}), 7.40 (d, J = 3.9 Hz, 1H, H_{13}), 7.19 (d, J = 8.2 Hz, 2H, $H_{4,6}$), 7.12 (d, J = 8.2 Hz, 2H, $H_{3,7}$), 4.40 (d, J = 6.1 Hz, 2H, H_8), 2.26 (s, 3H, H_1).

^{13}C NMR (75 MHz, DMSO) δ 156.3 (C_{10}), 151.6 (C_{12}), 148.4 (C_{15}), 136.4 (C_2), 135.8 (C_5), 129.1 ($C_{3,7}$), 127.6 ($C_{4,6}$), 115.8 (C_{13}), 113.6 (C_{14}), 42.3 (C_8), 20.8 (C_1).

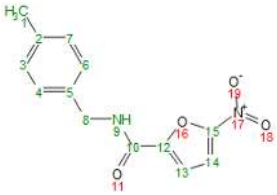

VI. 2. 15. Compound 7d – 2-(5-nitrofuran-2-carbonyl)-2,3-dihydro-1H-pyrrolo[3,4-b]quinolin-9(4H)-one

Compound **4** (300 mg, 1 mmol) is dissolved in dry tetrahydrofuran (1 mL), under inert (N_2) atmosphere. Triethylamine (1.11 mL, 8 eq.) is added to the solution, under inert atmosphere. The mixture reacted for 30 min, at r.t. 5-Nitro-2-furoyl chloride (193 mg, 1.1 eq.) is added to the reaction. The mixture reacted o.n., at r.t., under inert atmosphere.

The solvent is evaporated under reduced pressure and dried under vacuum. The product is isolated and purified through liquid chromatography, using a silica gel column and a gradient of hexane:ethyl acetate and ethyl acetate:methanol mixtures as the mobile phase. The solvent is evaporated under reduced pressure and dried under vacuum to obtain an orange powder. The product was not obtained pure [in **Annex 2 – Structural Characterization Spectra**, an HPLC chromatogram is presented], and due to low quantity further purification was not viable. Thus, no spectroscopy characterization was performed. $\eta < 6.2\%$.

ESI$^+$ – MS m/z (abund.): 368 $[M+ACN+H]^+$ (100%), 214 $[M+H-C_4H_2ONO_2]^+$ (24%), 226 $[M+3ACN+2H]^{2+}$ (12%), 409 $[M+2ACN+H]^+$ (8%).

VI. 2. 16. Compound 8a – (*E*)-2-(3-(((5-nitrofuran-2-yl)methylene) amino)benzyl)-2,3-dihydro-1*H*–pyrrolo[3,4-*b*]quinolin-9(4*H*)-one

Compound **6a** (50 mg, 0.17 mmol) is dissolved in toluene (2 mL). The mixture is transferred to a new recipient with activated molecular sieves and is put under reflux (110 ºC). 5-nitro-2-furaldehyde (27 mg, 1.1 eq.) and p-toluenesulfonic acid (2.6 μL, 0.1 eq.) are added to the reaction. The mixture reacts for 5h, at 110 ºC. The mixture is filtered and washed with methanol. The filtrate is evaporated under reduced pressure and dried under vacuum. The product is purified through liquid chromatography, using a silica gel column and a 9:1 dichloromethane:methanol mixture as the mobile phase. The solvent is evaporated under reduced pressure and dried under vacuum to obtain a black powder. m.p.: 62 – 64 ºC. $\eta = 22.8\%$

ESI$^+$ – MS m/z (abund.): 229 $[M+ACN+H]^{2+}$ (60%), 290 $[M+H-CHC_4H_2ONO_2]^+$ (8%), 415 $[M+H]^+$ (34%), 433 $[M+NH_4]^+$ (28%).

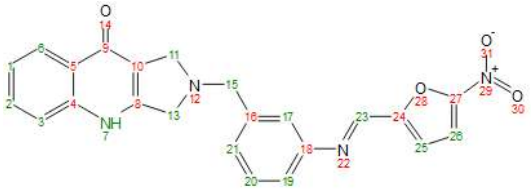

^{1}H NMR (300 MHz, $CDCl_3$) δ 11.07 (s, 1H, H_7), 9.84 (s, 1H, H_{23}), 7.74 (d, J = 7.9 Hz, 2H, $H_{6,26}$), 7.45 – 7.39 (m, 2H, $H_{2,3}$), 7.36 – 7.32 (m, 2H, $H_{1,25}$), 7.23 – 7.18 (m, 1H, H_{17}), 7.14 (d, J = 7.9 Hz, 3H, $H_{19,20,21}$), 3.49 (s, 2H, H_{13}), 2.34 (s, 4H, H_{15}).

VI. 2. 17. Compound 8b – (*E*)-2-(4-(((5-nitrofuran-2-yl)methylene) amino)benzyl)-2,3-dihydro-1*H*-pyrrolo[3,4-*b*]quinolin-9(4*H*)-one

Compound **6b** (75 mg, 0.26 mmol) is dissolved in dry tetrahydrofuran (2 mL). The mixture is transferred to a new recipient with activated molecular sieves and is put under reflux (67 ºC). 5-nitro-2-furaldehyde (40 mg, 1.1 eq.) and p-toluenesulfonic acid (4.0 μL, 0.1 eq.) are added to the reaction. The mixture reacts for 5h, at 67 ºC. The mixture is filtered and washed with methanol. The filtrate is evaporated under reduced pressure and dried under vacuum. The product is purified through liquid chromatography, using a silica gel column and a 95:5 dichloromethane:methanol mixture as the mobile phase. The solvent is evaporated under reduced pressure and dried under vacuum to obtain a black powder. m.p.: 64 – 66 ºC. $\eta = 11.5\%$

ESI$^+$ – MS m/z (abund.): 229 $[M+ACN+2H]^{2+}$ (100%), 217 $[CH_2C_6H_4NO_2+H]^+$ (17%), 187 $[M+H-CH_2C_6H_4NO_2]^+$ (13%), 457 $[M+CAN+H]^+$ (9%), 415 $[M+H]^+$ (6%).

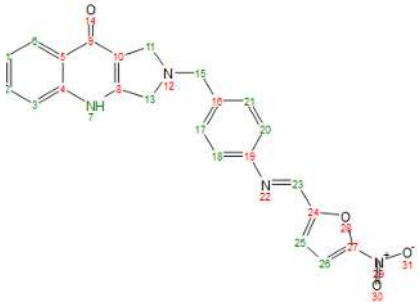

^{1}H NMR (300 MHz, Acetone-d_6) δ 9.76 (s, 1H, H_7), 8.65 – 8.63 (m, 1H, H_{23}), 7.67 – 7.65 (m, 1H, H_6), 7.54 – 7.49 (m, 2H,$H_{2,26}$), 7.41 – 7.36 (m, 3H, $H_{1,3,25}$), 7.09 (d, J = 8.3 Hz, 2H, $H_{18,20}$), 6.64 (d, J = 7.8 Hz, 2H, $H_{17,21}$), 3.82 (s, 2H, H_{13}), 3.68 (s, 2H, H_{15}), 3.64 – 3.59 (m, 2H, H_{15}).

VI. 2. 18. Compound 8c – (*E*)-2-(4-((((5-nitrofuran-2-yl)methylene) amino)methyl)benzyl)-2,3-dihydro-1*H*-pyrrolo[3,4-*b*]quinolin-9(4*H*) -one

Compound **6c** (100 mg, 0.33 mmol) is dissolved in toluene (2 mL). The mixture is transferred to a new recipient with activated molecular sieves and is put under reflux (110 ºC). 5-Nitro-2-furaldehyde (50 mg, 1.1 eq.) and p-toluenesulfonic acid (5.0 μL, 0.1 eq.) are added to the reaction. The mixture reacts for 5h, at 110 ºC. The mixture is filtered and washed with methanol. The filtrate is evaporated under reduced pressure and dried under vacuum. The product is purified through liquid chromatography, using a silica gel column and a 95:5 dichloromethane:methanol mixture as the mobile phase. The solvent is evaporated under reduced pressure and dried under vacuum to obtain a brown paste. η = 12.2%

ESI$^+$ – MS m/z (abund.): 141 $[M-PYQCH_2C_6H_4CH_2+H]^{2+}$ (100%), 255 $[M+2ACN+2H]^{2+}$ (32%), 237 $[M+2Na]^{2+}$ (17%), 429 $[M+H]^+$ (8%).

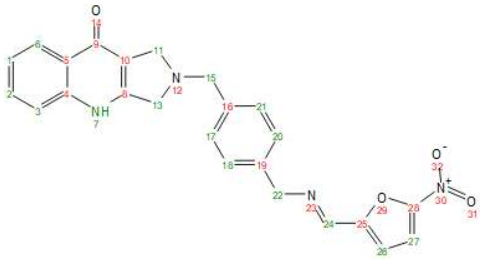

^{1}H NMR (300 MHz, DMSO-d_6) δ 12.38 (s, 1H, H_7), 8.16 – 8.11 (m, 2H, $H_{6,27}$), 8.09 (s, 1H, H_{24}), 7.74 – 7.65 (m, 3H, $H_{18,20,26}$), 7.60 – 7.52 (m, 2H, $H_{2,3}$), 7.41 – 7.32 (m, 3H, $H_{1,17,21}$), 5.12 (s, 2H, H_{13}), 4.91 (s, 2H, H_{15}), 4.81 (s, 2H, H_{11}), 4.63 (s, 2H, H_{22}).

VI. 2. 19. Compound 9 – (4-(bromomethyl)phenyl)methanamine

4-(Bromomethyl)benzonitrile (100 mg, 0.51 mmol) is dissolved in dry tetrahydrofuran (5 mL), under inert (N_2) atmosphere. Lithium aluminium hydride ($LiAlH_4$) (79 mg, 4.1 eq.) is added to the solution in an ice bath. The mixture reacts for 5h, at r.t. Distilled water (0.5 mL) and a sodium hydroxide (NaOH) solution (20% (m/V)) (0.2 mL) are added drop by drop in an ice bath to quench the excess $LiAlH_4$. The product is extracted with dichloromethane. The organic phase is dried with anhydrous sodium sulphate, filtered, evaporated under reduced pressure, and dried under vacuum. An orange yellow paste is obtained. η = 38.0%.

^{1}H NMR (300 MHz, $CDCl_3$) δ 7.23 – 7.08 (m, 4H, $H_{1,3,4,6}$), 3.80 (s, 2H, H_8), 3.64 (s, 2H, H_7), 2.32 (s, 2H, H_9).

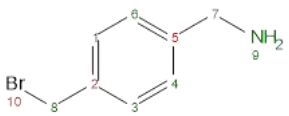

VI. 3. Biological and biochemical studies

VI. 3. 1. UV spectrometry

Stock solutions of the hybrid compounds were prepared: 5.0 x 10^{-3} M in methanol (MeOH) for compounds **7a** and **8a**, 2.5 x 10^{-3} M in MeOH for compounds **7b** and **8b**, and 1.0 x 10^{-3} M in DMSO for compounds **7c'** and **8c**. Then, all stock solutions were diluted in acetonitrile (ACN) to obtain the solutions with the desired concentrations.

The UV spectra of compounds **7c'** and **8c** were recorded using the Shimadzu UV-Visible Spectrometer UV-1603. For the data acquisition and processing, the UV-1601PC software was used. All spectra were recorded using quartz cells with an optical path length of 1 cm. Blank samples were prepared by measuring the same volume of solvent used in compound samples, without adding the compound.

In **Table VI.1**, the relative wavelength maximums used in the HPLC analyses are presented for compounds **7c'** and **8c**, as well as the correspondent absorbance, and the concentration of the sample solution used.

Table VI.1 | Wavelengths used for each hybrid compound and respective absorbance.

Compound	λ (nm)	Abs	[ ] (M)
(7c')	312.4	2.126	1.0 x 10^{-4}
(8c)	319.4	1.413	1.0 x 10^{-4}

VI. 3. 2. Solubility Assessment

A stock solution with a concentration of 1.0 x 10^{-3} M in DMSO was prepared for compound **7c',** compound **8c,** and the external standard (salicylic acid). For the calibration curve, the stock solution was diluted in DMSO directly on a 96-well plate to obtain three different concentrations: 10 µM, 100 µM, and 220 µM, with a final volume of 200 µL. For the solubility reading, the stock solution was diluted in PBS directly on a 96-well plate to obtain a final concentration of 200 µM, with a final volume of 200 µL.

The plate was incubated in a stirred (25 rpm) thermostatic bath (Lab Companion BS-06), at 37 ºC, for 2 hours; and centrifuged at 3500 rpm for 25 minutes (Eppendorf 5430r). Then, the supernatant was analysed by HPLC, using a 55:45 methanol:water mixture as the mobile phase and 319 nm as the detection wavelength. The calibration curves were performed in duplicate and are presented in **Annex 1 – Calibration Curves,** while the solubility readings were performed in triplicate.

VI. 3. 3. Stability Assessment in PBS

A stock solution with a concentration of 1.0 x 10^{-3} M in DMSO was prepared for compounds **7c'** and **8c.** Then, a volume of 125 µL of stock solution was diluted in 1 mL of PBS. The mixture was incubated in a thermostatic bath (Julabo F-12), at 37 ºC, for 96 hours. Periodically, in the aforementioned times, samples were collected from the mixture and analysed by HPLC, using a 55:45 methanol:water mixture as the mobile phase and 319 nm as the detection wavelength. The assay was performed in duplicate.

VI. 3. 4. Stability Assessment in Human Plasma

A stock solution with a concentration of 1.0 x 10^{-2} M in DMSO was prepared for compounds **7c'** and **8c**. Then, a volume of 40 µL of stock solution was diluted in 2.5 mL of human plasma [80% (v/v) in PBS]. Source plasma was collected by voluntary healthy donors and separated from its cellular components by centrifugation. Plasma samples were pooled, to mitigate intrapersonal variation, and fractioned. Each fraction (2 mL) was diluted in PBS (0.5mL). It is relevant to note that besides all requirements to donate blood, voluntary donors were required to not be taking any drug.

The mixture was incubated in a stirred (25rpm) thermostatic bath (Lab Companion BS-06), at 37 ºC, for 48 hours. The human plasma was incubated 10 minutes before the addition of compounds **7c'** and **8c** to guarantee the plasma proteins were active at the time of the addition of the compounds. Periodically, in the aforementioned times, samples (100 µL) were collected from the mixture and immediately diluted in cold ACN (200 µL, dilution 1:3), in order to both stop chemical degradation (by decrease of temperature) and enzymatic degradation (by inactivation of the enzymes and inducing enzyme denaturation and/or precipitation). For compound **8c**, samples stopped being collected after no chromatogram peak was detected. Samples were then centrifuged (Beckman and Coulter ™ Microfuge ® 18 Centrifuge) during 10 min at 5000 rpm and the supernatant was analysed by HPLC, using a 55:45 methanol:water mixture as the mobile phase and 319 nm as the detection wavelength. The assay was performed in duplicate.

VI. 3. 5. Metabolic Assays in Liver Microsomes

Mice liver microsomes (20 mg of protein per mL) were extracted from male Sprague-Dawley mice. Both liver microsomes and NADPH Regenerating System Solutions A [31 mM $NADP^+$, 66mM glucose-6-phosphate, 66mM $MgCl_2$] and B [40 U/mL glucose-6-phosphate dehydrogenase in 5mM sodium citrate] were ordered from BD Gentest ™.

A stock solution with a concentration of 1.0 x 10^{-2} M in DMSO was prepared for compounds **7c'** and **8c**. A volume of 8 µL of stock solution was added to a mixture comprising 160 µL of PBS, 570 µL of deionized water and 20 µL of mice liver microsomes. After the collection of the first sample (t = 0 min), 40 µL of NADPH Regenerating System Solution A and 8 µL of NADPH Regenerating System Solution B were added to the mixture. As the metabolic enzymes are only active in the presence of the co-factors contained in solutions A and B, this procedure accounts that in the first sample (t = 0 min) no metabolic activity is considered.

The mixture was incubated in a stirred (25rpm) thermostatic bath (Lab Companion BS-06), at 37 ºC, for 1 hour. The mixture was incubated for 10 minutes before the first sampling to guarantee the compounds were solubilized and the microsomes were functional. Periodically, in the aforementioned times, samples (80 µL) were collected from the mixture and immediately diluted in cold ACN (80 µL, dilution 1:2), in order to both stop chemical degradation (by decrease of temperature) and enzymatic degradation (by inactivation of the enzymes and inducing enzyme denaturation and/or precipitation). Samples were then centrifuged (Beckman and Coulter ™ Microfuge ® 18 Centrifuge) during 3 min at 10000 rpm and the supernatant was analysed by HPLC,

using a 55:45 methanol:water mixture as the mobile phase and 319 nm as the detection wavelength.

VI. 3. 6. Antimycobacterial Screening

The antimycobacterial screening assay was performed following the broth micro-dilution method. Two 10 mL cultures of *M. tuberculosis* H37Rv pMSp12:GFP and two 10 mL cultures of *M. tuberculosis* cydKO pMSp12:GFP were grown to an optical density (OD_{600}) of 0.6 – 0.8 in two different screening media: Middlebrook 7H9 broth medium supplemented with glucose, casitone, 0.05% tyloxapol and kanamycin, and Middlebrook TH9 broth medium supplemented with glucose, bovine albumin, dextrose, catalase, 0.05% Tween-80, and kanamycin. The cultures were then diluted 1:100 in their respective media.

Stock solutions of 10mM in DMSO were prepared for the compounds to be tested. The solutions were diluted in the screening media across 10 wells in a 96-well microtiter plate, with two-fold serial dilutions, to a final volume of 50 µL of compound in each plate. 50 µL of the diluted *M. tuberculosis* culture was then added to each plate. The compound concentration range assayed was 125 – 0.244 µM. Rifampicin at a concentration of two times the MIC was used as a minimum growth control, and 5% DMSO was used as a maximum growth control.

The microtiter plate was sealed in a secondary container and incubated at 37 ºC with 5% CO_2 and humidification. The relative fluorescence [excitation wavelength: 485 nm, emission wavelength: 520 nm] was measured using a plate reader (FLUOstar OPTIMA, BMG LABTECH), at day 7 and day 14 and when concordant, day 14 data was reported. The raw fluorescence data were archived and analysed using the CDD Vault from Collaborative Drug Discovery, in which data were normalized to the minimum and maximum inhibition controls to generate a dose–response curve, using the Levenberg–Marquardt damped least-squares method, from which the MIC_{90} was calculated. MIC_{90} was considered to be the lowest concentration of each compound that inhibits growth of more than 90% of the bacterial population.

VI. 3. 7. Cytotoxicity Assays

The compounds' cytotoxicity was assayed using the MTT assay. HEK 293T cells (ATCC CRL 11268) were cultured in 96-well plates (5×10^3 cells/wall) and fixed for 24h before addition of two concentrations of compounds **6c**, **7c'**, and **8c** in dimethyl sulfoxide (20 and 50 µM). Compounds were incubated at 37 ºC, for 48h.

MTT (3-(4,5-dimethylthiazol-2-yl)-2,5-diphenyltetrazolium bromide) was added to plates at a final concentration of 400 mg/mL per well, followed by incubation at 37 ºC, for 3h. After incubation, the medium was removed, and the formazan crystals were dissolved in a 4:1 dimethyl sulfoxide/glycine buffer (pH 10.5). The plates were shaken for 15 min, and cell viability was then assessed by measuring formazan uptake at 550 nm.

Chapter VII

References

Chapter VII – References

[1] E. L. Stockbridge, T. L. Miller, E. K. Carlson, and C. Ho, "Predictors of latent tuberculosis infection treatment completion in the US private sector : an analysis of administrative claims data," *BMC Public Health*, vol. 18, no. 662, pp. 1–13, 2018, doi: 10.1186/s12889-018-5578-3.

[2] World Health Organization, "Global Tuberculosis Report 2022," Geneva, 2022.

[3] A. B. Hogan *et al.*, "Potential impact of the COVID-19 pandemic on HIV, tuberculosis, and malaria in low-income and middle-income countries: a modelling study," *Lancet Glob. Heal.*, vol. 8, no. 9, pp. e1132–e1141, 2020, doi: 10.1016/S2214-109X(20)30288-6.

[4] A. A. Velayati, P. Farnia, and S. Hoffner, "Drug-resistant Mycobacterium tuberculosis: Epidemiology and role of morphological alterations," *J. Glob. Antimicrob. Resist.*, vol. 12, pp. 192–196, 2018, doi: 10.1016/j.jgar.2017.10.006.

[5] P. K. Drain *et al.*, "Incipient and subclinical tuberculosis: A clinical review of early stages and progression of infection," *Clin. Microbiol. Rev.*, vol. 31, no. 4, 2018, doi: 10.1128/CMR.00021-18.

[6] World Health Organization, "Global tuberculosis report 2021," Geneva, 2021. [Online]. Available: https://www.who.int/publications/i/item/9789240037021.

[7] S. Gagneux, "Ecology and evolution of Mycobacterium tuberculosis," *Nat. Rev. Microbiol.*, vol. 16, no. 4, pp. 202–213, 2018, doi: 10.1038/nrmicro.2018.8.

[8] M. Woodman, I. L. Haeusler, and L. Grandjean, "Tuberculosis genetic epidemiology: A latin american perspective," *Genes (Basel).*, vol. 10, no. 1, 2019, doi: 10.3390/genes10010053.

[9] G. T. Mashabela, T. J. De Wet, and D. F. Warner, "Mycobacterium tuberculosis metabolism," *Microbiol. Spectr.*, vol. 7, no. 4, pp. 1107–1128, 2019, doi: 10.1128/9781683670131.ch67.

[10] H. Eoh *et al.*, "Metabolic anticipation in Mycobacterium tuberculosis," *Nat. Microbiol.*, vol. 2, no. May, pp. 1–7, 2017, doi: 10.1038/nmicrobiol.2017.84.

[11] U. Banerjee, S. Sankar, A. Singh, and N. Chandra, "A Multi-Pronged Computational Pipeline for Prioritizing Drug Target Strategies for Latent Tuberculosis," *Front. Chem.*, vol. 8, no. December, pp. 1–18, 2020, doi: 10.3389/fchem.2020.593497.

[12] R. K. Maurya, S. Bharti, and M. Y. Krishnan, "Triacylglycerols: Fuelling the hibernating mycobacterium tuberculosis," *Front. Cell. Infect. Microbiol.*, vol. 9, no. JAN, pp. 1–8, 2019, doi: 10.3389/fcimb.2018.00450.

[13] J. B. Torrelles and L. S. Schlesinger, "Integrating Lung Physiology, Immunology, and Tuberculosis," *Trends Microbiol.*, vol. 25, no. 8, pp. 688–697, 2017, doi: 10.1016/j.tim.2017.03.007.

[14] J. Parmer, L. Allen, and W. Walton, "Tuberculosis : A New Screening Recommendation and an Expanded Approach to Elimination in the United States," *Am. J. Nurs.*, vol. 117, no. 8, pp. 24–34, 2017, doi: 10.1097/01.NAJ.0000521946.45448.90.

[15] L. Luies and I. du Preez, "The echo of pulmonary tuberculosis: Mechanisms of clinical symptoms and other disease-induced systemic complications," *Clin. Microbiol. Rev.*, vol. 33, no. 4, pp. 1–19, Oct. 2020, doi: 10.1128/CMR.00036-20/ASSET/CD599B44-9A03-44EE-B002-F1BA54F78626/ASSETS/GRAPHIC/CMR.00036-20-F0002.JPEG.

[16] T. Parbhoo, S. L. Sampson, and J. M. Mouton, "Recent Developments in the Application of Flow Cytometry to Advance our Understanding of Mycobacterium tuberculosis Physiology and Pathogenesis," *Cytom. Part A*, vol. 97, no. 7, pp. 683–693, 2020, doi: 10.1002/cyto.a.24030.

[17] L. I. Rankine-Wilson, T. Shapira, C. S. Emani, and Y. Av-Gay, "From infection niche to therapeutic target: The intracellular lifestyle of Mycobacterium tuberculosis," *Microbiol. (United Kingdom)*, vol. 167, no. 4, 2021, doi: 10.1099/MIC.0.001041.

[18] M. Z. Khan, P. Kaur, and V. K. Nandicoori, "Targeting the messengers: Serine/threonine protein kinases as potential targets for antimycobacterial drug development," *IUBMB Life*, vol. 70, no. 9, pp. 889–904, 2018, doi: 10.1002/iub.1871.

[19] J. K. Sia and J. Rengarajan, "Immunology of mycobacterium tuberculosis infections," *Microbiol. Spectr.*, vol. 7, no. 4, pp. 1056–1086, 2019, doi: 10.1128/9781683670131.ch64.

[20] J. L. Khawbung, D. Nath, and S. Chakraborty, "Drug resistant Tuberculosis: A review," *Comp. Immunol. Microbiol. Infect. Dis.*, vol. 74, p. 101574, 2021, doi: 10.1016/j.cimid.2020.101574.

[21] V. Peddireddy, S. N. Doddam, and N. Ahmed, "Mycobacterial dormancy systems and host responses in tuberculosis," *Front. Immunol.*, vol. 8, no. FEB, pp. 1–19, 2017, doi: 10.3389/fimmu.2017.00084.

[22] C. E. Dodd and L. S. Schlesinger, "New concepts in understanding latent tuberculosis," *Curr. Opin. Infect. Dis.*, vol. 30, no. 3, pp. 316–321, 2017, doi: 10.1097/QCO.0000000000000367.

[23] T. Q. Mai *et al.*, "Tuberculosis risk factors and Mycobacterium tuberculosis transmission among HIV-infected patients in Vietnam," *Tuberculosis*, vol. 115, no. December 2018, pp. 67–75, 2019, doi: 10.1016/j.tube.2019.02.001.

[24] A. M. Cadena, S. M. Fortune, and J. L. Flynn, "Heterogeneity in tuberculosis," *Nat. Rev. Immunol.*, vol. 17, no. 11, pp. 691–702, 2017, doi: 10.1038/nri.2017.69.

[25] E. W. Tiemersma, M. J. van der Werf, M. W. Borgdorff, B. G. Williams, and N. J. D. Nagelkerke, "Natural history of tuberculosis: Duration and fatality of untreated pulmonary tuberculosis in HIV negative patients: A systematic review," *PLoS One*, vol. 6, no. 4, 2011, doi: 10.1371/journal.pone.0017601.

[26] K. Dheda *et al.*, "The epidemiology , pathogenesis , transmission , diagnosis , and management of multidrug-resistant , extensively drug-resistant , and incurable tuberculosis," *Lancet Respir. Med.*, vol. 2600, no. 17, pp. 291–360, 2017, doi: 10.1016/S2213-2600(17)30079-6.

[27] N. Dookie, S. Rambaran, N. Padayatchi, S. Mahomed, and K. Naidoo, "Evolution of drug resistance in Mycobacterium tuberculosis: A review on the molecular determinants of resistance and implications for personalized care," *J. Antimicrob. Chemother.*, vol. 73, no. 5, pp. 1138–1151, 2018, doi: 10.1093/jac/dkx506.

[28] H. M. A. Hameed *et al.*, "Molecular targets related drug resistance mechanisms in MDR-, XDR-, and TDR-Mycobacterium tuberculosis strains," *Front. Cell. Infect. Microbiol.*, vol. 8, no. APR, 2018, doi: 10.3389/fcimb.2018.00114.

[29] S. Tiberi *et al.*, "Tuberculosis: progress and advances in development of new drugs, treatment regimens, and host-directed therapies," *Lancet Infect. Dis.*, vol. 18, no. 7, pp. e183–e198, 2018, doi: 10.1016/S1473-3099(18)30110-5.

[30] V. L. Campodónico, D. Rifat, Y. M. Chuang, T. R. Ioerger, and P. C. Karakousis, "Altered Mycobacterium tuberculosis cell wall metabolism and physiology associated with RpoB mutation H526D," *Front. Microbiol.*, vol. 9, no. MAR, p. 494, 2018, doi: 10.3389/fmicb.2018.00494.

[31] K. Floyd, P. Glaziou, A. Zumla, and M. Raviglione, "The global tuberculosis epidemic and progress in care, prevention, and research: an overview in year 3 of the End TB era," *Lancet Respir. Med.*, vol. 6, no. 4, pp. 299–314, 2018, doi: 10.1016/S2213-2600(18)30057-2.

[32] D. Sharma and D. Bisht, "M. tuberculosis hypothetical proteins and proteins of unknown function: Hope for exploring novel resistance mechanisms as well as future target of drug resistance," *Front. Microbiol.*, vol. 8, no. MAR, pp. 1–5, 2017, doi: 10.3389/fmicb.2017.00465.

[33] F. Conradie *et al.*, "Treatment of Highly Drug-Resistant Pulmonary Tuberculosis," *N. Engl. J. Med.*, vol. 382, no. 10, pp. 893–902, 2020, doi: 10.1056/nejmoa1901814.

[34] M. J. A. Reid *et al.*, "Building a tuberculosis-free world: The Lancet Commission on tuberculosis," *Lancet*, vol. 393, no. 10178, pp. 1331–1384, 2019, doi: 10.1016/S0140-6736(19)30024-8.

[35] P. K. Deb, N. A. Al-Shar'i, K. N. Venugopala, M. Pillay, and P. Borah, "In vitro anti-TB properties, in silico target validation, molecular docking and dynamics studies of substituted 1,2,4-oxadiazole analogues against Mycobacterium tuberculosis," *J. Enzyme Inhib. Med. Chem.*, vol. 36, no. 1, pp. 869–884, 2021, doi: 10.1080/14756366.2021.1900162.

[36] M. A. Ejalonibu *et al.*, "Dual targeting approach for Mycobacterium tuberculosis drug discovery: insights from DFT calculations and molecular dynamics simulations," *Struct. Chem.*, vol. 31, no. 2, pp. 557–571, 2020, doi: 10.1007/s11224-019-01422-w.

[37] A. Campaniço, R. Moreira, and F. Lopes, "Drug discovery in tuberculosis. New

drug targets and antimycobacterial agents," *Eur. J. Med. Chem.*, vol. 150, pp. 525–545, 2018, doi: 10.1016/j.ejmech.2018.03.020.

[38] A. Washburn *et al.*, "Dual-targeting GroEL/ES chaperonin and protein tyrosine phosphatase B (PtpB)inhibitors: A polypharmacology strategy for treating Mycobacterium tuberculosis infections," *Bioorganic Med. Chem. Lett.*, vol. 29, no. 13, pp. 1665–1672, 2019, doi: 10.1016/j.bmcl.2019.04.034.

[39] P. Nahid *et al.*, *Treatment of drug-resistant tuberculosis an official ATS/CDC/ERS/IDSA clinical practice guideline*, vol. 200, no. 10. 2019.

[40] A. G. Flynn, K. Aiona, M. K. Haas, R. Reves, and R. Belknap, "Clinical characteristics of active tuberculosis diagnosed after starting treatment for latent tuberculosis infection," *Clin. Infect. Dis.*, vol. 71, no. 5, pp. 1320–1323, 2020, doi: 10.1093/cid/ciz1157.

[41] M. A. Huaman and T. R. Sterling, "Treatment of Latent Tuberculosis Infection — An Update," *Clin. Chest Med.*, vol. 40, no. 4, pp. 839–848, 2019, doi: 10.1016/j.ccm.2019.07.008.

[42] Y. Eun, G. Jung, and N. W. Schluger, "Advances in the diagnosis and treatment of latent tuberculosis infection," *Curr. Opin. Infect. Dis.*, vol. 33, no. 2, pp. 166–172, 2020, doi: 10.1097/QCO.0000000000000629.

[43] A. Campaniço, S. G. Harjivan, D. F. Warner, R. Moreira, and F. Lopes, "Addressing Latent Tuberculosis: New Advances in Mimicking the Disease, Discovering Key Targets, and Designing Hit Compounds," *Int. J. Mol. Sci.*, vol. 21, no. 22, p. 8854, Nov. 2020, doi: 10.3390/ijms21228854.

[44] J. Furin, H. Cox, and M. Pai, "Tuberculosis," *Lancet*, vol. 393, no. 10181, pp. 1642–1656, 2019, doi: 10.1016/S0140-6736(19)30308-3.

[45] D. Menzies *et al.*, "Four Months of Rifampin or Nine Months of Isoniazid for Latent Tuberculosis in Adults," *N. Engl. J. Med.*, vol. 379, no. 5, pp. 440–453, 2018, doi: 10.1056/nejmoa1714283.

[46] L. A. Ronald *et al.*, "Estimated Impact of World Health Organization Latent Tuberculosis Screening Guidelines in a Region With a Low Tuberculosis Incidence : Retrospective Cohort Study," *Clin. Infect. Dis.*, vol. 69, no. 12, pp. 2101–2108, 2019, doi: 10.1093/cid/ciz188.

[47] E. J. Hasenoehrl, T. J. Wiggins, and M. Berney, "Bioenergetic Inhibitors: Antibiotic Efficacy and Mechanisms of Action in Mycobacterium tuberculosis," *Front. Cell. Infect. Microbiol.*, vol. 10, no. January, pp. 1–26, 2021, doi: 10.3389/fcimb.2020.611683.

[48] S. Bajeli, N. Baid, M. Kaur, G. P. Pawar, V. D. Chaudhari, and A. Kumar, "Terminal Respiratory Oxidases: A Targetables Vulnerability of Mycobacterial Bioenergetics?," *Front. Cell. Infect. Microbiol.*, vol. 10, no. November, pp. 1–22, 2020, doi: 10.3389/fcimb.2020.589318.

[49] C. S. Foo, K. Pethe, and A. Lupien, "Oxidative Phosphorylation — an Update on a New , Essential Target Space for Drug Discovery in Mycobacterium tuberculosis," *Appl. Sci.*, vol. 10, no. 7, Apr. 2020, doi:

doi.org/10.3390/app10072339.

[50] Y. Cai *et al.*, "Host immunity increases Mycobacterium tuberculosis reliance on cytochrome bd oxidase," *PLoS Pathog.*, vol. 17, no. 7, pp. 1–17, 2021, doi: 10.1371/journal.ppat.1008911.

[51] I. K. Iqbal, S. Bajeli, A. K. Akela, and A. Kumar, "Bioenergetics of Mycobacterium: An Emerging Landscape for Drug Discovery," *Pathog. 2018, Vol. 7, Page 24*, vol. 7, no. 1, p. 24, Feb. 2018, doi: 10.3390/PATHOGENS7010024.

[52] B. J. Berube, D. Russell, L. Castro, S. Choi, P. Narayanasamy, and T. Parish, "Novel MenA Inhibitors Are Bactericidal against Mycobacterium," *Antimicrob. Agents Chemother.*, vol. 63, no. 6, pp. 1–7, 2019.

[53] S. Gupta, Z. Fatima, and S. Kumawat, "Study of the bioenergetics to identify the novel pathways as a drug target against Mycobacterium tuberculosis using Petri net," *BioSystems*, vol. 209, no. March, p. 104509, 2021, doi: 10.1016/j.biosystems.2021.104509.

[54] M. A. Wani and D. K. Dhaked, "Targeting the cytochrome bc1 complex for drug development in M. tuberculosis: review," *Mol. Divers.*, no. 0123456789, 2021, doi: 10.1007/s11030-021-10335-y.

[55] A. M. Thompson and W. A. Denny, *Inhibitors of enzymes in the electron transport chain of Mycobacterium tuberculosis*, 1st ed., vol. 52. Elsevier Inc., 2019.

[56] K. K. Roy and M. A. Wani, "Emerging opportunities of exploiting mycobacterial electron transport chain pathway for drug-resistant tuberculosis drug discovery," *Expert Opin. Drug Discov.*, vol. 15, no. 2, pp. 231–241, 2020, doi: 10.1080/17460441.2020.1696771.

[57] N. C. Cardoso, K. Chibale, and V. Singh, "Implications of Mycobacterium tuberculosis Metabolic Adaptability on Drug Discovery and Development," *ACS Infect. Dis.*, vol. 8, no. 3, pp. 414–421, 2022, doi: 10.1021/acsinfecdis.1c00627.

[58] B. J. Berube and T. Parish, "Combinations of respiratory chain inhibitors have enhanced bactericidal activity against mycobacterium tuberculosis," *Antimicrob. Agents Chemother.*, vol. 62, no. 1, 2018, doi: 10.1128/AAC.01677-17.

[59] A. Harikishore, S. S. M. Chong, P. Ragunathan, R. W. Bates, and G. Grüber, "Targeting the menaquinol binding loop of mycobacterial cytochrome bd oxidase," *Mol. Divers.*, vol. 25, no. 1, pp. 517–524, 2021, doi: 10.1007/s11030-020-10034-0.

[60] V. B. Borisov, "Bioenergetics and Reactive Nitrogen Species in Bacteria," 2022.

[61] B. Wiseman *et al.*, "Structure of a functional obligate complex III2IV2 respiratory supercomplex from Mycobacterium smegmatis," *Nat. Struct. Mol. Biol.*, vol. 25, no. 12, pp. 1128–1136, 2018, doi: 10.1038/s41594-018-0160-3.

[62] G. A. Harrison *et al.*, " Identification of 4-Amino-Thieno[2,3- d]Pyrimidines as QcrB Inhibitors in Mycobacterium tuberculosis ," *mSphere*, vol. 4, no. 5, 2019,

doi: 10.1128/msphere.00606-19.

[63] A. Lupien *et al.*, "New 2-Ethylthio-4-methylaminoquinazoline derivatives inhibiting two subunits of cytochrome bc1 in Mycobacterium tuberculosis," *PLoS Pathog.*, vol. 16, no. 1, pp. 1–19, 2020, doi: 10.1371/journal.ppat.1008270.

[64] G. C. Moraski *et al.*, "Intracellular and in vivo evaluation of imidazo [2,1-b]thiazole-5-carboxamide antituberculosis compounds," *PLoS One*, vol. 15, no. 1, pp. 1–19, 2020, doi: 10.1371/journal.pone.0227224.

[65] N. S. Chandrasekera *et al.*, "Improved Phenoxyalkylbenzimidazoles with Activity against Mycobacterium tuberculosis Appear to Target QcrB," *ACS Infect. Dis.*, vol. 3, no. 12, pp. 898–916, 2017, doi: 10.1021/acsinfecdis.7b00112.

[66] T. Friedrich, D. Wohlwend, and V. B. Borisov, "Recent Advances in Structural Studies of Cytochrome bd and Its Potential Application as a Drug Target," *Int. J. Mol. Sci.*, vol. 23, no. 6, 2022, doi: 10.3390/ijms23063166.

[67] C. S. Foo *et al.*, "Arylvinylpiperazine Amides, a New Class of Potent Inhibitors Targeting QcrB of Mycobacterium tuberculosis," *MBio*, vol. 9, no. 5, pp. 1–13, Nov. 2018, doi: 10.1128/mBio.01276-18.

[68] A. Moosa *et al.*, "Susceptibility of Mycobacterium Mutants to Compounds Targeting the," vol. 61, no. 10, pp. 3–7, 2017.

[69] B. S. Lee, N. P. Kalia, X. E. F. Jin, E. J. Hasenoehrl, M. Berney, and K. Pethe, "Inhibitors of energy metabolism interfere with antibiotic-induced death in mycobacteria," *J. Biol. Chem.*, vol. 294, no. 6, pp. 1936–1943, 2019, doi: 10.1074/jbc.RA118.005732.

[70] G. F. dos S. Fernandes, C. M. Chin, and J. L. dos Santos, "Potential molecular targets for antituberculosis drug discovery," *Quim. Nova*, vol. 40, no. 5, pp. 572–585, 2017, doi: 10.21577/0100-4042.20170016.

[71] L. Brulíkov, M. Urban, and V. Slachtov, "Small organic molecules targeting the energy metabolism of Mycobacterium tuberculosis," *Eur. J. Med. Chem.*, vol. 212, 2021, doi: 10.1016/j.ejmech.2020.113139.

[72] V. K. Gupta, M. M. Kumar, D. Singh, D. Bisht, and S. Sharma, "Drug targets in dormant Mycobacterium tuberculosis: can the conquest against tuberculosis become a reality?," *Infect. Dis. (Auckl).*, vol. 50, no. 2, pp. 81–94, 2018, doi: 10.1080/23744235.2017.1377346.

[73] J. Verma and N. Subbarao, "Designing novel inhibitors against cyclopropane mycolic acid synthase 3 (PcaA): targeting dormant state of Mycobacterium tuberculosis," *J. Biomol. Struct. Dyn.*, vol. 39, no. 17, pp. 6339–6354, 2021, doi: 10.1080/07391102.2020.1797534.

[74] E. L. Nuermberger, "Preclinical Efficacy Testing of New Drug Candidates," *Microbiol. Spectr.*, vol. 5, no. 3, 2017, doi: 10.1128/microbiolspec.TBTB2-0034-2017.Correspondence.

[75] S. Sundararajan and R. Muniyan, "Latent tuberculosis: interaction of virulence

factors in Mycobacterium tuberculosis," *Mol. Biol. Rep.*, vol. 48, no. 8, pp. 6181–6196, 2021, doi: 10.1007/s11033-021-06611-7.

[76] J. P. Sarathy, G. Gruber, and T. Dick, "Re-understanding the mechanisms of action of the anti-mycobacterial drug bedaquiline," *Antibiotics*, vol. 8, no. 4, 2019, doi: 10.3390/antibiotics8040261.

[77] A. B. Jeon *et al.*, "2-Aminoimidazoles Collapse Mycobacterial Proton Motive Force and Block the Electron Transport Chain," *Sci. Rep.*, vol. 9, no. 1, pp. 1–13, 2019, doi: 10.1038/s41598-018-38064-7.

[78] J. Odingo *et al.*, "In Vitro Evaluation of Novel Nitazoxanide Derivatives against Mycobacterium tuberculosis," *ACS Omega*, vol. 2, no. 9, pp. 5873–5890, Sep. 2017, doi: 10.1021/ACSOMEGA.7B00892/ASSET/IMAGES/LARGE/AO-2017-00892Q_0003.JPEG.

[79] W. Yu *et al.*, "Sterilizing effects of novel regimens containing TB47, clofazimine, and linezolid in a murine model of tuberculosis," *Antimicrob. Agents Chemother.*, vol. 65, no. 10, 2021, doi: 10.1128/AAC.00706-21.

[80] W. Yu *et al.*, "TB47 and clofazimine form a highly synergistic sterilizing block in a second-line regimen for tuberculosis in mice," *Biomed. Pharmacother.*, vol. 131, no. July, p. 110782, 2020, doi: 10.1016/j.biopha.2020.110782.

[81] S. Zeng, J. Zhang, M. Sun, X. Zhang, G. M. Cook, and T. Zhang, "Nitric oxide-dependent electron transport chain inhibition by the cytochrome bc1inhibitor and pretomanid combination kills mycobacterium tuberculosis," *Antimicrob. Agents Chemother.*, vol. 65, no. 9, 2021, doi: 10.1128/AAC.00956-21.

[82] S. M. S. Chong *et al.*, "Antituberculosis Activity of the Antimalaria Cytochrome *bcc* Oxidase Inhibitor SCR0911.," *ACS Infect. Dis.*, vol. 6, no. 4, pp. 725–737, Mar. 2020, doi: 10.1021/ACSINFECDIS.9B00408.

[83] A. Calcaterra *et al.*, "The pictet-spengler reaction updates its habits," *Molecules*, vol. 25, no. 2, 2020, doi: 10.3390/molecules25020414.

[84] S. P. Roche, J. J. Youte Tendoung, and B. Tréguier, "Advances in dearomatization strategies of indoles," *Tetrahedron*, vol. 71, no. 22, pp. 3549–3591, 2015, doi: 10.1016/j.tet.2014.06.054.

[85] W. Jiang, X. Zhang, and Z. Sui, "Potassium superoxide as an alternative reagent for winterfeldt oxidation of β-carbolines," *Org. Lett.*, vol. 5, no. 1, pp. 43–46, 2003, doi: 10.1021/ol0271279.

[86] M. Mentel, M. Peters, J. Albering, and R. Breinbauer, "The Witkop-Winterfeldt oxidation converts tetrahydropyridoindoles into pyrroloquinolones and cinnolines by an unprecedented scaffold rearrangement," *Tetrahedron*, vol. 67, no. 5, pp. 965–970, 2011, doi: 10.1016/j.tet.2010.11.110.

[87] M. Mentel and R. Breinbauer, "The Witkop-Winterfeldt-Oxidation of Indoles," *Curr. Org. Chem.*, vol. 11, no. 2, pp. 159–176, 2006, doi: 10.2174/138527207779316426.

[88] P. Klövekorn *et al.*, "From off-to on-target: New BRAF-inhibitor-template-derived compounds selectively targeting mitogen activated protein kinase

kinase 4 (MKK4)," *Eur. J. Med. Chem.*, vol. 210, 2021, doi: 10.1016/j.ejmech.2020.112963.

[89] A. V. Aksenov *et al.*, "Electrophilically activated nitroalkanes in synthesis of 3,4-dihydroquinozalines," *Molecules*, vol. 26, no. 14, pp. 1–15, 2021, doi: 10.3390/molecules26144274.

[90] F. Zafar *et al.*, "Physicochemical and Pharmacokinetic Analysis of Anacardic Acid Derivatives," *ACS Omega*, vol. 5, no. 11, pp. 6021–6030, 2020, doi: 10.1021/acsomega.9b04398.

[91] C. Fink *et al.*, "Evaluating the Role of Solubility in Oral Absorption of Poorly Water-Soluble Drugs Using Physiologically-Based Pharmacokinetic Modeling," *Clin. Pharmacol. Ther.*, vol. 107, no. 3, pp. 650–661, Mar. 2020, doi: 10.1002/CPT.1672.

[92] G. Tambosi *et al.*, "Challenges to improve the biopharmaceutical properties of poorly water-soluble drugs and the application of the solid dispersion technology," *Matéria (Rio Janeiro)*, vol. 23, no. 4, Dec. 2018, doi: 10.1590/S1517-707620180004.0558.

[93] E. Freitas, "Hit optimization to improve aqueous solubility of compounds with antimycobacterial activity," p. 50, 2020.

[94] L. Di and E. H. Kerns, "Stability challenges in drug discovery," *Chem. Biodivers.*, vol. 6, no. 11, pp. 1875–1886, 2009, doi: 10.1002/cbdv.200900061.

[95] L. Di, E. H. Kerns, Y. Hong, and H. Chen, "Development and application of high throughput plasma stability assay for drug discovery," *Int. J. Pharm.*, vol. 297, no. 1–2, pp. 110–119, Jun. 2005, doi: 10.1016/j.ijpharm.2005.03.022.

[96] S. Roth *et al.*, "Crossing the Border: From Keto- to Imine Reduction in Short-Chain Dehydrogenases/Reductases," *ChemBioChem*, vol. 21, no. 18, pp. 2615–2619, Sep. 2020, doi: 10.1002/cbic.202000233.

[97] X. Liu and L. Jia, "The Conduct of Drug Metabolism Studies Considered Good Practice (I): Analytical Systems and In Vivo Studies," *Curr. Drug Metab.*, vol. 8, no. 8, pp. 815–821, Dec. 2007, doi: 10.2174/138920007782798153.

[98] Z. Zhang and W. Tang, "Drug metabolism in drug discovery and development," *Acta Pharm. Sin. B*, vol. 8, no. 5, pp. 721–732, Sep. 2018, doi: 10.1016/j.apsb.2018.04.003.

[99] T. Iwatsubo, H. Suzuki, and Y. Sugiyama, "Prediction of species differences (rats, dogs, humans) in the in vivo metabolic clearance of YM796 by the liver from in vitro data," *J. Pharmacol. Exp. Ther.*, vol. 283, no. 2, pp. 462–469, Nov. 1997, Accessed: Nov. 20, 2022. [Online]. Available: https://pubmed.ncbi.nlm.nih.gov/9353358/.

[100] D. Canudo, "Desenvolvimento de moléculas híbridas tendo como alvo a cadeia respiratória do Mycobacterium tuberculosis," Universidade de Lisboa, 2021.

[101] S. G. Franzblau *et al.*, "Comprehensive analysis of methods used for the evaluation of compounds against Mycobacterium tuberculosis," *Tuberculosis*, vol. 92, no. 6, pp. 453–488, Nov. 2012, doi: 10.1016/j.tube.2012.07.003.

[102] V. Srivastava, C. Rouanet, R. Srivastava, B. Ramalingam, C. Locht, and B. S. Srivastava, "Macrophage-specific Mycobacterium tuberculosis genes: identification by green fluorescent protein and kanamycin resistance selection," *Microbiology*, vol. 153, no. 3, pp. 659–666, Mar. 2007, doi: 10.1099/mic.0.2006/000547-0.

[103] D. A. Smith, L. Di, and E. H. Kerns, "The effect of plasma protein binding on in vivo efficacy: misconceptions in drug discovery," *Nat. Rev. Drug Discov.*, vol. 9, no. 12, pp. 929–939, Dec. 2010, doi: 10.1038/nrd3287.

[104] R. Tangallapally, R. Yendapally, A. Daniels, R. Lee, and R. Lee, "Nitrofurans as Novel Anti-tuberculosis Agents: Identification, Development and Evaluation," *Curr. Top. Med. Chem.*, vol. 7, no. 5, pp. 509–526, 2007, doi: 10.2174/156802607780059772.

[105] R. P. Tangallapally *et al.*, "Synthesis and evaluation of nitrofuranylamides as novel antituberculosis agents," *J. Med. Chem.*, vol. 47, no. 21, pp. 5276–5283, 2004, doi: 10.1021/jm049972y.

Annexes

Annex 1 – Calibration Curves

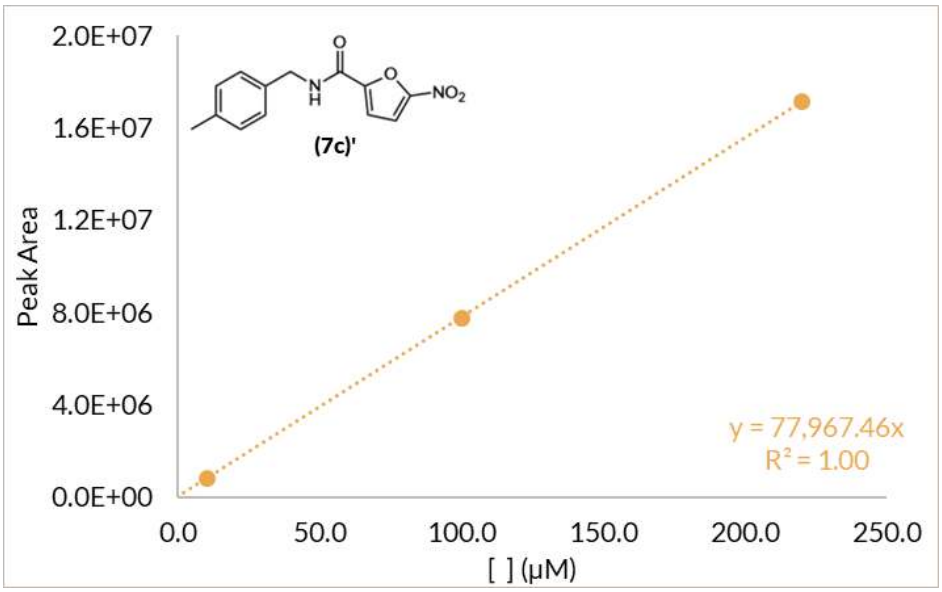

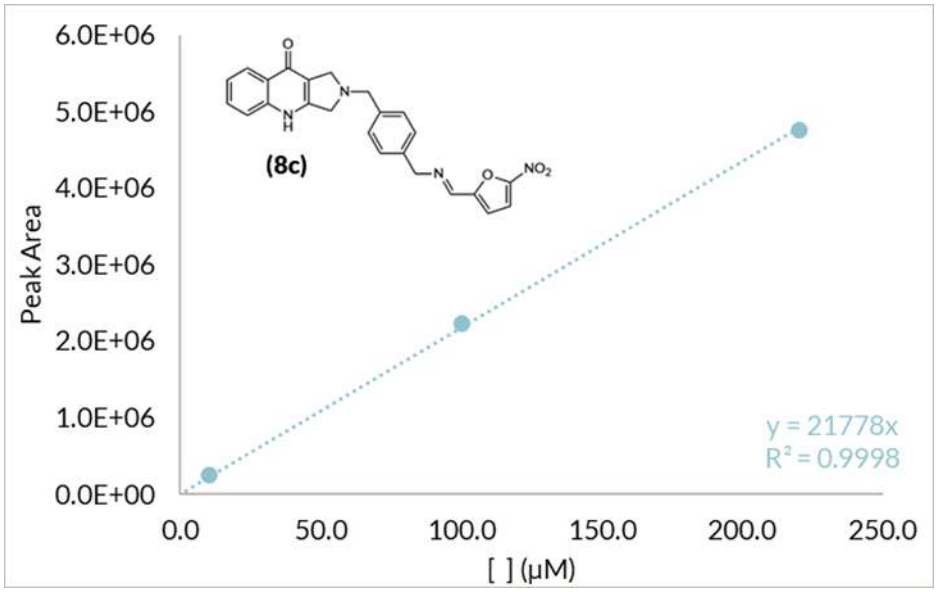

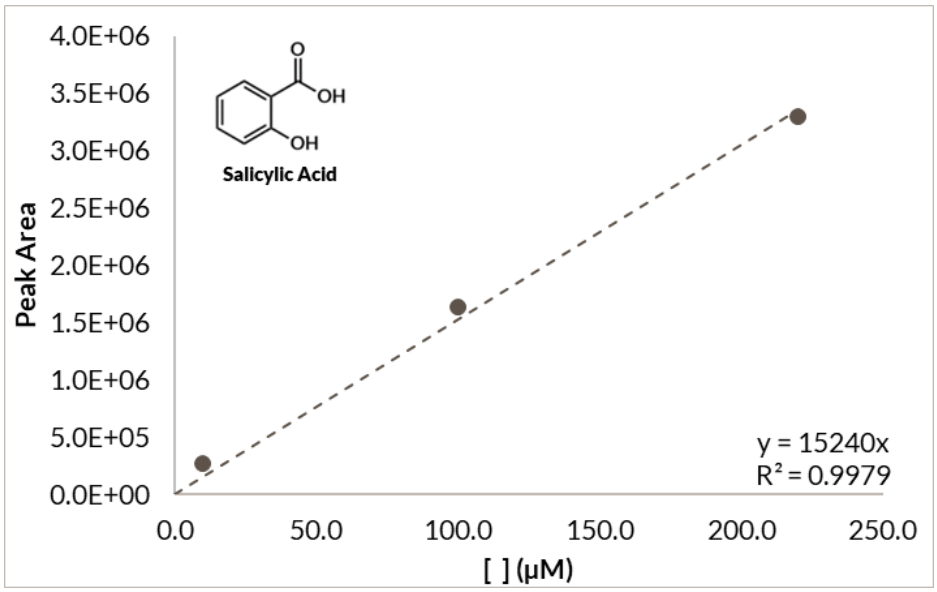

Annex 2 – Structural Characterization Spectra

Compound 1

^{1}H NMR

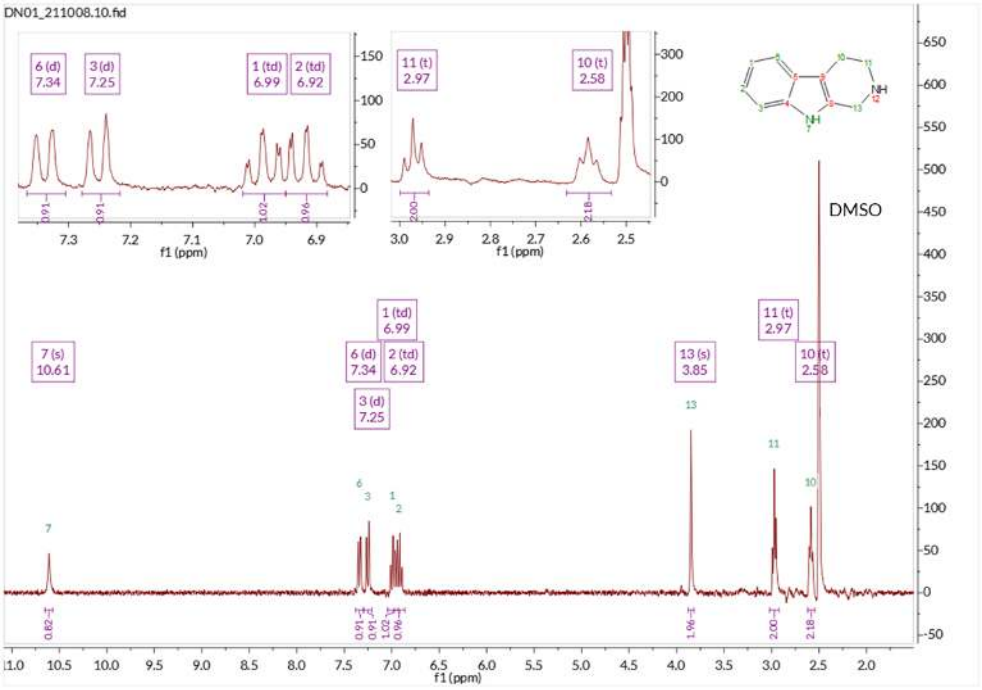

Compound 2

^{1}H NMR

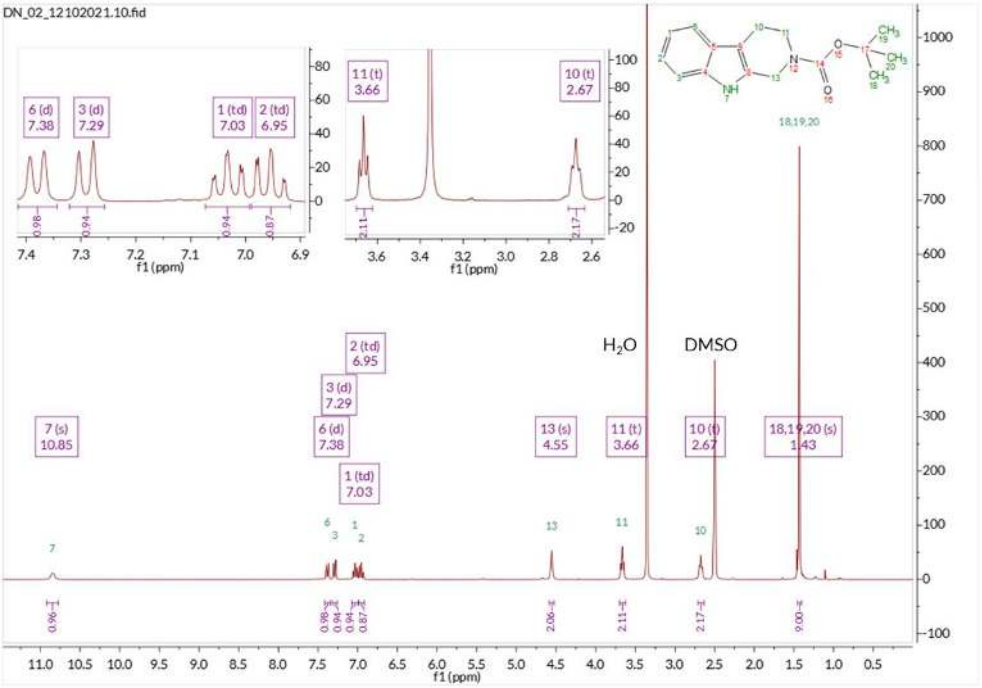

Compound 3

^{1}H NMR

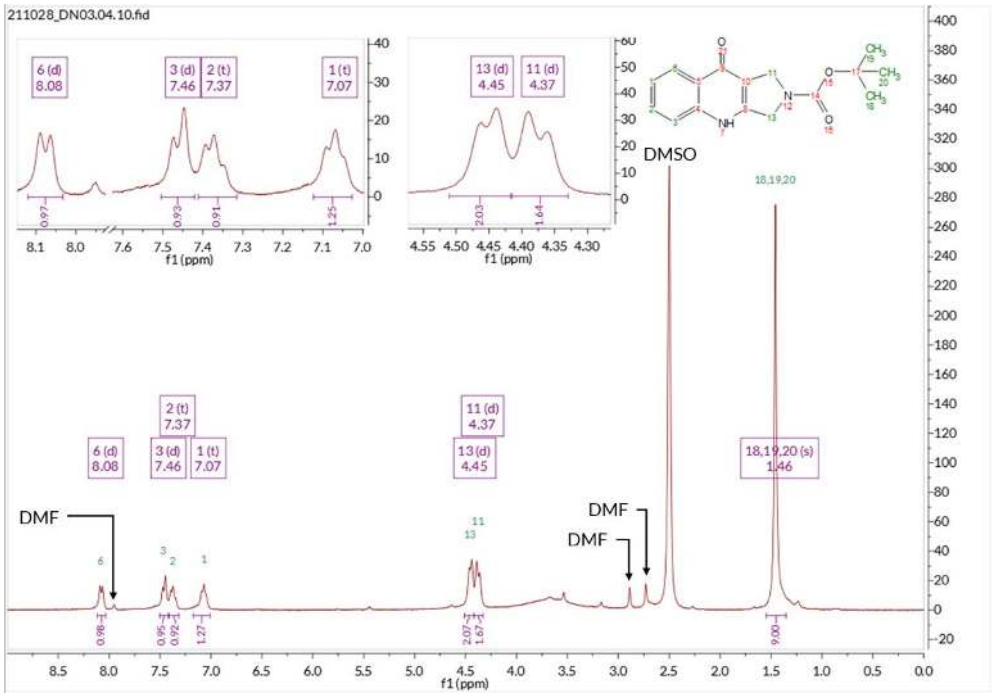

Compound 4

^{1}H NMR

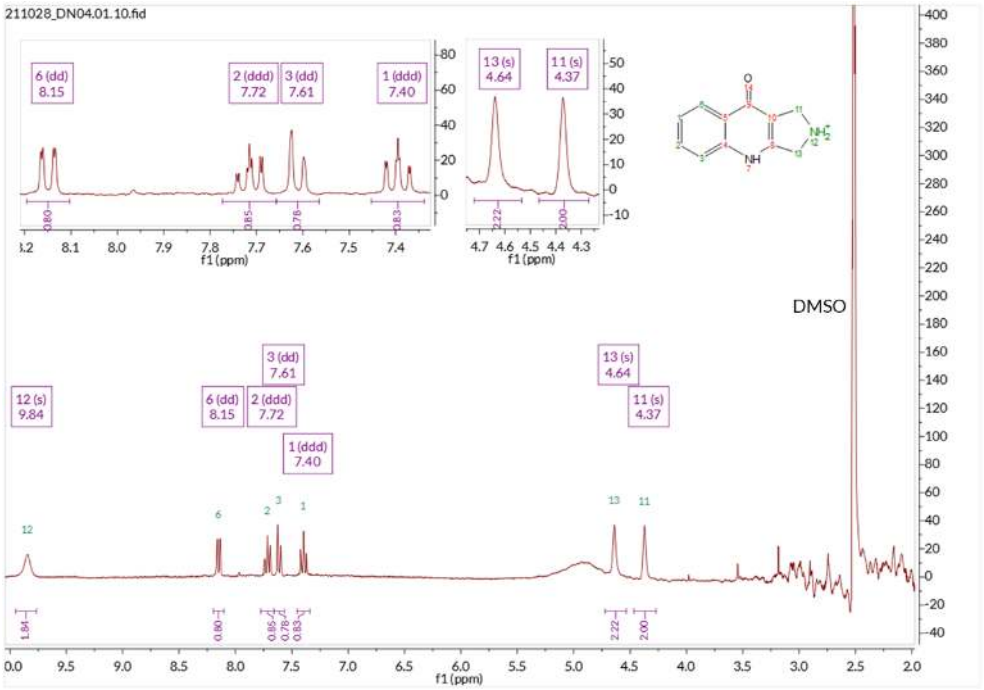

Compound 5a

ESI – MS

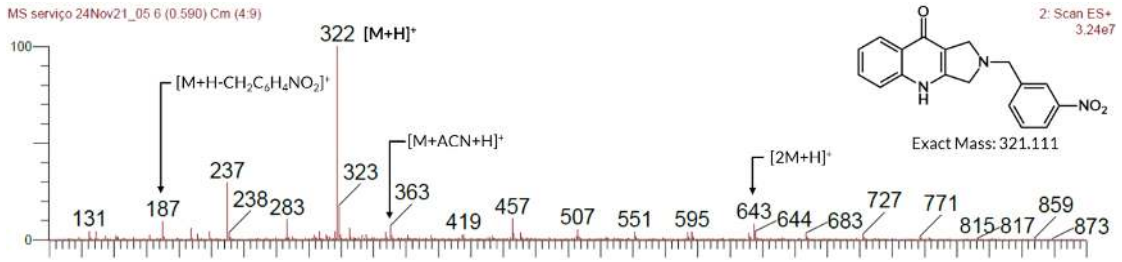

^{1}H NMR

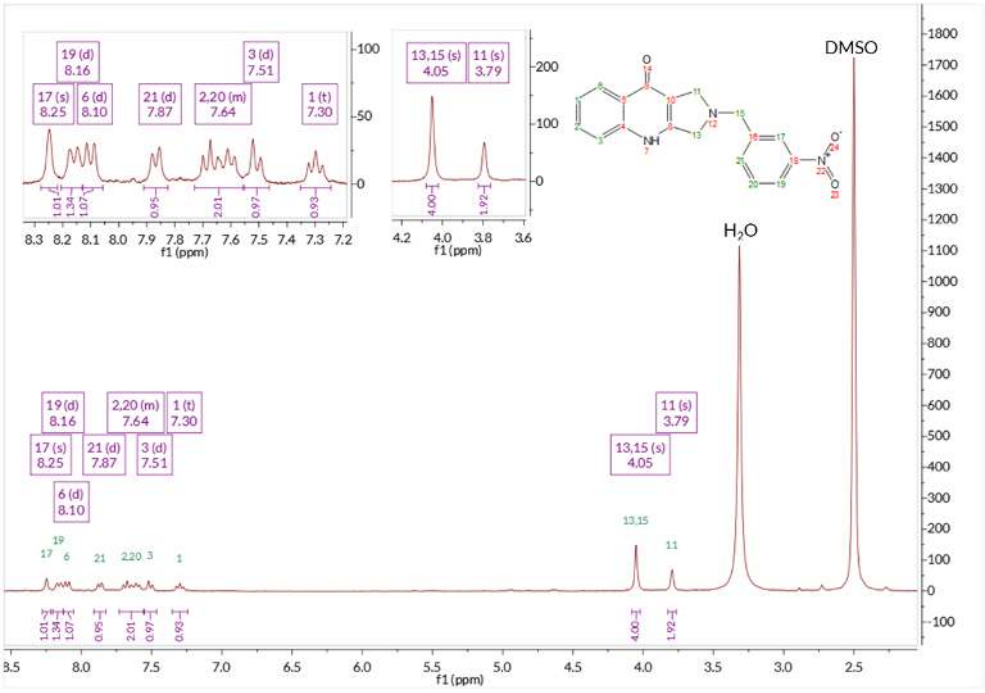

Compound 5b

^{1}H NMR

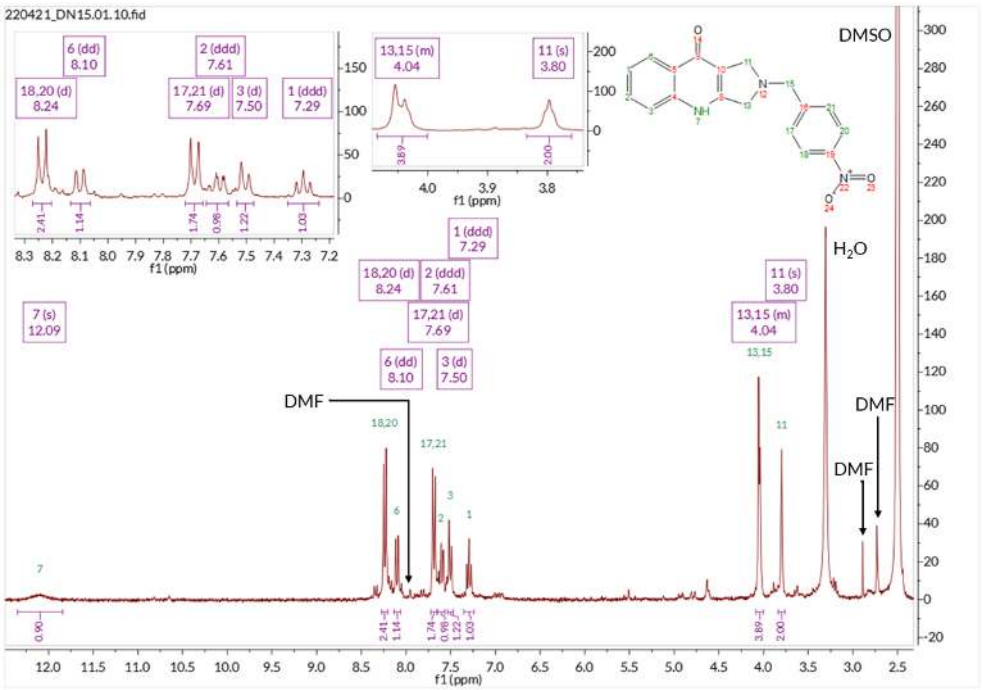

Compound 5c

^{1}H NMR

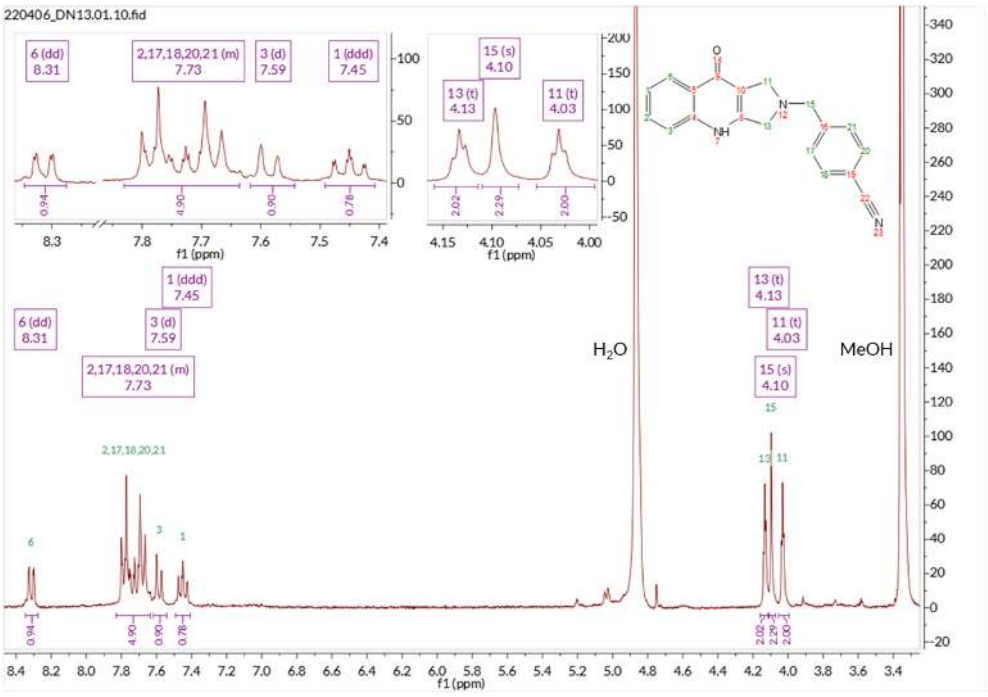

Compound 6a

ESI – MS

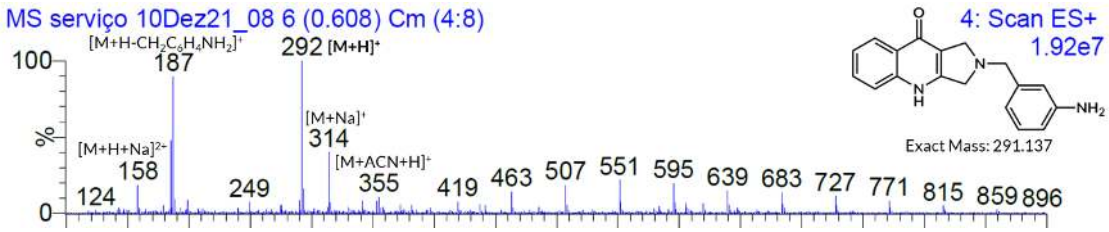

^{1}H NMR

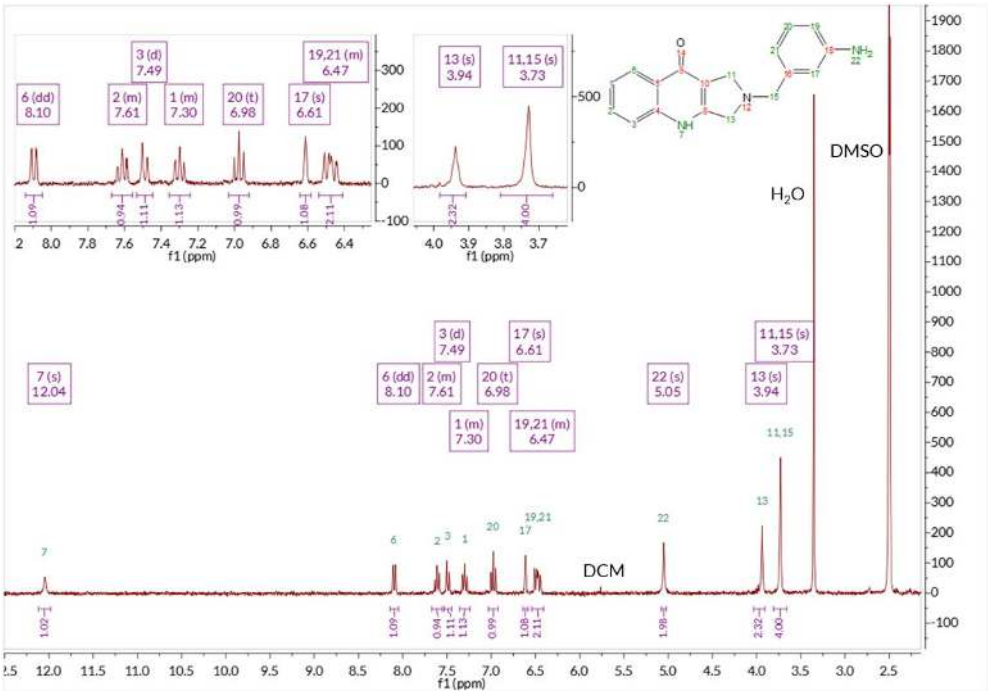

Compound 6b

^{1}H NMR

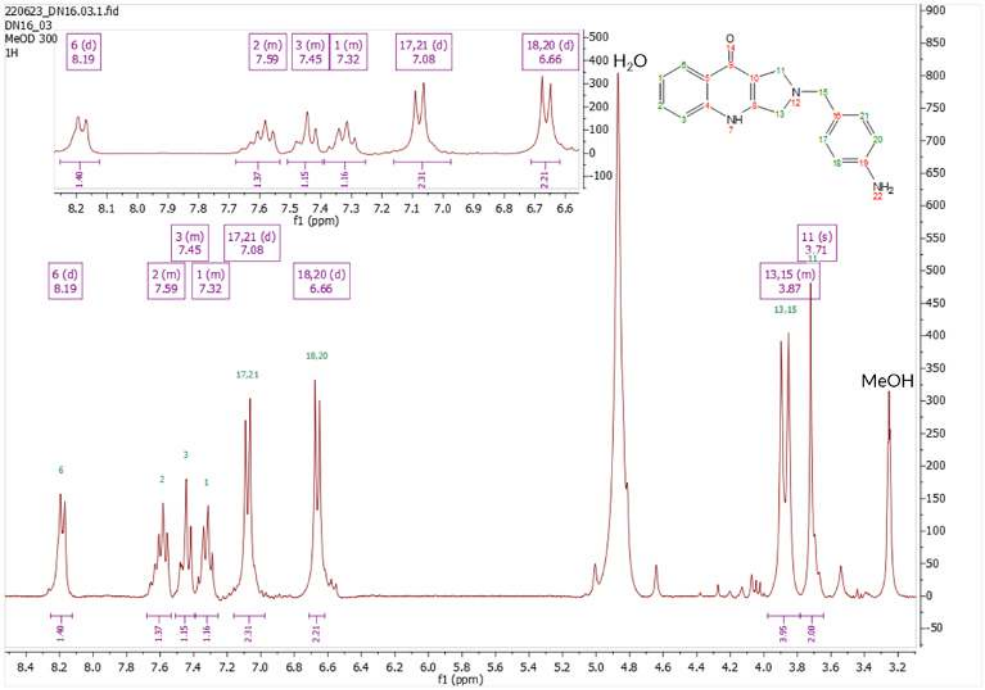

Compound 6c

^{1}H NMR

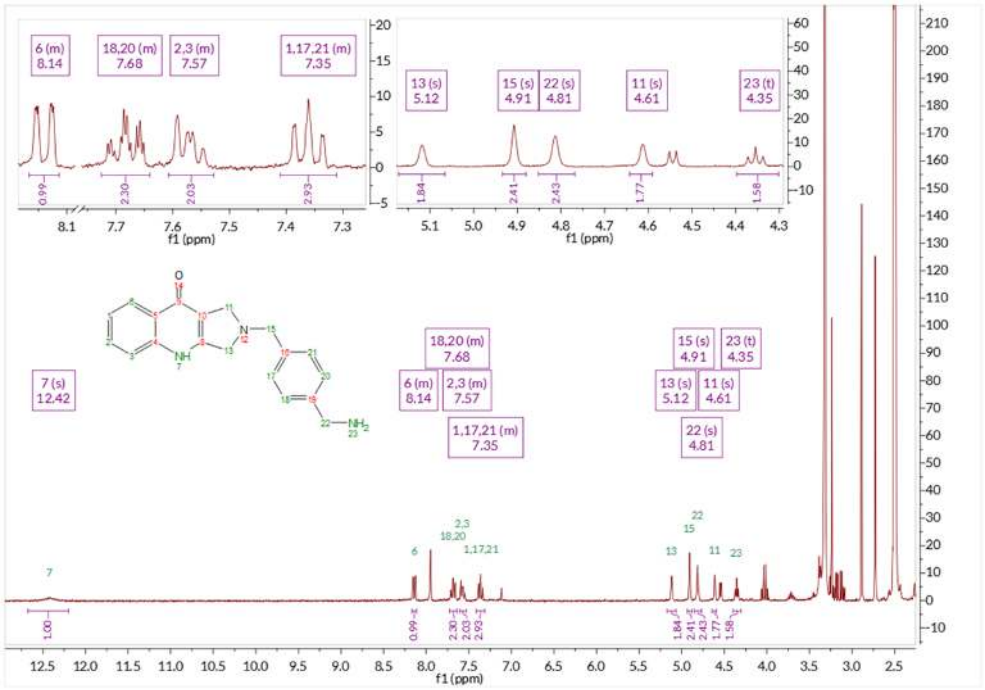

^{1}H–^{1}H COSY

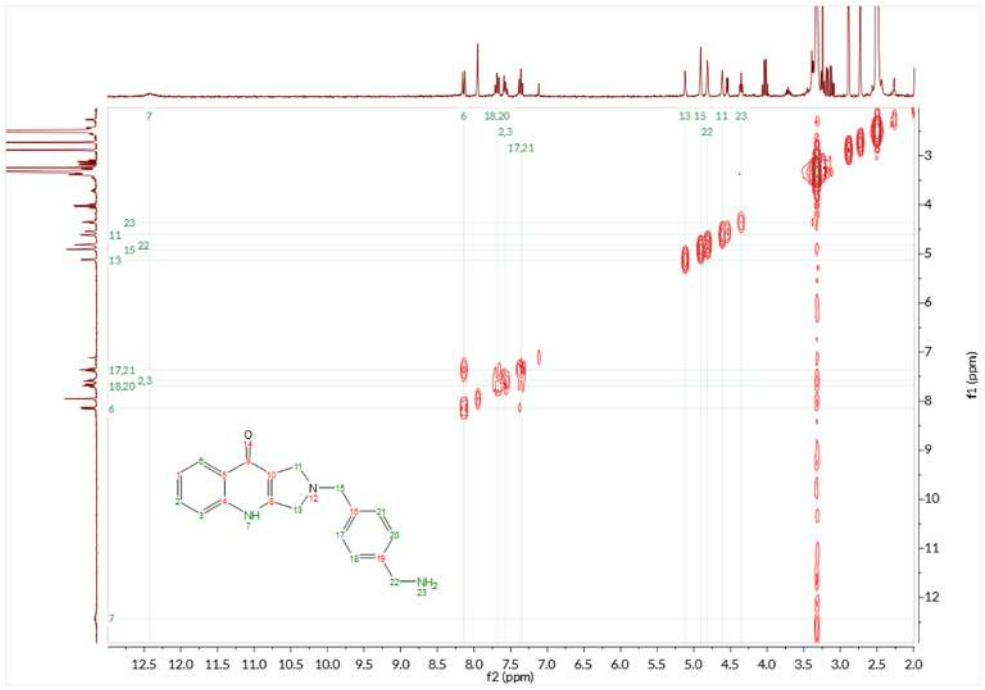

Compound 7a

ESI – MS

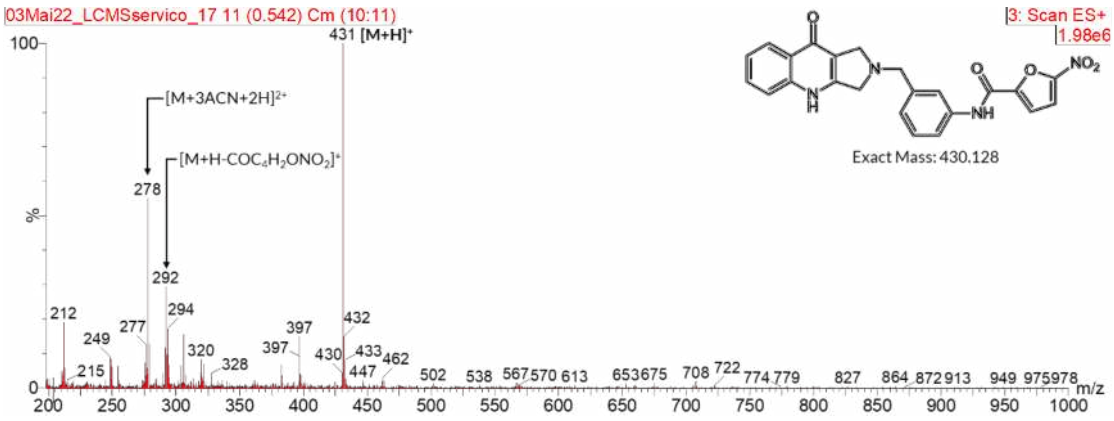

^{1}H NMR

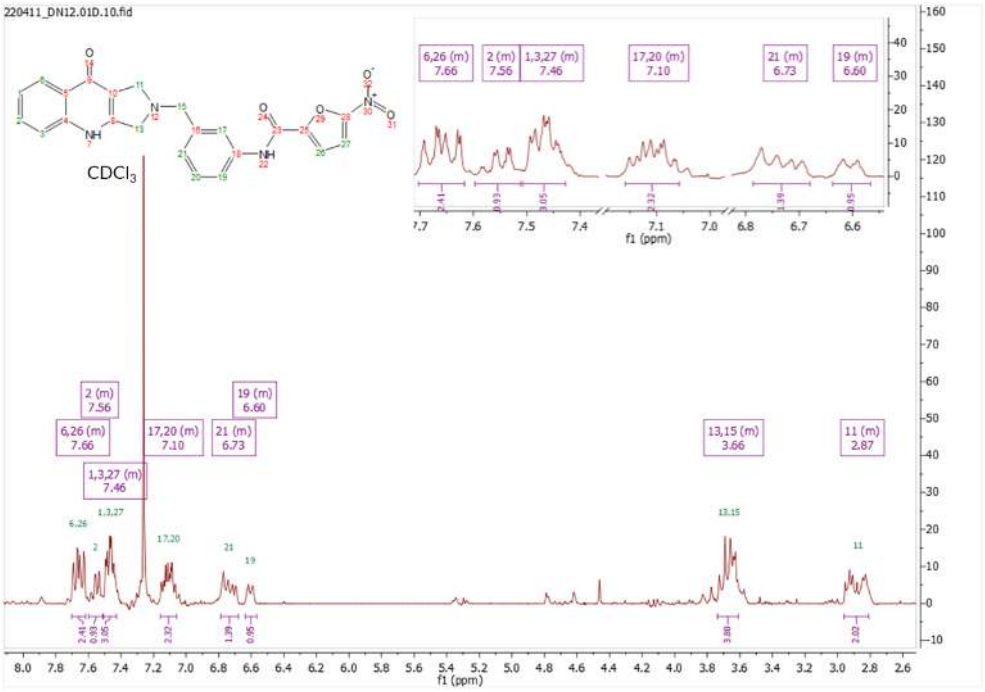

Compound 7b

ESI – MS

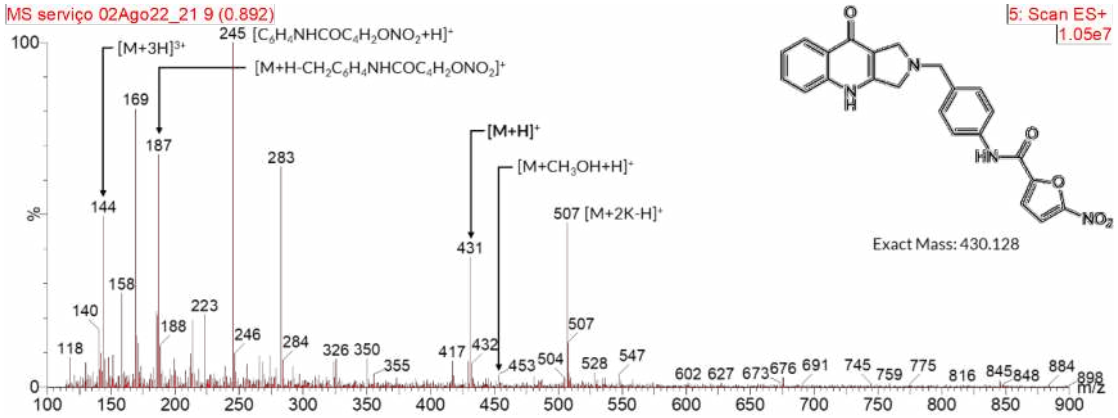

^{1}H NMR

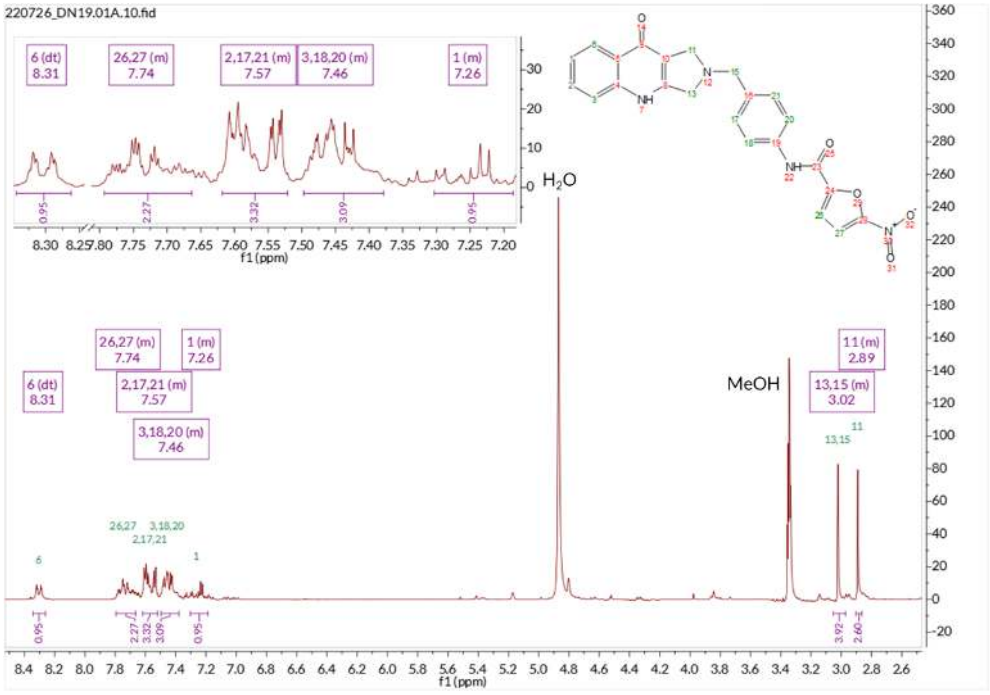

Compound 7c

ESI – MS

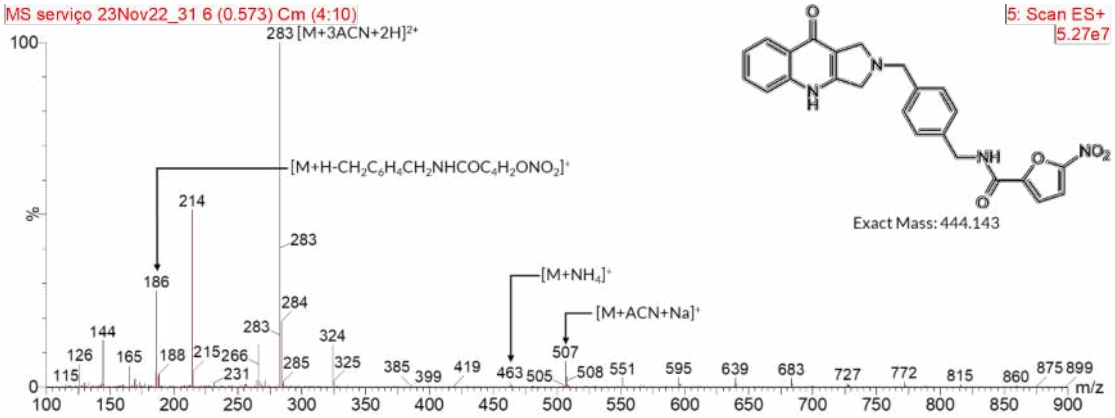

^{1}H NMR

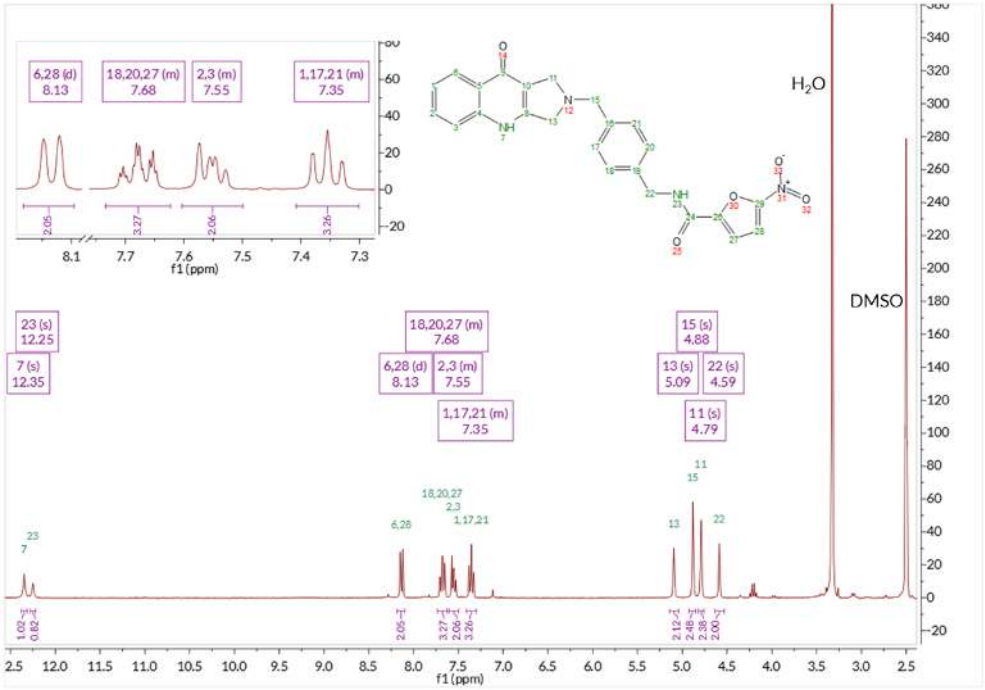

^{13}C NMR

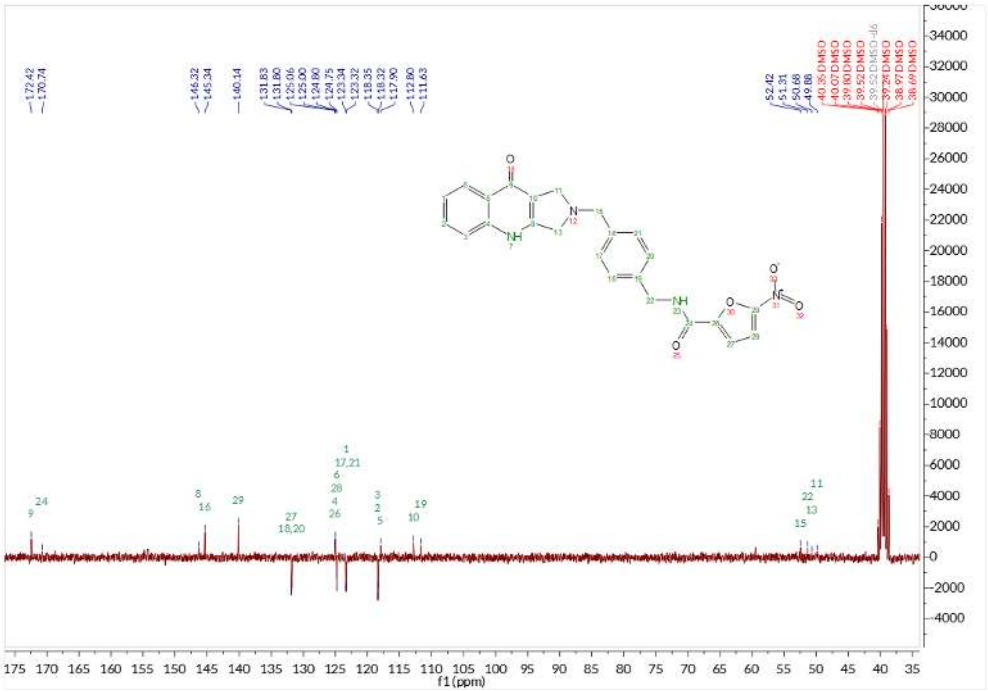

$^{1}H–^{1}H$ COSY

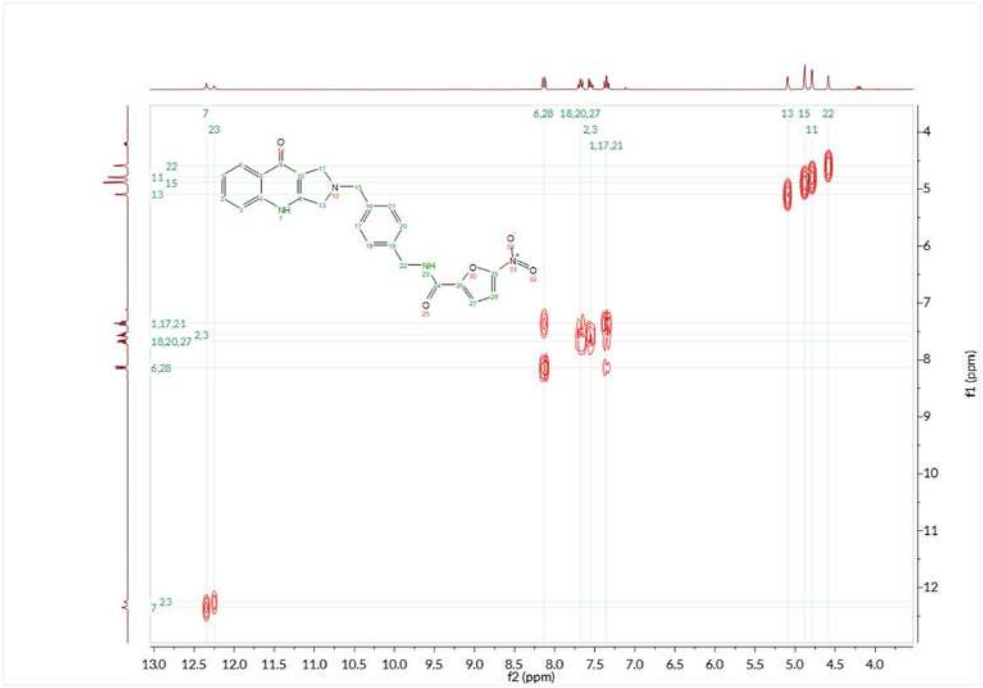

$^{1}H–^{13}C$ HMQC

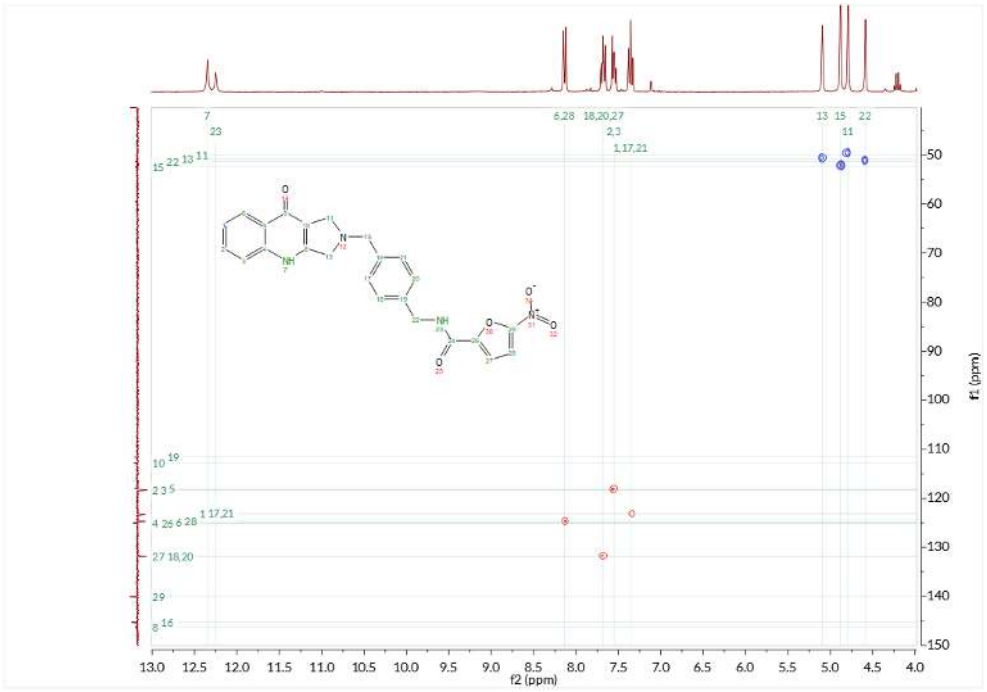

$^{1}H–^{13}C$ HMBC

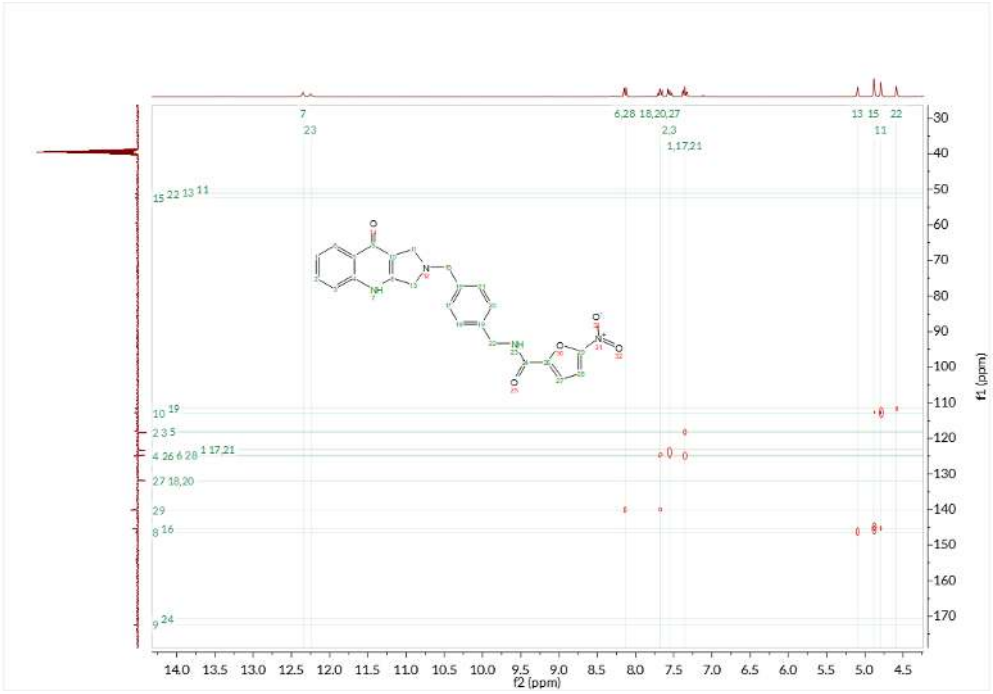

Compound 7c'

ESI – MS

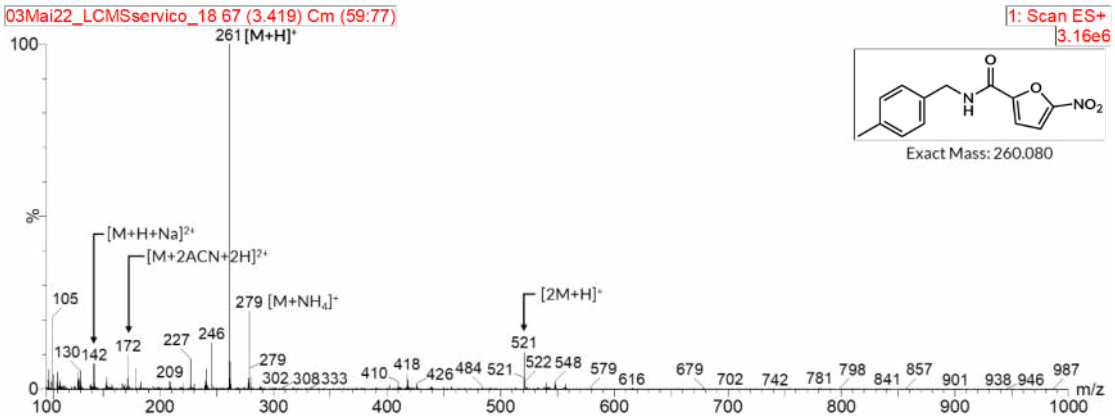

^{1}H NMR

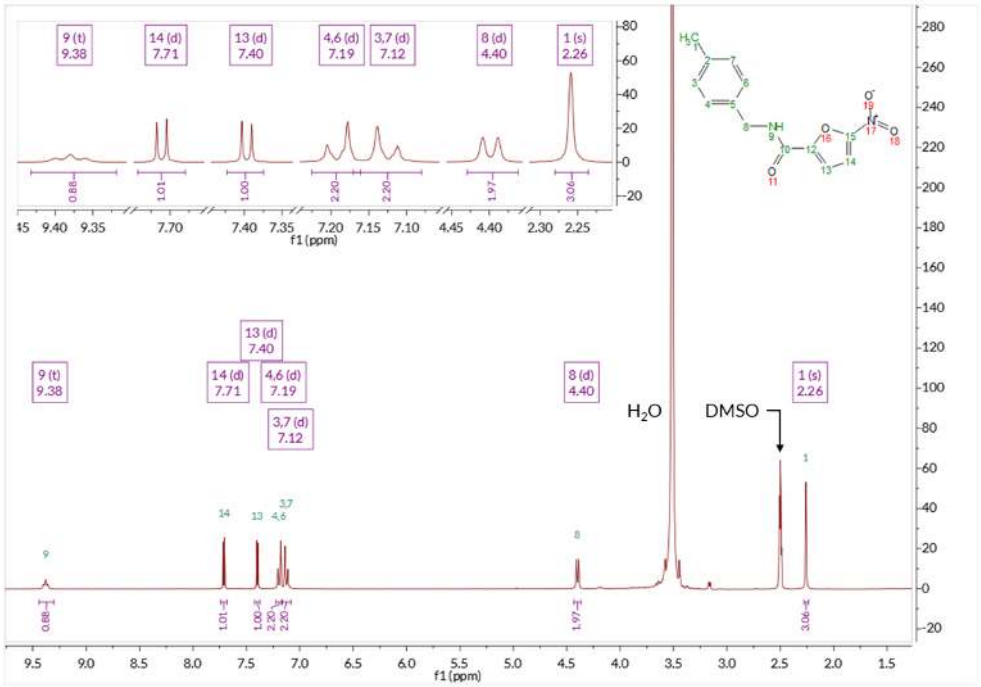

^{13}C NMR

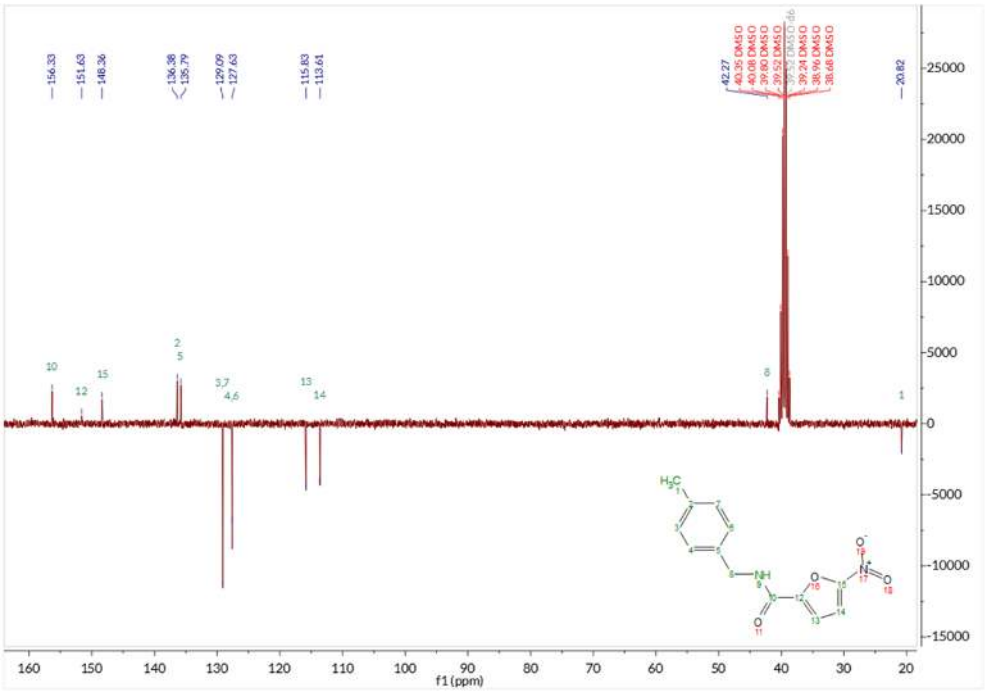

$^{1}H–^{1}H$ COSY

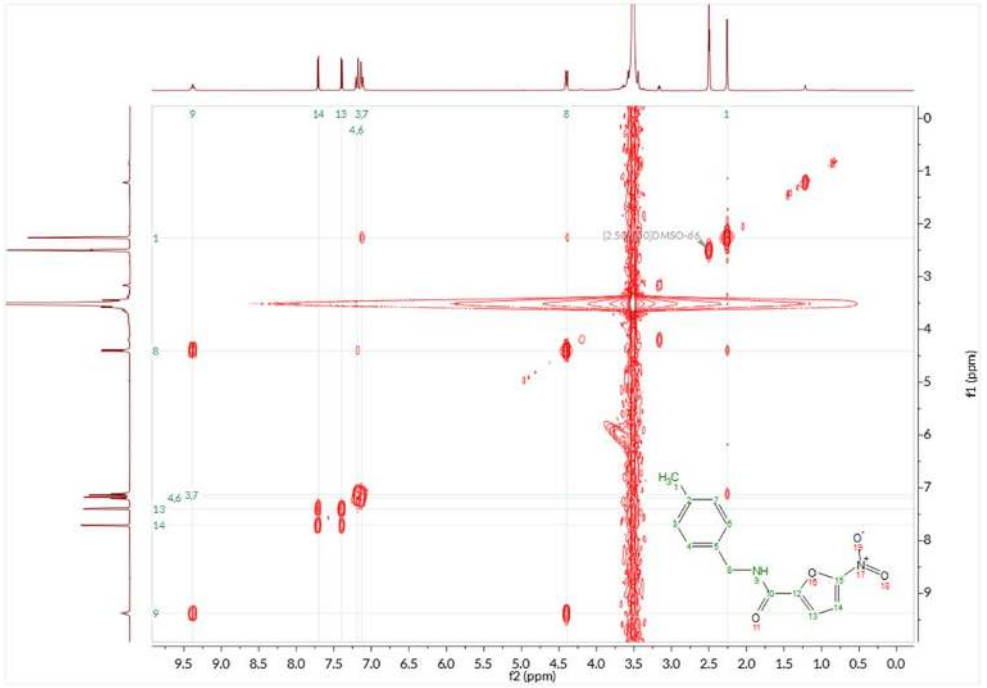

$^{1}H–^{13}C$ HMQC

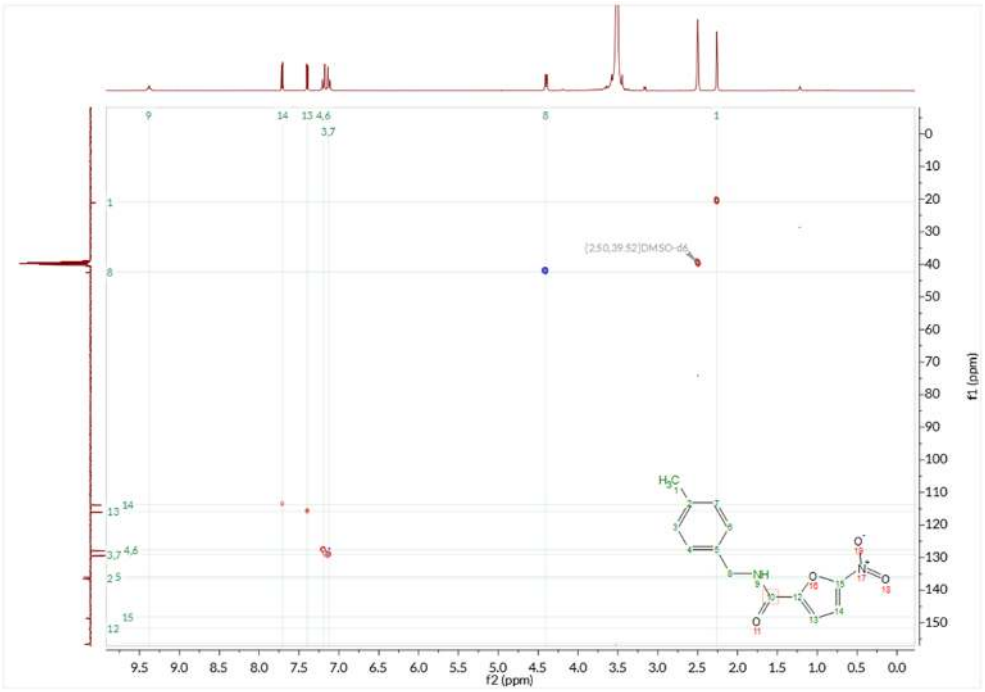

$^{1}H–^{13}C$ HMBC

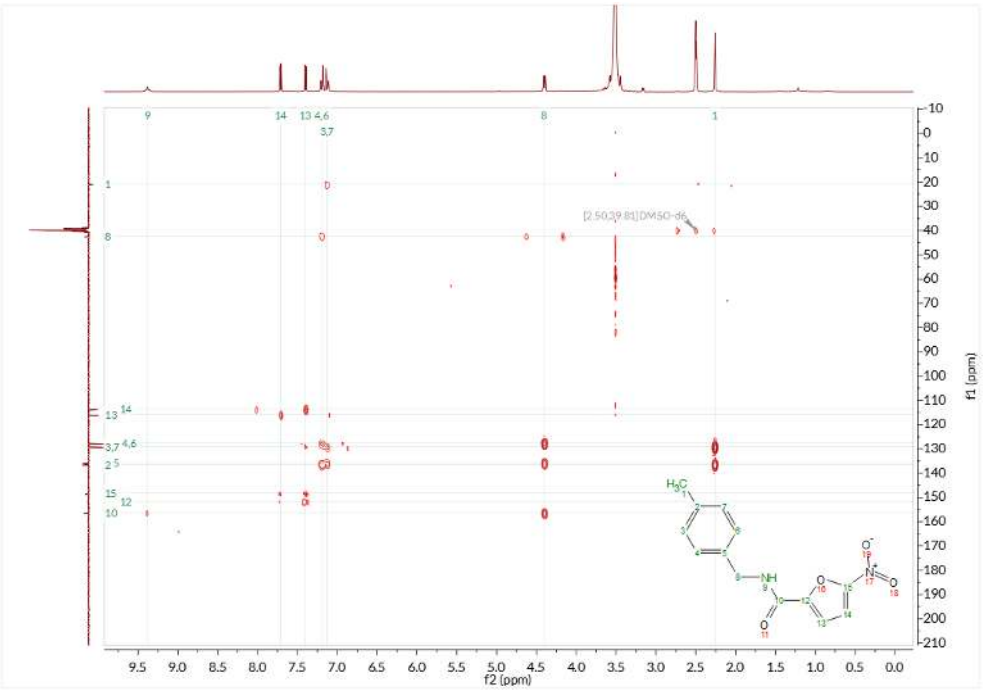

Compound 7d

HPLC chromatogram [detection wavelength: 315 nm]

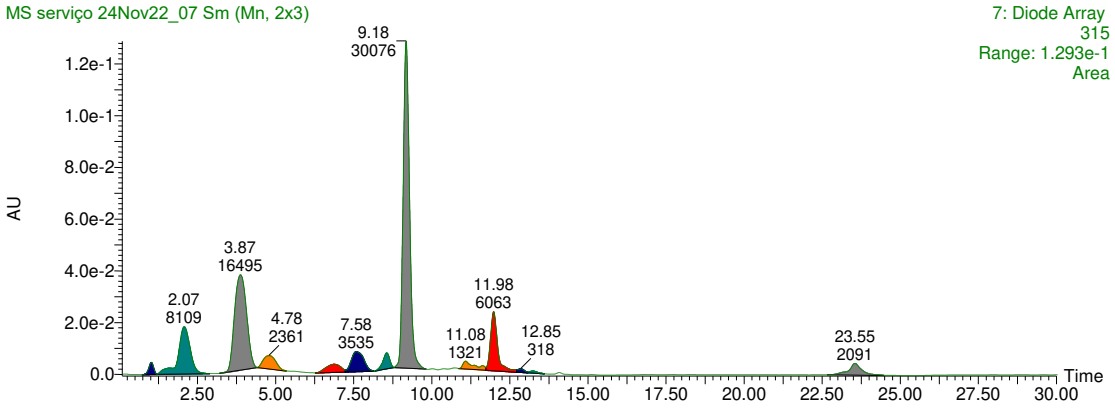

ESI – MS [spot at 11.98 min]

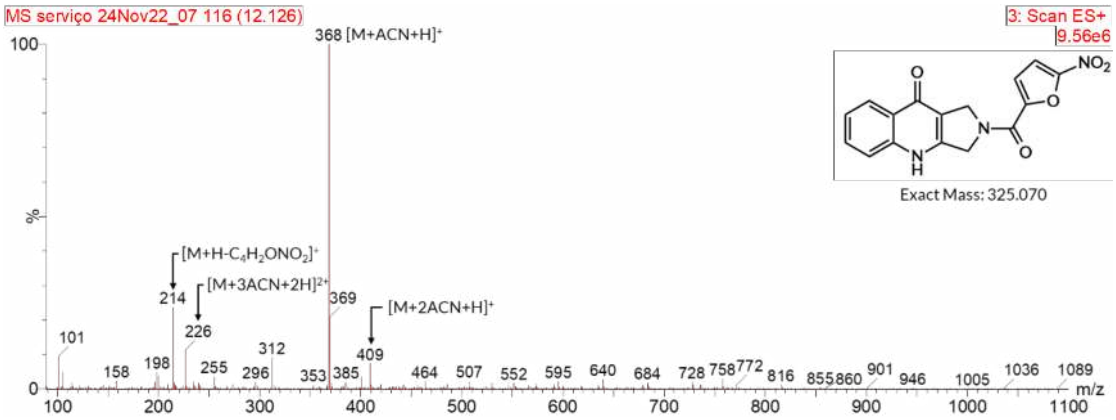

Compound 8a

ESI – MS

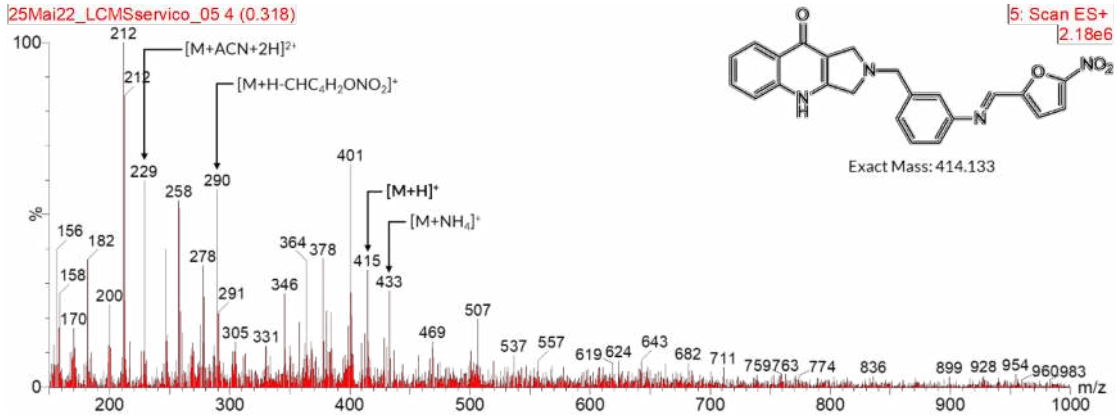

^{1}H NMR

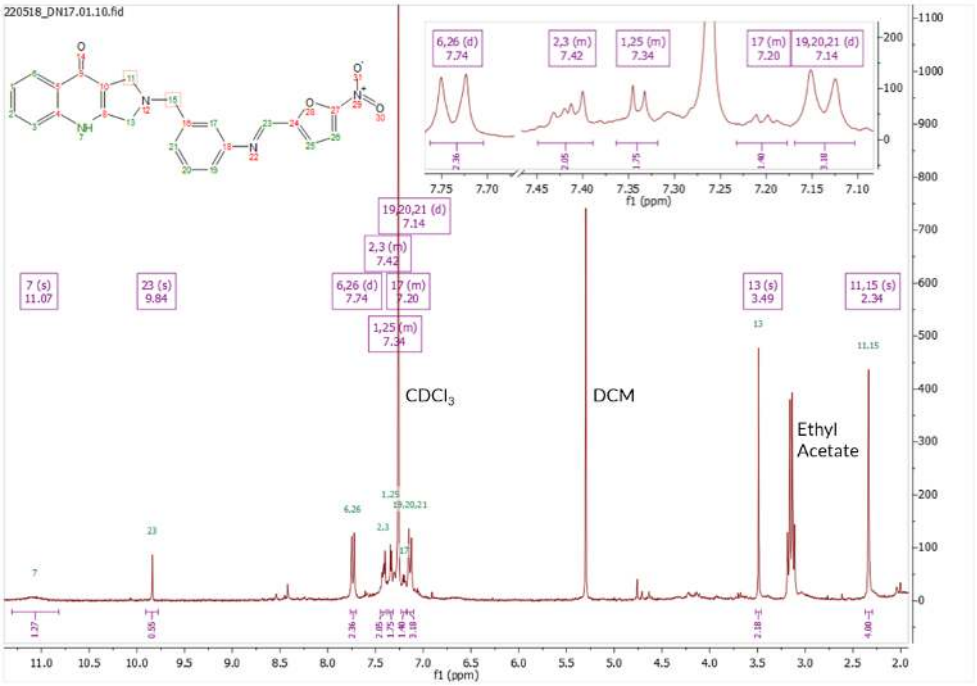

Compound 8b

ESI – MS

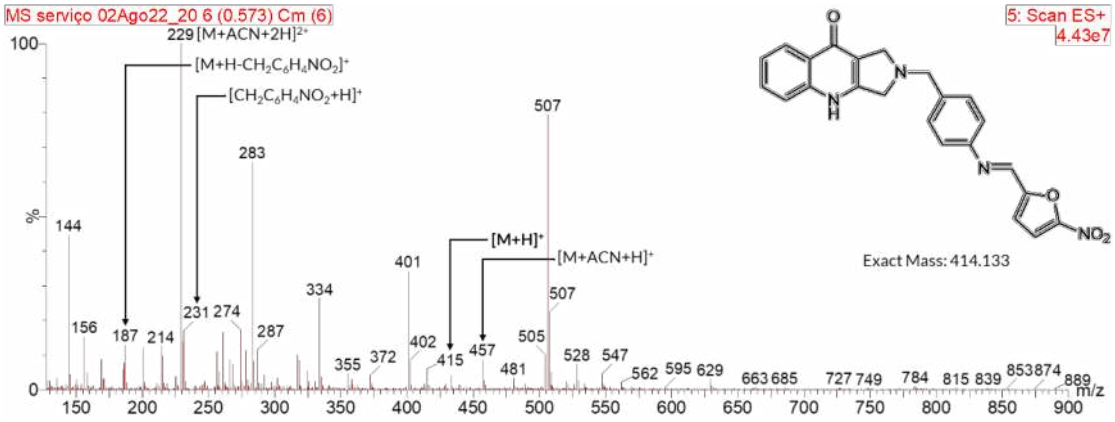

^{1}H NMR

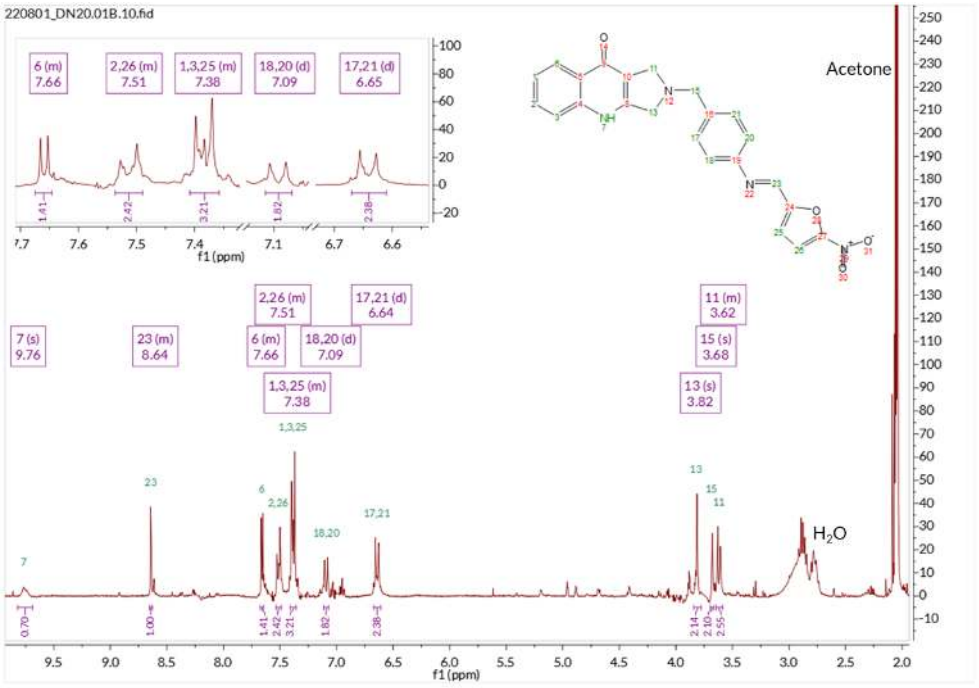

Compound 8c

ESI – MS

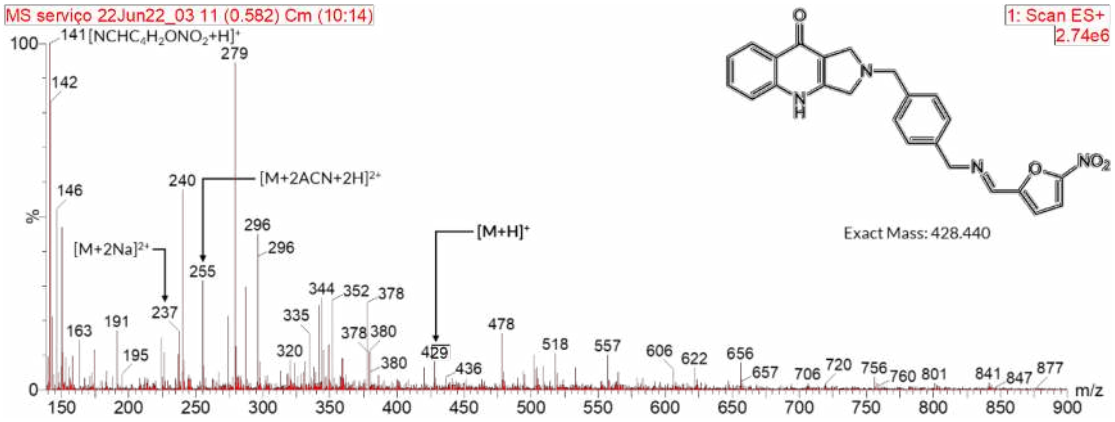

^{1}H NMR

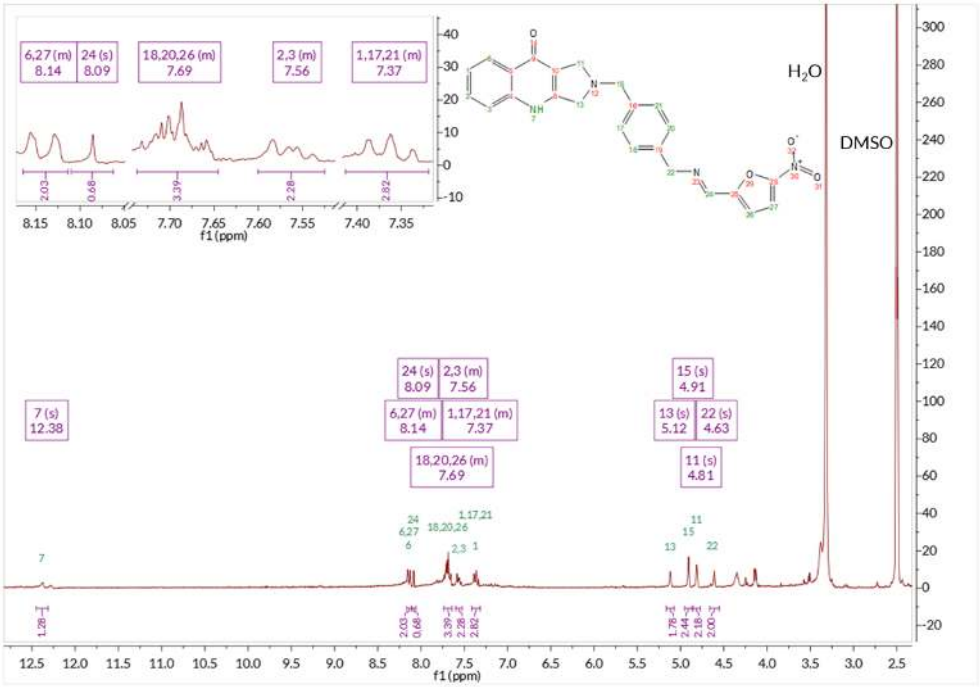

^{1}H–^{1}H COSY

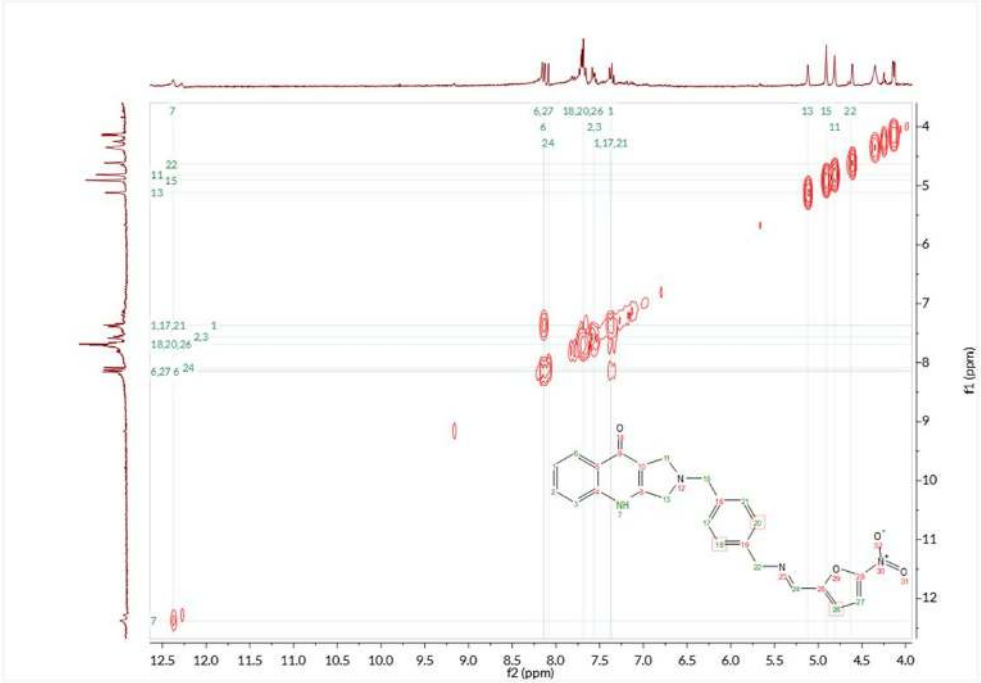

Compound 9

^{1}H NMR